

**TRACING TIME IN THE OCEAN: UNRAVELING  
DEPOSITIONAL AND PRESERVATIONAL TIMESCALES  
USING COMPOUND-SPECIFIC RADIOCARBON ANALYSIS  
OF BIOMARKERS FROM MARINE SEDIMENTS**

Dissertation zur Erlangung des Doktorgrades

Dr. rer. nat.

am Fachbereich Geowissenschaften der Universität Bremen

vorgelegt von

**Stephanie Kusch**

März, 2010



Gutachter der Dissertation

**Prof. Dr. Gesine Mollenhauer  
Prof. Dr. Kai-Uwe Hinrichs**



*It is the tension between creativity and scepticism  
that has produced the stunning and unexpected findings of science.*

Carl Edward Sagan  
(1934-1996)



## **ERKLÄRUNG**

Name: Stephanie Kusch

Datum: 11.03.2010

Anschrift: Graudenzer Str. 12, 28201 Bremen

Hiermit versichere ich, dass ich

1. die Arbeit ohne unerlaubte fremde Hilfe angefertigt habe,
2. keine anderen als die von mir angegebenen Quellen und Hilfsmittel benutzt habe und
3. die den benutzen Werken wörtlich oder inhaltlich entnommenen Stellen als solche kenntlich gemacht habe.

Bremen, den 11.03.2010

---

Unterschrift



## TABLE OF CONTENTS

ABSTRACT .....	I
KURZFASSUNG .....	III
1. INTRODUCTION .....	1
1.1 Radiocarbon .....	3
1.2 Geochemical methods used for compound-specific radiocarbon analysis.....	11
1.2.1 Bulk sample analysis.....	12
1.2.2 Calcareous microfossil analysis.....	12
1.2.3 Lipid analysis .....	13
1.2.4 Gas chromatography.....	14
1.2.5 Preparative Capillary Gas Chromatography .....	15
1.2.6 High Performance Liquid Chromatography .....	16
1.2.7 Isotope Ratio Mass Spectrometry.....	17
1.3 Biomarkers used for compound-specific radiocarbon analysis.....	18
1.4 Motivation and goals of this thesis.....	20
2. MANUSCRIPT I .....	23
Timescales of lateral sediment transport in the Panama Basin as revealed by compound-specific radiocarbon ages of alkenones, total organic carbon and foraminifera .....	23
3. MANUSCRIPT II .....	49
Controls on the age of terrigenous organic matter in Black Sea sediments .....	49
4. MANUSCRIPT III .....	77
Implications for chloro- and pheopigments synthesis and preservation from combined compound-specific $\delta^{13}\text{C}$ , $\delta^{15}\text{N}$ , and $\Delta^{14}\text{C}$ analysis.....	77
5. SUMMARY AND PERSPECTIVES .....	97
6. REFERENCES.....	103
7. ACKNOWLEDGEMENTS .....	125
8. APPENDIX.....	127



## ABSTRACT

Carbon cycle dynamics between the different inorganic and organic carbon pools play an important role in controlling the atmospheric chemical composition, thus, regulating the Earth's climate. Atmospheric CO<sub>2</sub> is fixed into biomass by photosynthesis of terrestrial and marine primary producers. Until final burial in marine sediments, the biologically fixed carbon that escapes remineralisation undergoes exchange between various active carbon reservoirs. Until now, the timescales on which terrestrial and marine organic matter is exchanged between the terrigenous, oceanic, and sedimentary carbon pool as well as the residence time in the respective reservoirs are still poorly understood. Compound-specific radiocarbon analysis of biomarkers provides a powerful tool to determine the temporal scales of such exchange processes. Here, the timescales of different physicochemical and sedimentological processes are resolved including timescales of lateral sediment transport within the ocean, terrestrial residence times of terrigenous organic matter prior to delivery to the ocean, and timescales of organic matter preservation in the ocean.

Radiocarbon ages of co-occurring alkenones, foraminiferal tests, and total organic carbon (TOC) were measured to estimate the timescales of lateral sediment transport within the Panama Basin. Such transport processes are likely to occur at the sediment-water interface prior to initial sedimentation or following resuspension and can lead to prolonged residence times of organic matter in the water column before final burial in the sediments. Accordingly, this process may cause age offsets between organic matter easily prone to resuspension (alkenones) and denser sediment constituents (foraminifera). In Panama Basin late glacial to Holocene sediments from cores ME0005-24JC, Y69-71P, and MC16 all sediment constituents mostly agree well in age, indicating no significant addition of pre-aged alkenones or contribution of aged terrigenous organic matter. Therefore, lateral sediment transport is not inferred. However, evidence from previous studies indicates strong sediment focusing at the investigated core locations. Thus, if lateral transport occurs, radiocarbon ages of alkenones, TOC, and foraminifera indicate rapid, syndepositional (i.e. within decades), and local nepheloid layer transport rather than remobilization of aged sediments. Transport within only a few decades inhibits temporal decoupling of proxies from different grain size fractions, thus, validating multi-proxy paleoceanographic reconstructions in the study area. Nevertheless, anomalously old foraminiferal tests were found in one glacial depth interval of core Y69-71P resulting from downslope transport along the northern Carnegie Ridge. This process might bias paleoceanographic reconstructions for core Y69-71P based on foraminifera.

Radiocarbon ages of long-chain vascular plant *n*-alkanes and *n*-fatty acids, and TOC were determined to estimate their average terrestrial residence time prior to burial

## ABSTRACT

---

in Black Sea sediments and the underlying controlling factors. Storage of terrigenous organic matter in terrestrial reservoirs, such as soils, is likely to produce age offsets between marine and terrigenous organic matter in marine sediments, which is critical when continental climate is reconstructed. Average terrestrial residence times in different river drainage areas of the Black Sea deduced from  $n\text{-C}_{29+31}$  alkanes and  $n\text{-C}_{28+30}$  fatty acids of river mouth stations range from  $900\pm70$  years to  $4400\pm170$  years. River catchment size is the major morphological control on terrestrial residence time in climatically similar drainage areas. A climatic controlling factor cannot unambiguously be determined, but Mediterranean climate appears to increase continental carbon turnover compared to continental climate. Along-transect data imply petrogenic  $n\text{-C}_{29+31}$  alkanes contribute to the vascular plant  $n\text{-C}_{29+31}$  alkanes. As a result,  $n\text{-C}_{28+30}$  fatty acids provide better estimates of average terrestrial residence time. Along-transect data furthermore reveal that  $n\text{-C}_{29+31}$  alkanes as well as  $n\text{-C}_{28+30}$  fatty acids are supplied by both riverine (nearshore) and aeolian (offshore) transport mechanisms. Interestingly, aeolian vascular plant biomarkers are pre-aged as well although to a lesser extent than riverine biomarkers, which are up to 3500 years older. The aged aeolian biomarkers are likely to result from admixture of lipids blown out of agriculturally degraded soils of the northern Black Sea catchment and lipids directly abraded from leaf surfaces.

Preservation timescales of marine chloro- and pheopigments, which can directly be linked to photosynthesis, were estimated using radiocarbon ages of chlorophyll *a*, pheophytin *a*, pyropheophytin *a*, and cyclopheophorbide *a* enol as well as co-occurring TOC and bivalve shells from Black Sea core top sediments. Additionally, stable carbon and nitrogen isotopic compositions were determined to reconstruct the environmental conditions during the time of pigment synthesis. Since primary chloro- and pheopigments rapidly decompose in multiple ways including (autolytic) cell senescence, photo-oxidation, enzymatic or hydrolysis reactions, microbial and viral lysis, and grazing, their potential to be preserved as intact pigments in sediments is considered to be low. However, the radiocarbon concentrations of mainly phytoplanktonic chlorophyll *a*, pheophytin *a*, pyropheophytin *a*, and cyclopheophorbide *a* enol, which translate into ages of 40 up to 1200 years, imply preservation is much more efficient than expected. Preservation most likely results from mechanisms such as association with minerals or eutrophication-induced hypoxia and light limitation. The stable nitrogen isotopic composition of the pigments identifies nitrate utilization as the major nitrogenous nutrient uptake pathway especially at near-coast stations. Towards more offshore stations an isotopic depletion indicates N<sub>2</sub>-fixation as an additional nutrient utilization pathway. The long-term stable carbon and nitrogen isotopic variability appears to be as strong as the seasonal isotopic variations of the nutrient source, growth period, and habitat.

## KURZFASSUNG

Der globale Kohlenstoffkreislauf ist durch Austauschprozesse zwischen verschiedenen organischen und anorganischen sowie aktiven und passiven Kohlenstoffreservoirn, wie beispielsweise der Erdatmosphäre, den Ozeanen, mariner und terrestrischer Biomasse und Sedimenten, charakterisiert. Dabei umfassen die größten Kohlenstoffflüsse des aktiven Kreislaufes den Austausch zwischen Atmosphäre und Ozean (Lösung und Ausgasung von CO<sub>2</sub>) und Atmosphäre und Vegetation (Photosynthese und Respiration mariner und terrestrischer Biomasse). Die photosynthetische Bindung anorganischen Kohlenstoffs in organische Biomasse und deren Ablagerung in Sedimenten stellt den Übergang vom aktiven in den passiven Kohlenstoffkreislauf dar. Vor einer solchen, endgültigen Sequestrierung findet der aktive Kohlenstofftransfer zwischen Reservoirn auf sehr unterschiedlichen, weitestgehend unbekannten Zeitskalen statt. Dazu gehören unter anderem die Zeitskalen, auf welchen terrigene und marine organische Substanz zwischen den kontinentalen, ozeanischen und sedimentären Kohlenstoff-Pools zirkuliert und zwischengespeichert wird. Mit Hilfe komponenten-spezifischer Radiokarbondatierungen von Biomarkern ist es möglich die Zeitskalen der Kohlenstoffdynamik innerhalb eines Reservoirs und zwischen Reservoirn zu bestimmen. Diese Methodik wurde in der vorliegenden Dissertation angewandt um die Zeitskalen von lateralem Sedimenttransport innerhalb des Ozeans zu erfassen, terrigene Verweildauern organischer Substanz vor ihrer Ablagerung in marinen Sedimenten zu bestimmen, sowie die Zeitskalen der Erhaltung organischer Verbindungen innerhalb der ozeanischen Wassersäule und Sedimenten abzuschätzen.

Die Zeitskalen lateralens Sedimenttransports im Panama-Becken wurden anhand der Radiokarbon-Alter von Alkenonen, Foraminiferen sowie des gesamt-organischen Kohlenstoffs bestimmt. Lateraler Sedimenttransport findet vor der ersten Ablagerung oder nach Resuspension besonders an der Grenze zwischen Wassersäule und Sedimentoberfläche statt. Dies kann zu verlängerter Aufenthaltsdauer des organischen Materials in der Wassersäule und somit zu Alterunterschieden zwischen leicht suspendierbarem Material geringer Dichte (Alkenone) und weniger leicht suspendierbarem Material höherer Dichte (Foraminiferen) führen. In den untersuchten spätglazialen und holozänen Sedimenten des Panama-Beckens, stimmen die Alter aller untersuchten Komponenten der Kerne ME0005-24JC, Y69-71P, und MC16 fast immer gut überein. Dies schließt Zutrag von vorgealterten Alkenonen oder terrigenem organischen Material aus und impliziert daher selbst keinen lateralen Transport. Vorangehende Arbeiten haben allerdings starke Sedimentfokussierung an den Kernpositionen aufgezeigt. Aufgrund der guten Altersübereinstimmung lässt sich daher schließen, dass wenn lateraler Transport stattfindet es eine schnelle und lokale Umlagerung frische

sedimentierten organischen Materials in Nepheloid-Schichten innerhalb von Dekaden gibt und keine Remobilisierung vorgealterter Sedimente stattfindet. Solch schneller Transport innerhalb von Dekaden verhindert eine Entkopplung von Proxies verschiedener Korngrößen. Somit ist im Untersuchungsgebiet keine Beeinträchtigung von Paläo-Rekonstruktionen basierend auf der Korrelation verschiedener Proxies zu befürchten. Allerdings finden sich ungewöhnlich alte Foraminiferen in einer glazialen Kerntiefe von Kern Y69-71P, die höchstwahrscheinlich vom nördlichen Carnegie Rücken gespült wurden. Dieser Prozess kann eine Beeinträchtigung paläo-ozeanographischer Studien des Sedimentkerns Y69-71P hervorrufen, die auf Foraminiferen beruhen.

Durchschnittliche terrigene Verweildauern cutiulärer Pflanzenwachse vor ihrer Ablagerung in Schwarzmeer-Sedimenten und die zugrunde liegenden Kontrollparameter wurden mit Hilfe der Radiokarbon-Alter langkettiger *n*-Alkane und *n*-Fettsäuren sowie des gesamt-organischen Kohlenstoffs bestimmt. Die Zwischenspeicherung terrigenen organischen Materials in kontinentalen Reservoirs wie Böden führt zu einem Altersunterschied zwischen marinem und terrestrischem organischen Material in marinen Sedimenten. Dies ist ein kritischer Prozess für Paläo-Rekonstruktionen kontinentalen Klimas mit Hilfe solcher Pflanzenwachse aus marinen Sedimenten. Die durchschnittlichen Verweildauern von *n*-C<sub>29+31</sub> Alkanen und *n*-C<sub>28+30</sub> Fettsäuren mündungsnaher Proben verschiedener Flusseinzugsgebiete des Schwarzen Meeres reichen von 900±70 bis 4400±170 Jahre. Hierbei ist die Größe des Einzugsgebietes der maßgebliche morphologische Faktor für das durchschnittliche terrigene Reservoiralter in klimatisch ähnlichen Einzugsgebieten. Eine klimatische Kontrolle kann nicht eindeutig herausgestellt werden, jedoch scheint mediterranes Klima die terrestrische Verweildauer im Vergleich zu humiderem, kälterem, kontinentalen Klima zu verlängern. Die Proben entlang von Transekten zeigen eine Mischung petrogener und pflanzlicher *n*-C<sub>29+31</sub> Alkane an, sodass *n*-C<sub>28+30</sub> Fettsäuren grundsätzlich besser zur Bestimmung durchschnittlicher kontinentaler Reservoiralter geeignet sind. Die Transektdaten zeigen weiterhin, dass die *n*-C<sub>29+31</sub> Alkane und *n*-C<sub>28+30</sub> Fettsäuren in Küstennähe durch Flusseintrag, im offenen Schwarzen Meer dagegen durch Windeintrag bereit gestellt werden. Hierbei zeigt sich, dass auch die äolischen Pflanzen-Biomarker vorgealtert sind, obwohl die fluvialen Biomarker nochmals bis zu 3500 Jahre älter sind. Die Voralterung der äolischen Biomarker resultiert höchstwahrscheinlich aus der Zusammenführung von Lipiden, welche aus landwirtschaftlich degradierten Böden ausgeblasen werden und Lipiden, welche direkt von Blattoberflächen abradiert werden.

Degradations-Zeitskalen von Chloro- und Pheopigmenten wurden mit Hilfe der komponenten-spezifischen Radiokarbonalter von Chlorophyll *a*, Pheophytin *a*, Pyropheophytin *a* und Cyclopheophorbide *a* enol, sowie der Radiokarbonalter von

Muschelschalen und des gesamt-organischen Kohlenstoffs aus Oberflächensedimenten des Schwarzen Meeres rekonstruiert. Zusätzlich wurde die stabile Kohlenstoff und Stickstoff-Isotopenzusammensetzung zur Bestimmung der Umweltbedingungen zur Zeit der Pigmentsynthese bestimmt. Da primäre Chloro- und Pheopigmente sehr schnell und durch verschiedene Prozesse wie autolytischer Zellzerfall, Photooxidation, Enzym- oder Hydrolyse-Reaktionen, mikrobielle und virale Lyse und Prädation degradieren, wird ihr Potential in Sedimenten erhalten als gering eingeschätzt. Trotz dieser Prozesse liegen die gemessenen Alter Chlorophyll *a*, Pheophytin *a*, Pyropheophytin *a* und Cyclopheophorbide *a* enol zwischen 40 und 1200 Jahren. Dies zeigt, dass die Erhaltung von Pigmenten wesentlich besser ist als erwartet. Die Erhaltung ist höchstwahrscheinlich durch die Assoziation der Pigmente an Mineraloberflächen oder in Mineralporen oder Hypoxie und Lichtlimitierung der Wassersäule während eutropher Phasen begründet. Die stabilen Stickstoff-Isotope weisen besonders an den küstennahen Kernpositionen auf Nitrat-Assimilation als den hauptsächlichen Nährstoffaufnahmeprozess hin. Küstenfern deutet eine Abreicherung der Stickstoff-Isotope Stickstofffixierung als zusätzlichen Nährstoffaufnahmeprozess an. Hierbei erscheint die langzeitliche Variabilität der Kohlenstoff- und Stickstoff-Isotope eben so stark zu variieren wie durch saisonale Isotopen-Schwankungen der Nährstoffquelle und Abhängigkeit von der Wachstumsperiode und dem Lebensraum (Wassertiefe).



## 1. INTRODUCTION

The global carbon cycle is characterised by exchange processes between various inorganic and organic carbon reservoirs (Figure 1.1). The short- and long-term variability of these carbon transfer processes determines the atmospheric chemical composition and, thus, regulates the Earth's climate. Understanding the present carbon cycle has, therefore, become a matter of great urgency for society since the effects of human activities on atmospheric chemistry and global climate are believed to be, as yet, unprecedented (e.g., Bindoff et al., 2007; Forster et al., 2007).

Major carbon reservoirs include the atmosphere, oceans, terrestrial and marine biosphere and fossil carbon (including fossil fuels, kerogen, sedimentary rocks and the Earth's crust). The exchange processes of carbon from one reservoir to another cover all timescales from days to millions of years. Over shorter timescales (<1,000 years) carbon exchange primarily affects the terrestrial and marine biosphere. Via photosynthesis inorganic carbon, fixed as atmospheric CO<sub>2</sub>, is reduced into carbohydrates to produce organic biomass, which is subsequently exchanged throughout the biosphere by heterotrophy. The reverse process of respiration and remineralisation, oxidise the organic carbon, and result in the release of CO<sub>2</sub> into the atmosphere (Falkowski, 2003). On timescales of <10,000 years (e.g., from Glacial to Interglacial) carbon transfer between the atmosphere, biosphere, and oceans includes carbon burial into, and redistribution from, marine surface sediments and terrestrial soils. Over timescales of millions of years carbon exchange and the levels of CO<sub>2</sub> in the atmosphere are also controlled by carbon released from the Earth's interior, including that released from sedimentary rocks, as well

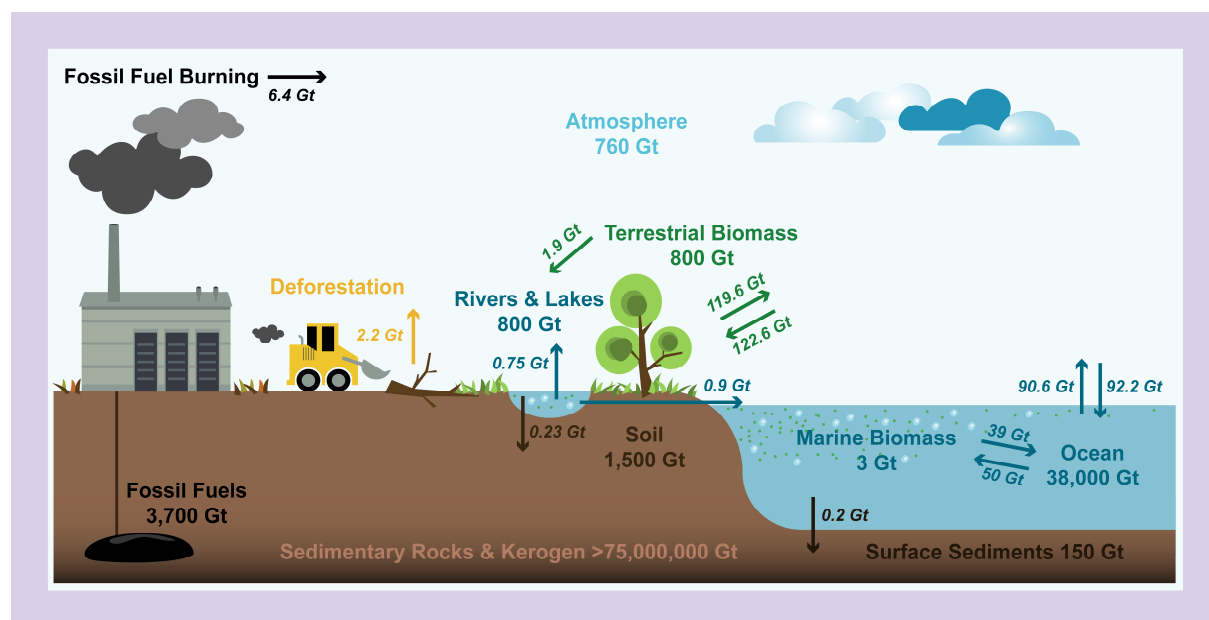


**Figure 1.1** The global carbon cycle. Carbon reservoir sizes ("rivers & lakes" include lacustrine sediments) include anthropogenic perturbations. Annual exchange between the reservoirs is shown in italics (data from Cole et al., 2007; Denman et al., 2007; Houghton, 2003a; Houghton, 2003b; Sundquist and Visser, 2003).

as crust and mantle carbon redistribution (Sundquist and Visser, 2003). These basic temporal dimensions of the global carbon cycle have been understood for several decades. However, insights into precise timescales of the respective short-, medium- and long-term carbon exchange processes have been more difficult to constrain. There is a reasonable knowledge of the timescales involved in the long-term carbon transfer that affects the atmospheric chemistry through interaction with the oceanic and fossil carbon reservoirs. The influence this has over the Earth's climate has been deduced from, e.g., trapped air bubbles inside ice sheets or marine and terrestrial carbonates, and fossil organic carbon (e.g., Freeman and Hayes, 1992; Koch et al., 1992; Pearson and Palmer, 2000; Petit et al., 1999). Likewise, the timescales of the very short-term carbon cycling between the atmosphere and the biosphere through marine and terrestrial carbon fixation as well as the timescales of "anthropogenic carbon transfer" mainly by fossil fuel combustion and deforestation, are well known since they are accessible through direct monitoring (Houghton, 2003a). However, the detailed timescales of most carbon exchange processes coupling terrestrial and marine primary production to final burial in marine surface sediments are rather vague or unknown, due to the lack of insights into potential intermediate time lags. Since compound-specific radiocarbon analysis was first introduced to the Earth Sciences (Eglinton et al., 1996), a powerful tool has become available that illuminates such aspects of the global carbon cycle. It provides the opportunity to trace chemical, physical, and biological pathways, and the rates of organic carbon dynamics that play an important role in regulating the global carbon cycle exchange between the biosphere and geosphere (Levin and Hesshaimer, 2000). Moreover, compound-specific radiocarbon analysis of biomarkers can help in understanding the timescales over which carbon fixed in terrestrial biomass is supplied to the oceans and buried in marine sediments (Drenzek, 2007; Drenzek et al., 2007; Mollenhauer and Eglinton, 2007; Pearson and Eglinton, 2000; Smittenberg et al., 2006). Likewise, the timescales over which carbon fixed in marine biomass is ultimately stored in sediments can be assessed. It allows transport processes within single reservoirs to be identified, and determines their timescales (Drenzek, 2007; Mollenhauer et al., 2003; Mollenhauer et al., 2006; Ohkouchi et al., 2002). Furthermore, metabolic carbon fixation pathways and the respective carbon sources can be identified, and preservation or degradation pathways and their timescales can be understood (Hansman et al., 2009; Ingalls et al., 2006; Pearson et al., 2005; Petsch et al., 2001; Rethemeyer et al., 2004). Moreover, in marine sediments compound-specific radiocarbon analysis furthermore offers the potential for sediment chronologies to be improved, or it can be used as a primary chronological tool for paleoceanographic studies in regions where other materials cannot be used (Ingalls et al., 2004; Ohkouchi et al., 2003).

## 1.1 RADIOCARBON

### 1.1.1 GLOBAL DISTRIBUTION OF RADIOCARBON

Carbon naturally occurs as three isotopes, which differ in their number of neutrons and, thus, their atomic weight: the stable isotopes  $^{12}\text{C}$  (98.89%) and  $^{13}\text{C}$  (1.11%) and the cosmogenic nuclide  $^{14}\text{C}$  ( $1.176 \times 10^{-12}\%$ ). The latter isotope, radiocarbon, is constantly produced in the lower stratosphere by collisions between low-energy cosmic ray neutrons and atmospheric nitrogen atoms ( $^{14}\text{N}$ ), which emit a proton. The newly produced  $^{14}\text{C}$  is rapidly oxidised to  $^{14}\text{CO}$  and  $^{14}\text{CO}_2$  and, thus, is quickly mixed within the atmosphere (Figure 1.2). Via photosynthesis  $^{14}\text{C}$  enters the terrestrial and the marine biosphere as a result of the uptake of atmospheric  $\text{CO}_2$  or seawater dissolved inorganic carbon (DIC) into plant biomass (Damon et al., 1978).

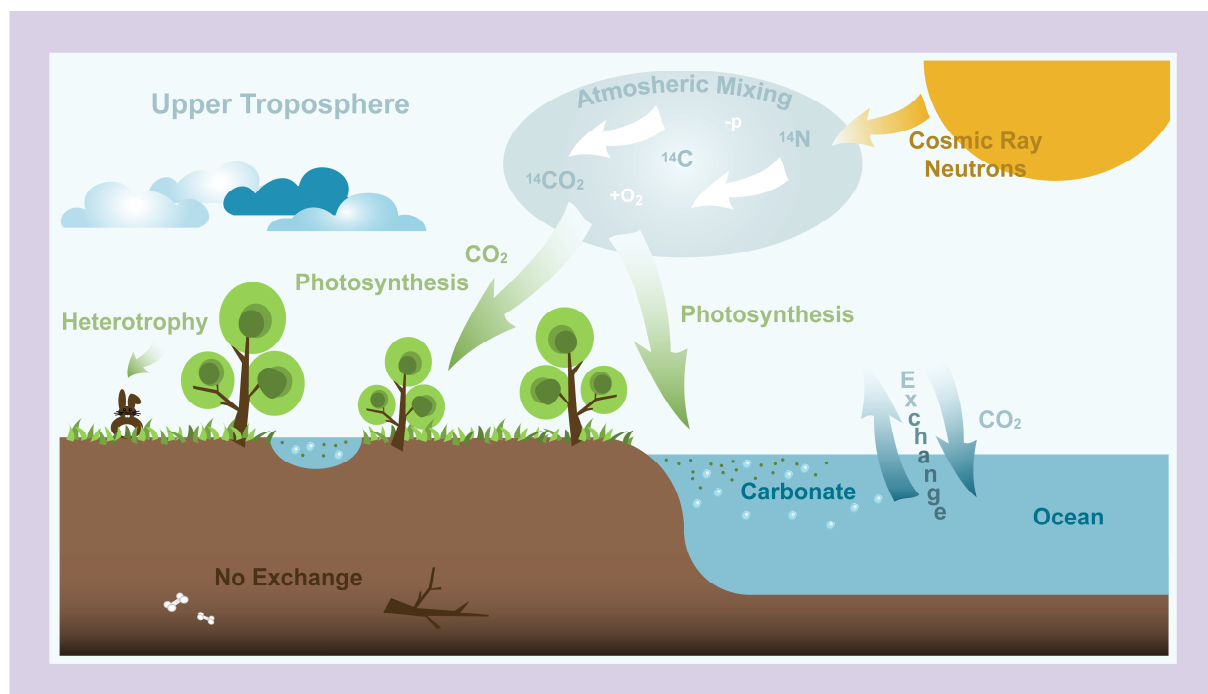


Figure 1.2 Simplified illustration of the distribution of radiocarbon (re-drawn after J. Ducette, WHOI).

The gas exchange between atmospheric  $^{14}\text{CO}_2$  and surface ocean seawater  $\text{DI}^{14}\text{C}$  species, i.e.  $^{14}\text{CO}_2(\text{aq}) \rightleftharpoons \text{H}^{14}\text{CO}_3^- \rightleftharpoons ^{14}\text{CO}_3^{2-}$ , is kinetically limited, delaying the isotopic equilibration between both pools. Furthermore, isotopic equilibration is delayed by removal of seawater  $\text{DI}^{14}\text{C}$  by advection and radioactive decay in the water column. Both processes reach a steady state balance causing an age offset between the atmosphere and the surface ocean, which is termed reservoir age. The reservoir age increases with increasing water depth. Thus, the surface ocean reservoir age increases when young surface seawater  $\text{DI}^{14}\text{C}$  and older bottom seawater  $\text{DI}^{14}\text{C}$ , which has been removed from exchange with atmospheric  $\text{CO}_2$  for up to 1,500 years, become admixed in areas of down- and upwelling triggered by the global ocean circulation. Presently the global mean

ocean reservoir age of surface waters ranges from approximately 300 to 500 years, with an average of 400 years commonly used. However, it differs significantly between regions; for example, at high latitudes or in upwelling areas ages of up to 1,300 years are reached (Bard, 1988; Hughen et al., 2004b; Southon et al., 1990; Stuiver and Braziunas, 1993). The reservoir age of seawater  $\text{DI}^{14}\text{C}$  will be incorporated into the living biomass and has to be considered when interpreting  $^{14}\text{C}$  data from marine samples. Photoautotrophic utilization will yield phytoplanktonic biomass  $^{14}\text{C}$  concentrations that reflect the respective surface  $\text{DI}^{14}\text{C}$ . Likewise, heterotrophic biomass grazing on phytoplankton will incorporate the phytoplanktonic  $^{14}\text{C}$  concentrations. Accordingly, heterotrophs from deeper waters, which consume phytoplanktonic detritus (particulate organic carbon; POC) settling rapidly through the water column, also mirror young surface water  $\text{DI}^{14}\text{C}$  concentrations, although the ambient seawater DIC is likely to have different  $^{14}\text{C}$  concentrations (Wang et al., 1998; Wang et al., 1996). Oceanic POC, however, does not generally show homogenous  $^{14}\text{C}$  concentrations, as it might also include old organic carbon (OC), such as terrestrial OC or adsorbed dissolved organic carbon (DOC) (Druffel et al., 1986). Deep ocean  $\text{DO}^{14}\text{C}$  has been shown to be significantly older (~6,400 years) than  $\text{DI}^{14}\text{C}$ , most likely due to recycling during deep water transit (Bauer et al., 1992; Druffel et al., 1992; Williams and Druffel, 1987). Heterotrophs utilizing POC and/or DOC will hence reflect the respective, probably low,  $^{14}\text{C}$  concentrations. Besides photosynthesis, chemosynthesis is a further pathway of primary production. Although chemosynthesis constitutes only minor amounts of carbon to primary production (<1%), it is of great importance for carbon fixation in some extreme environments, e.g., hydrothermal vents, cold seeps, or hot springs (Falkowski, 2003). Instead of seawater  $\text{DI}^{14}\text{C}$  uptake, marine chemosynthetic prokaryotes rely on different substrates, for example hydrogen ( $\text{H}_2$ ) or methane ( $\text{CH}_4$ ). Methane-oxidizing archaea building consortia with sulphate-reducing bacteria consume  $\text{CH}_4$  to produce biomass, a process that is termed anaerobic oxidation of methane (AOM) (Strous and Jetten, 2004; Valentine, 2002). The  $^{14}\text{CH}_4$  utilized to perform AOM is likely to be derived from remineralized fossil organic matter or gas seepage and thus have a low or unmeasurable  $^{14}\text{C}$  concentration (the latter is referred to as being radiocarbon dead, i.e. >50,000 years old) (Kessler et al., 2005; Pearson et al., 2005). The methanotrophs incorporate the low  $^{14}\text{C}$  concentrations of the substrate  $^{14}\text{CH}_4$  into their biomass and consequently appear to be old or radiocarbon dead.

Therefore, the substrate  $^{14}\text{C}$  concentrations taken up by photo- and chemosynthesis have to be known and considered when interpreting radiocarbon data. However, the incorporation of fossil radiocarbon can also be used to trace carbon assimilation to help identify substrates used for the production of organic biomass (Hansman et al., 2009; Ingalls et al., 2006; Pearson et al., 2005; Petsch et al., 2001; Rethemeyer et al., 2004).

In general, exchange processes between the atmosphere, biosphere, and hydrosphere are quick enough (compared to the half life of  $^{14}\text{C}$ ) to result in a dynamic equilibrium between  $^{14}\text{C}$  production and decay, displayed by a constant  $^{14}\text{C}/^{12}\text{C}$  ratio. As soon as these exchange processes stop by, e.g., the death of an organism,  $^{14}\text{C}$  incorporated into its biomass starts to decay to atomic nitrogen, through the emission of  $\beta$ -particles and antineutrinos with a half-life of 5,730 years, which reduces the residual  $^{14}\text{C}$  concentration. Thus, measuring the remaining  $^{14}\text{C}$  concentration of a carbon-containing sample and comparing it to the  $^{14}\text{C}$  concentration at the time of its formation, which is achieved by comparison with a standard material, can provide an age of the sample.

### 1.1.2 MEASURING RADIOCARBON

The radiocarbon dating method was introduced by W. Libby in 1949. At that time  $^{14}\text{C}$  concentrations were determined by measuring in situ radioactive decay through the counting of  $\beta$ -particles using liquid scintillation or proportional gas counters (Arnold and Libby, 1949; Willkomm, 1976). Since the late 1970s radiocarbon abundances in a sample have been measured directly using accelerator mass spectrometry (AMS). The advantage of AMS dating in comparison to conventional methods is its rapidity (hours rather than days) and the very high sensitivity, which have reduced the amount of sample required by three orders of magnitude and have recently allowed samples of less than 1 mg, or even as low as 5–25  $\mu\text{g}$  to be dated (Pearson et al., 1998; Santos et al., 2007; Shah and Pearson, 2007).

The principles of Accelerator Mass Spectrometry will be explained following the configuration of the 2.5 MV tandem accelerator of the National Ocean Sciences Accelerator Mass Spectrometry Facility (NOSAMS) at Woods Hole Oceanographic Institution (WHOI), where most of the compound-specific radiocarbon data reported in this thesis were measured.

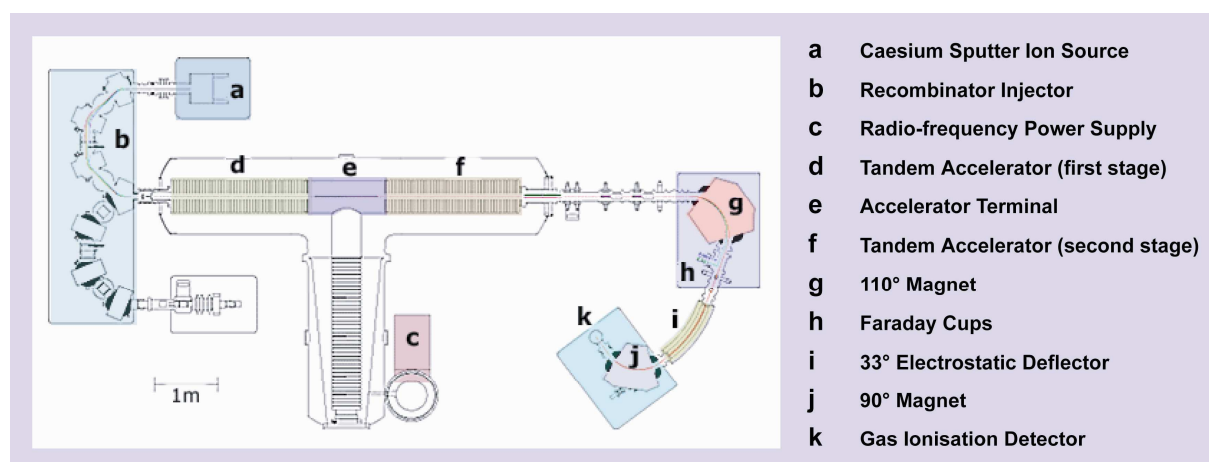


Figure 1.3 Schematic diagram of the NOSAMS tandemron AMS system (figure from NOSAMS, 2009a; modified).

For  $^{14}\text{C}$  measurements by AMS at NOSAMS, carbon has to be converted into graphite by reduction in excess hydrogen using iron (or cobalt) as catalyst. The iron-graphite mixture is then pressed into aluminium target cartridges, which are placed in a carousel and loaded into the AMS ion source (a in [Figure 1.3](#)). In the ion source the graphite is sputtered with heated caesium ions producing a negative ion beam, which consists of  $^{12}\text{C}^-$ ,  $^{13}\text{C}^-$ , and  $^{14}\text{C}^-$  and further elemental and molecular ions, but discriminates against  $^{14}\text{N}$ , the most abundant element with an atomic mass of 14, which does not form stable negative ions. The ion beam is produced at 40 kV and kept in vacuum before passing through a recombillator unit (b in [Figure 1.3](#)), which consists of an assembly of four magnets and two electrostatic lenses that split the negative ions according to their atomic masses 12, 13, and 14, remove other unwanted masses, and finally recombine the carbon ions for the accelerator. Inside the tandem accelerator the ion beam becomes accelerated to  $\sim$ 5,800 km/s (d in [Figure 1.3](#)) towards the accelerator terminal (e in [Figure 1.3](#)), which is at 2.5 mV, resulting in the ion beam gaining a kinetic energy of 2.5 meV. Here, the ion beam passes an electron stripper, a canal filled with argon gas in which the ion beam collides with argon atoms. These collisions remove 4 valence electrons from each of the carbon ions, thus, charging them positively ( $^{12}\text{C}^{3+}$ ,  $^{13}\text{C}^{3+}$  and  $^{14}\text{C}^{3+}$ ) whereby isobars with the atomic mass 14 ( $^{12}\text{CH}$ ,  $^{12}\text{CH}_2$ , and  $^{13}\text{CH}$  ions) are destroyed. Emerging from the electron stripper the  $^{12}\text{C}^{3+}$ ,  $^{13}\text{C}^{3+}$ , and  $^{14}\text{C}^{3+}$  ions are accelerated to a velocity of  $\sim$ 11,600 km/s (f in [Figure 1.3](#)) to produce a final kinetic energy of about 10 meV. Afterwards, a  $110^\circ$  magnet (g in [Figure 1.3](#)) separates the ion beam into three isotope beams by deflection according to atomic masses. The  $^{12}\text{C}$  and  $^{13}\text{C}$  stable isotope beams are collected in Faraday cups (h in [Figure 1.3](#)), whereas the  $^{14}\text{C}$  beam passes through a further  $33^\circ$  electrostatic deflector (i in [Figure 1.3](#)), removing ions with the wrong energy/charge ratio, and a  $90^\circ$  magnet (j in [Figure 1.3](#)), removing ions with the wrong momentum. Finally, the  $^{14}\text{C}$  ions are collected in a gas ionisation detector (k in [Figure 1.3](#)). The ratio of the relative abundances of the  $^{14}\text{C}$  particles detected in the ionisation detector and the  $^{12}\text{C}$  and  $^{13}\text{C}$  particles detected in the Faraday cups is compared with the frequently measured  $^{14}\text{C}/^{12}\text{C}$  and  $^{13}\text{C}/^{12}\text{C}$  ratios of a reference standard to report final AMS  $^{14}\text{C}$  concentrations (NOSAMS, 2008).

Currently, the AMS sensitivity limits radiocarbon dating to approximately 10 half lives or 60,000 yrs BP for sample sizes of 1 mg graphite (NOSAMS, 2008).

### 1.1.3 REPORTING RADIOCARBON DATA

As described above,  $^{14}\text{C}/^{12}\text{C}$  or  $^{14}\text{C}/^{13}\text{C}$  ratios of a sample measured by AMS ( $^{14}\text{C}/^{12}\text{C}$  ratio at NOSAMS) are expressed relative to the respective ratio of a reference standard reported as *fraction modern carbon* (fMC)

$$\text{fMC} = \left( \frac{^{14}\text{C}/^{12}\text{C}_{\text{sample}}}{^{14}\text{C}/^{12}\text{C}_{\text{standard}}} \right) \quad (1.1)$$

or, alternatively, *percent modern carbon* defined as,

$$\text{pMC} = \left( \frac{^{14}\text{C}/^{12}\text{C}_{\text{sample}}}{^{14}\text{C}/^{12}\text{C}_{\text{standard}}} \right) 100 \quad (1.2)$$

(NOSAMS, 2008; Stuiver and Polach, 1977). To account for isotopic fractionation the  $^{14}\text{C}/^{12}\text{C}$  ratio of the sample is normalized to a  $\delta^{13}\text{C}$  of  $-25\text{\textperthousand}$  relative to the Vienna PeeDee Belemnite (PDB), which is equivalent to the  $^{13}\text{C}$  isotopic composition of terrestrial wood. This correction is as follows,

$$^{14}\text{C}/^{12}\text{C}_{\text{sample}, \delta^{13}\text{C}} = ^{14}\text{C}/^{12}\text{C}_{\text{sample}} \cdot \left( \frac{(1 - 25/1000)}{(1 + \delta^{13}\text{C}/1000)} \right)^2 \quad (1.3)$$

This isotopic correction allows samples from different environments to be compared (Stuiver and Polach, 1977).

Likewise, the *modern* standard  $^{14}\text{C}/^{12}\text{C}$  ratio, the international reference for reporting  $^{14}\text{C}$  data agreed upon and defined as 95% of the activity of the NBS oxalic acid I standard\* in the year 1950 (the year which all radiocarbon ages are referred to, termed *present*), is normalized to a  $\delta^{13}\text{C}_{\text{VPDB}}$  value of  $-19\text{\textperthousand}$  (Stuiver and Polach, 1977). This isotopic correction adjusts the international reference standard to the value of pre-industrial wood in the year 1890 (an atmospheric  $^{14}\text{C}/^{12}\text{C}$  ratio of  $1.176 \times 10^{-12}$ ), containing no fossil fuel-derived carbon (Karlén et al., 1968), and can be mathematically expressed as,

$$^{14}\text{C}/^{12}\text{C}_{\text{standard}, \delta^{13}\text{C}} = 0.95 \cdot ^{14}\text{C}/^{12}\text{C}_{\text{standard}} \cdot \left( \frac{(1 - 19/1000)}{(1 + \delta^{13}\text{C}/1000)} \right)^2 \quad (1.4)$$

The reported fMC is further corrected for processing blanks, the addition of isotopically unknown C, in the AMS laboratory as well as for the statistical uncertainty of the AMS measurement. The respective fMC error is calculated using the larger of either an internal statistical error (counting statistics) or an external error (reproducibility of

---

\* the original National Bureau of Standards oxalic acid I standard was followed by the International Atomic Energy Agency oxalic acid II standard, which is in use today and is directly related to the oxalic acid I standard.

several measurements of each sample). Blank determination and correction for, e.g., chemical preparation should be applied independently.

As well as in terms of fMC, radiocarbon data might also be reported using the  $\Delta^{14}\text{C}$  notation. The  $\Delta^{14}\text{C}$  value corrects the fMC for the radioactive decay that took place between the year of sample collection and the year of the AMS measurement (y), and is defined as,

$$\Delta^{14}\text{C} = \left( \frac{\text{fMC}}{e^{\lambda(y-1950)}} - 1 \right) 1000\text{\textperthousand} \quad (1.5)$$

where  $\lambda$  is  $1/8267 \text{ yr}^{-1}$  (8,267 years being the mean life of  $^{14}\text{C}$  according to its half life of 5,730 years). This correction will always yield the same calculated  $\Delta^{14}\text{C}$  result for measurements of the same sample, even if they are made at different times.

If the true sample age is known (e.g., by comparison with tree rings or varve counting),  $\Delta^{14}\text{C}$  can be corrected for the decay between the year of sample death (x) and the year of the AMS measurement (y), using

$$\Delta^{14}\text{C} = (\text{fMC} \cdot e^{\lambda(1950-x)} - 1) 1000\text{\textperthousand} \quad (1.6)$$

to calculate the  $\Delta^{14}\text{C}$  value the sample had at the time of death or cessation of isotopic exchange with the atmosphere.

The radiocarbon age calculation, referred to as *conventional radiocarbon age* (t), is defined as,

$$t = -8033 \cdot \ln(\text{fMC}) \quad (1.7)$$

Underlying this equation is one basic assumption: the production of atmospheric  $^{14}\text{C}$  is assumed to have been constant throughout the past 100,000 years and equals the absolute international standard  $^{14}\text{C}/^{12}\text{C}$  ratio of  $1.176 \times 10^{-12}$ . Furthermore, the "incorrect" Libby half life of 5,568 years (mean life 8,033 years) is used to ensure that radiocarbon ages measured before the year 1962, when the true half life was determined (Godwin, 1962), can be compared with those of later measurements. Every conventional radiocarbon age is referred to the year 1950, which equals 0 years BP. Thus, for samples originating after 1950 a conventional radiocarbon age cannot be determined, they are termed >modern (Stuiver and Polach, 1977). As per convention, conventional radiocarbon ages are rounded off ([Table 1.1](#)).

Age	Nearest	Age Error	Nearest
<1000	5	<100	5
1000-9999	10	100-1000	10
10000-20000	50	>1000	100
>20000	100		

Table 1.1 Rounding off convention for conventional radiocarbon ages as reported by NOSAMS.

Conventional radiocarbon ages cannot be directly converted into calendar ages. This is because the basic assumption for conversion of  $^{14}\text{C}$  concentrations into conventional radiocarbon age – a constant atmospheric  $^{14}\text{C}$  production – is not fulfilled in nature. Atmospheric  $^{14}\text{C}$  concentrations are continuously fluctuating naturally as a result of the solar sunspot cycle and variations in the Earth's magnetic field intensity, which cause changes in the cosmic ray fluxes or among the active carbon reservoirs, e.g., controlled by deep ocean ventilation changes (e.g., Bard, 1998; Beck et al., 2001; Damon et al., 1978; Edwards et al., 1993; Goslar et al., 1995; Hughen et al., 2004a; Hughen et al., 1998; Mazaad et al., 1991; Stuiver et al., 1991; Stuiver and Quay, 1980; Suess, 1986). In addition to natural anomalies of atmospheric  $^{14}\text{C}$  concentrations, anthropogenic perturbations have become significant during the last  $\sim$ 150 years. Above-ground nuclear weapons testing, starting in 1945, caused the *modern* atmospheric  $^{14}\text{C}/^{12}\text{C}$  concentration in the northern hemisphere to almost double during the 1950s and 1960s (Figure 1.4) (Damon et al., 1978; Levin et al., 1985; Nydal and Lövseth, 1983).

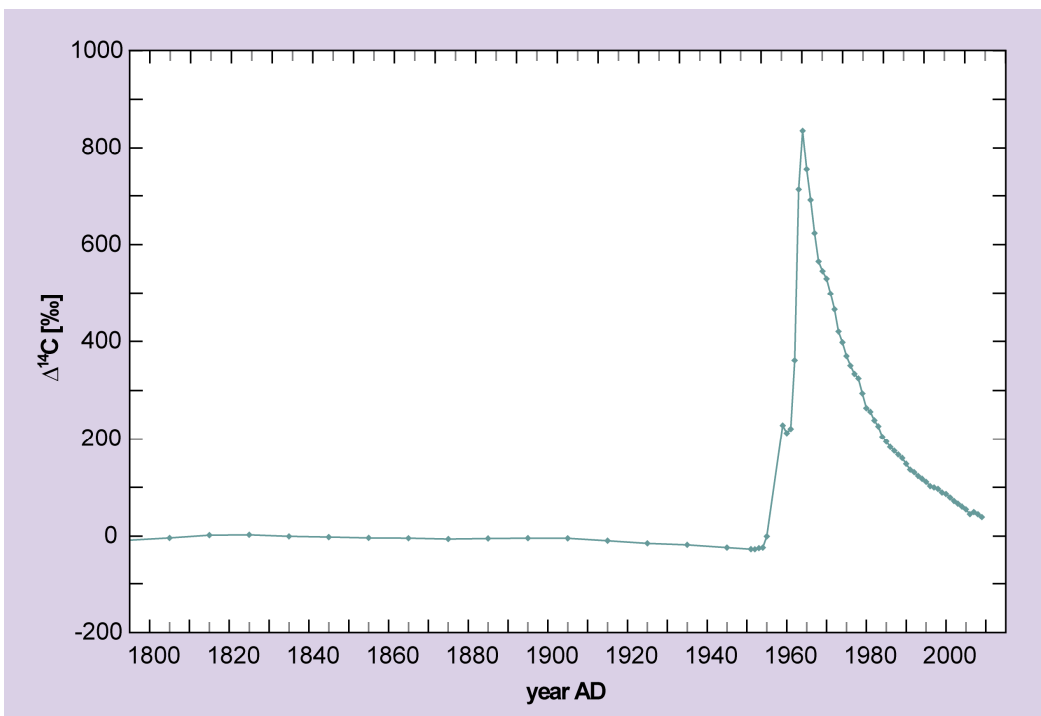
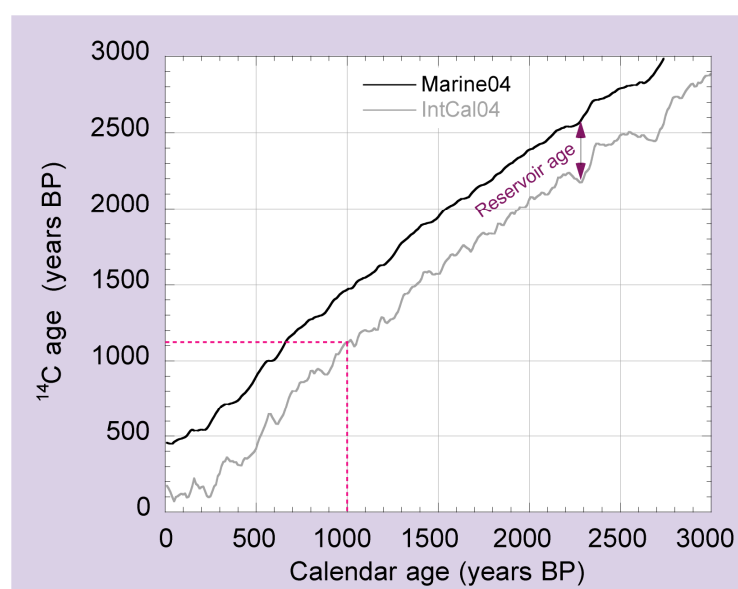


Figure 1.4 Atmospheric  $^{14}\text{CO}_2$  concentrations ( $\Delta^{14}\text{C}$ ) for the time period AD1795-2009 (data from Levin et al., 2008; Levin and Kromer, 1997; Levin et al., 1985; Stuiver and Becker, 1993; I. Levin, pers. comm.).

The bomb-induced change in atmospheric  $^{14}\text{C}$  concentrations, the so-called bomb-effect, peaked in 1963 since which it has decreased due to the uptake of carbon by the biosphere and hydrosphere. Recently it has almost equilibrated back to pre-bomb values. The immense perturbation has been used in artificial global tracer experiments, allowing the residence times and transfer rates of  $^{14}\text{C}$  and  $\text{CO}_2$  within and between the carbon reservoirs to be evaluated, e.g., oceanic circulation or soil organic matter turnover rates, data which were otherwise unobtainable (Broecker et al., 1991; Damon et al., 1978; Druffel et al., 2008; Key et al., 2004; Stuiver et al., 1983; Trumbore, 2009; Trumbore et al., 1996). A second anthropogenic perturbation, the release of  $^{12}\text{CO}_2$  by fossil fuel burning (Suess-effect or Industrial effect) since the industrialization counter-acts the bomb-effect (Damon et al., 1978; Suess, 1955).

Because of the changes in atmospheric  $^{14}\text{C}$  concentrations caused by the processes described above, the reporting of true calendar ages (absolute or calibrated ages) requires conventional radiocarbon ages to be compared with other geochronological ages that have been independently derived. Independent derivations include dendrochronological counting, laminae counting of varved limnic and marine sediments, ice core chronologies or coral, lake aragonite and speleothem stalagmite  $^{230}\text{Th}$ - $^{234}\text{U}$  ages (Bard et al., 1993; Bard et al., 1990; Beck et al., 2001; Beer et al., 1988; Fairbanks et al., 2005; Friedrich et al., 2004; Goslar et al., 2000; Hughen et al., 2004b; Reimer et al., 2004a; Schramm et al., 2000; Völker et al., 2000). All these data are included in international calibration data sets such as IntCal09, Marine09 or SHcal04 (McCormac et al., 2004; Reimer et al., 2009) (Figure 1.5) and can easily be accessed using calibration programs like CALIB6.0 (Stuiver et al., 2010), which determine the probability distribution of the sample's true age.



**Figure 1.5** Clipping of the IntCal04 and Marine04 calibration curves showing the deviation between conventional  $^{14}\text{C}$  age and calendar age as derived from dendrochronologically dated tree rings, foraminifera in varved sediments or  $^{230}\text{Th}/^{234}\text{U}$ -dated corals (from Hughen et al., 2004b; modified).

Probabilities are ranked and summed to find the 68.3% ( $1\sigma$ ) and 95.4% ( $2\sigma$ ) confidence intervals, which can be reported as calibrated age ranges (for precise description of the calibrated probability distribution calculation see Stuiver et al., 2010). For post-bomb samples a calibration cannot be achieved using CALIB6.0. Since there is no international convention for reporting post-bomb radiocarbon concentrations, Reimer et al. (2004c) recommended the use of fMC as defined in equation (1) but with a new symbol  $F^{14}\text{C}$  to prevent any confusion. They provide a compiled calibration data set using the calibration program CALIBomb (Reimer et al., 2004b).

In this thesis, calibrated ages are only used when terrestrial residence times are reported or an age model or sedimentation rates are provided for a core. When radiocarbon data of samples derived from different sources (e.g., marine biomarkers and calcareous microfossils) are compared, fMC,  $\Delta^{14}\text{C}$  or conventional radiocarbon ages are used since they are corrected for isotopic fractionation and can thus be compared.

## 1.2 GEOCHEMICAL METHODS USED FOR COMPOUND-SPECIFIC RADIOCARBON ANALYSIS

Due to the limitations of the processing blanks and statistical uncertainties in radiocarbon AMS measurements, compound-specific radiocarbon dating of single biomarkers, or a class of biomarkers, aims for sample sizes containing 50 to 300  $\mu\text{g C}$ , because lower amounts increase the likelihood of blank C addition (Mollenhauer and Rethemeyer, 2009). In several AMS laboratories blank-reducing techniques for “routine” small-scale  $^{14}\text{C}$  measurements allowing sample amounts down to  $\sim 25 \mu\text{g C}$  to be analysed have been developed (Pearson et al., 1998). For even smaller sample sizes, ultra-microscale measurements of only 5 to 25  $\mu\text{g}$ , processing blanks may represent up to 40% of the sample C (Shah and Pearson, 2007), thus,  $^{14}\text{C}$  data from such samples may be inconclusive if the precise overall blank cannot be reliably accounted for.

However, compound-specific radiocarbon dating necessitates the separation of complex mixtures into single compounds in high purity. Even the purification of 25  $\mu\text{g}$  of biomarker C from marine sediments, where high resolution is highly desirable but sample availability is often limited, requires dedicated techniques, which are described below. Even after applying these techniques, solitary compound-specific radiocarbon data have to be analysed considering the overall sedimentary context to allow a reasonable interpretation of process-timescales. Thus, radiocarbon analysis of other co-occurring sediment constituents (e.g., total organic carbon or calcareous microfossils) and also knowledge of basic sedimentary parameters (e.g., % $\text{C}_{\text{org}}$ ) are required. The methods used to acquire these will also briefly be described in the context of their relevance to the interpretation of radiocarbon data.

### 1.2.1 BULK SAMPLE ANALYSIS

Radiocarbon dating of TOC has long been used as stratigraphic tool in paleoceanography. It has been shown, however, that TOC consists of a broad mixture of OC from various sources, including marine and terrestrial production (e.g., Eglinton et al., 1996) and vertical, as well as lateral, supply, rather than from the overlying water column alone (e.g., Mollenhauer et al., 2005a; Ohkouchi et al., 2002). Nevertheless, in comparison with marine biomarker or calcareous microfossil radiocarbon data, sedimentary TOC  $^{14}\text{C}$  ages allow the contribution of pre-aged material, such as that derived from the continent, to be identified.

Furthermore, elemental data, e.g.,  $\% \text{C}_{\text{org}}$  or  $\text{C}_{\text{org}}/\text{N}_{\text{total}}$  ratios help to interpret estimates of preservation, freshness of organic matter, or terrigenous and marine organic matter input (e.g., Meyers, 1994). They are also crucial for radiocarbon analysis of bulk sedimentary TOC, since the  $\% \text{C}_{\text{org}}$  needs to be known to gauge how much sample is required to yield 1 mg C for AMS analysis (NOSAMS, 2009b).

All bulk sample measurements of  $\% \text{C}_{\text{org}}$  and  $\% \text{N}_{\text{total}}$  reported in this thesis were determined using a Vario EL III Elemental Analyser (EA).

### 1.2.2 CALCAREOUS MICROFOSSIL ANALYSIS

Calcareous microfossils like planktonic or benthic foraminiferal tests and mollusc shells (e.g., bivalves) provide a good stratigraphic control parameter for compound-specific radiocarbon analysis of biomarkers. In comparison to organic matter, foraminifera are less prone to resuspension once they have reached the sediment due to their physical properties, i.e., they reside in the coarse grain-size fraction and have a high density resulting in water column sinking rates of  $\geq 100$  m to 1,000 m per day according to their shell weight (Berger and Piper, 1972; Fok-Pun and Komar, 1983; Takahashi and Be, 1984). On the contrary, organic matter is very buoyant; average phytoplankton sinking rates are on the order of  $\leq 1$  m per day (Bienfang, 1980; Bienfang, 1981) and may only be enhanced by ballast material, such as minerals, faecal pellets or TEP (transparent extrapolymeric particles) (De La Rocha and Passow, 2007). Thus, foraminifera are most likely to offer the most reliable stratigraphic tool for marine sediments, but sedimentary processes, such as bioturbation always need to be considered (*for a detailed description of processes biasing foraminiferal  $^{14}\text{C}$  ages see manuscript I*). The benefit of using planktonic rather than benthic species is that they utilize surface water DI $^{14}\text{C}$ , which has  $^{14}\text{C}$  concentrations closest to atmospheric  $^{14}\text{CO}_2$  values. Radiocarbon data for benthic foraminifera, on the other hand, have to be corrected for the local reservoir DI $^{14}\text{C}$  effect, which might be unknown. In coastal regions bivalve shells can also provide surface ocean DIC  $^{14}\text{C}$  concentrations since most species inhabit the intertidal to shallow-water benthic zone.

For radiocarbon analysis of foraminiferal  $\text{CaCO}_3$ , sediment samples are wet-sieved ( $>125 \mu\text{m}$  fraction) using tap water and hand-picked to sample single-species assemblages. Resulting foraminiferal tests may be ultrasonicated in water or 3% peroxide solution and rinsed with deionised water if they are contaminated (e.g., sediment containing different  $\text{CaCO}_3$  in and on the test). Clean foraminifera are hydrolyzed with 100%  $\text{H}_3\text{PO}_4$  in a vacuum at 60 °C to convert the carbonate of the sample into  $\text{CO}_2$  (McNichol et al., 1994). Resulting  $\text{CO}_2$  is converted into graphite for the AMS.

### 1.2.3 LIPID ANALYSIS

To prepare lipid biomarkers for compound-specific radiocarbon analysis different wet chemical techniques have to be used for the entire purification process or for basic separation before Preparative Column Gas Chromatography or preparative High Performance Liquid Chromatography can be applied.

Organics were extracted from freeze-dried sediments for most of the samples analysed in this thesis using a Soxhlet apparatus (Figure 1.6). During extraction with a Soxhlet, an organic solvent (mixture) is constantly heated in a round-bottom flask to evaporation. The solvent vapour moves up a distillation sidearm and condenses in a cooled condenser to reflux into the Soxhlet containing an extraction thimble with the sediment, thus, extracting the total lipid extract (TLE). The Soxhlet extractor empties back into the round-bottom flask through a siphon side arm at a certain filling level to rerun.

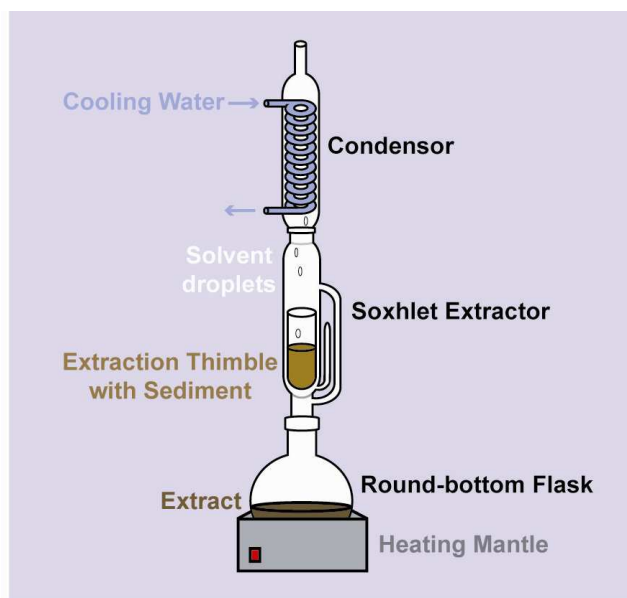


**Figure 1.6** Simplified diagram of a Soxhlet apparatus. The Soxhlet extractor is equipped with a bypass sidearm for solvent vapour ascent and a reflux siphon determining the filling level.

Beside Soxhlet extraction, extraction of some of the samples was performed using accelerated solvent extraction (ASE) (see *manuscript I*) or ultrasonication (see *manuscript III*). Further wet chemical methods used for the lipid biomarker purification in this thesis include

- saponification: applied to break ester-bound molecules of the TLE into their respective alkanoic acids (*n*-fatty acids) and *n*-alkanols,
- SiO<sub>2</sub>-column chromatography: used to separate neutral lipids into molecule groups according to polarity,
- AgNO<sub>3</sub>-silica gel column chromatography: performed to separate saturated from unsaturated molecules,
- Al<sub>2</sub>O<sub>3</sub>-column chromatography: used to separate polar from apolar molecules,
- urea adduction: undertaken to separate branched/cyclic from straight-chain molecules,
- desulfurization: applied to samples from anoxic sediments to remove sulphur-containing molecules, and
- methylation: used to substitute polar compounds like *n*-fatty acids with an apolar methyl-group amenable for Gas Chromatography.

The exact analytical procedures are described in detail in *manuscripts I, II and III*.

#### 1.2.4 GAS CHROMATOGRAPHY

During sample preparation of lipid biomarkers for compound-specific radiocarbon analysis, splits of each sample were measured on a Gas Chromatograph (GC) (Figure 1.7) equipped with a Flame Ionisation Detector (FID) in order to monitor sample purity after each analytical isolation step.

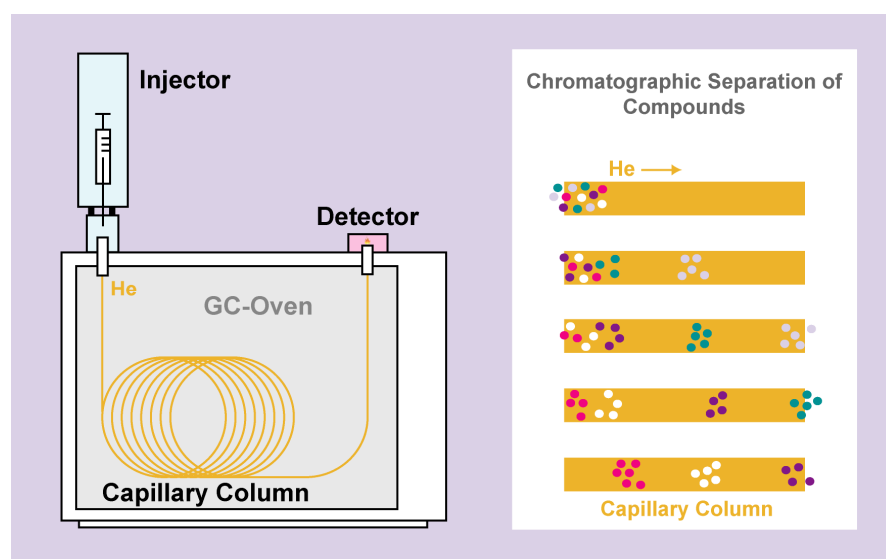


**Figure 1.7** Schematic of a Gas Chromatograph and the chromatographic separation. Compounds are separated on the chromatographic column by repeated partitioning between the mobile (e.g., He gas) and the stationary phase (e.g., silica capillary column).

Additionally, Gas Chromatography was used to access basic data, such as biomarker concentrations or Average Chain Length (ACL) and the Carbon Preference Index (CPI) for homologues series of *n*-alkanes and *n*-fatty acids. Such basic parameters help to estimate whether biomarkers concentrations in a sample are high enough to maintain compound-specific radiocarbon analysis and can help to evaluate the sources and maturity of the respective compounds (*for definition of these parameters see manuscript II*).

All GC purity checks and geochemical proxy data reported in this thesis were measured using HP5890 Series II plus GC systems equipped with both split/splitless or on-column injectors and FID.

### 1.2.5 PREPARATIVE CAPILLARY GAS CHROMATOGRAPHY

The use of a Preparative Capillary Gas Chromatograph (PCGC) for the isolation of apolar biomarkers for compound-specific radiocarbon analysis of geological samples was first demonstrated by Eglinton et al. (1996). Unlike standard GCs, a PCGC is equipped with a splitter at the end of the capillary column inside the GC oven, which allows the gaseous sample to be split between a FID and a Preparative Fraction Collector (PFC) in a ratio of about 1:99 (FID:PFC) (Figure 1.8). The PFC is equipped with capillaries linked to U-shaped sample tubes, which can either be cooled or heated and allow sufficient amounts of single compounds to be trapped in high purities according to their elution time. The PFC has to be adapted for high sample recovery for every method (*for detailed description of PCGC methods for the purification of *n*-alkanes and fatty acid methyl esters see manuscript II*).

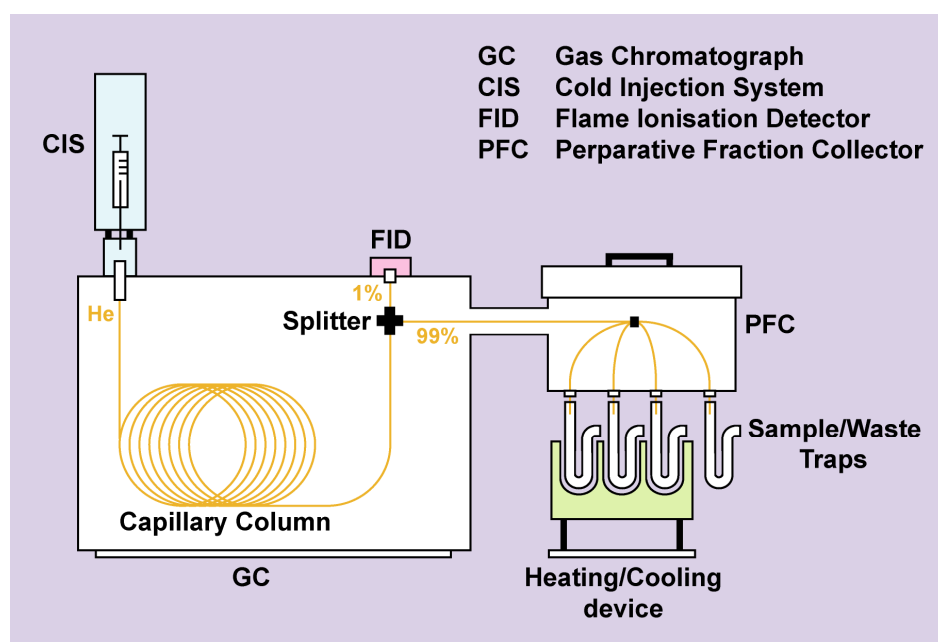


Figure 1.8 Diagram of the PCGC system used for biomarker purification in this thesis.

The huge benefit of a PCGC over wet chemical techniques is the possibility of separating compounds from homologues series according to their chain length. Such homologues series, e.g., *n*-alkanes, *n*-fatty acids or *n*-alcohols, are characterized by contributions from various sources, whereas the longer chain length homologues ( $\geq n\text{-C}_{26}$  fatty acid or  $n\text{-C}_{27}$  alkane) are mainly produced by vascular plants, thus, making them useful biomarkers to trace continental climate, for example (Eglinton and Hamilton, 1967; Eglinton and Eglinton, 2008).

Isolation of lipid biomarkers for this thesis was achieved using an Agilent 6890N GC system equipped with a Gerstel 7683 series Cold Injection System (CIS) and connected with a Gerstel PFC. Blank tests of PCGC sample purification for AMS  $^{14}\text{C}$  analysis were performed as described by Mollenhauer and Rethemeyer (2009).

### 1.2.6 HIGH PERFORMANCE LIQUID CHROMATOGRAPHY

Another method that can isolate single compounds in sufficient quantity and purity for compound-specific radiocarbon analysis is High Performance Liquid Chromatography (HPLC) equipped with a fraction collector (Figure 1.9). In contrast to a PCGC, HPLC is also amenable to polar and high molecular weight molecules, such as pigments or glycerol dialkyl glycerol tetraether (GDGTs). For these compounds either a Diode Array Detector (DAD) or a Mass Spectrometer (MS) is used for detection (*for detailed description of pigment purification using HPLC/DAD see manuscript III, for GDGT analysis using HPLC/APCI-MS see manuscript II*). The MS can be run simultaneously with the isolation process if the system is equipped with an active splitter.

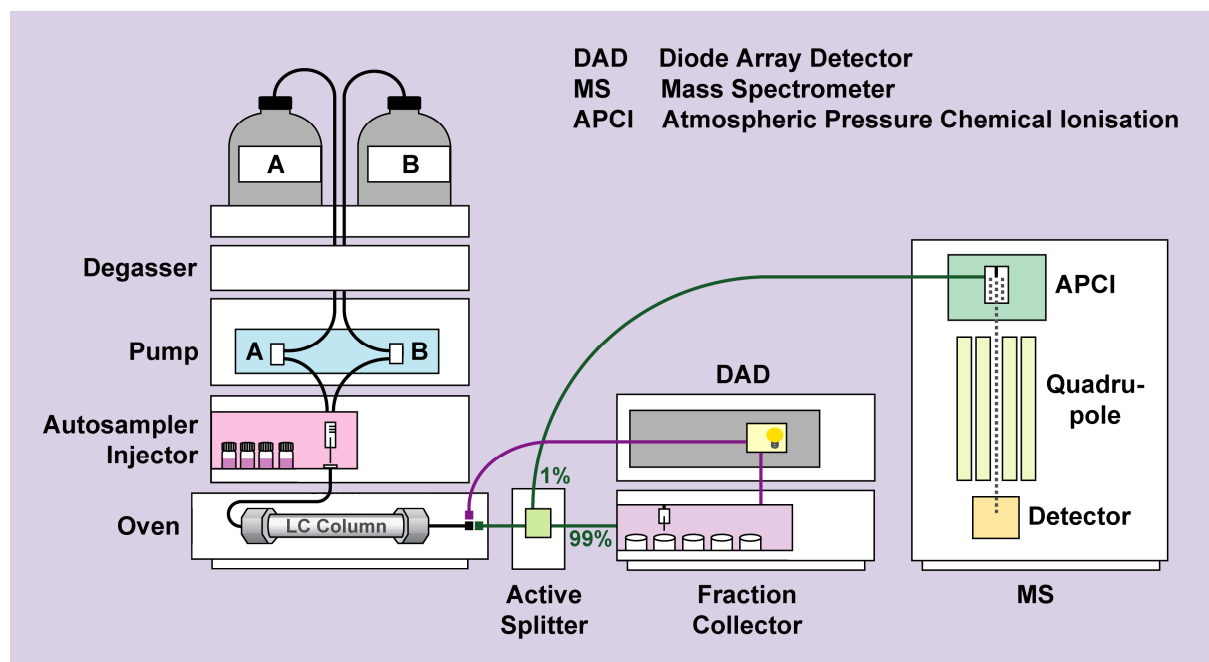


Figure 1.9 Diagram of an HPLC system suitable for either pigment purification/analysis (purple setup), or GDGT purification/analysis (green setup) as used in this thesis.

Furthermore, several new proxies ( $\text{TEX}_{86}$ , BIT, MBT/CBT), derived from GDGT analysis using HPLC methods, have recently been introduced allowing environmental conditions to be estimated, such as sea surface temperature (SST), riverine terrigenous organic matter input and continental mean annual temperatures (Hopmans et al., 2004; Schouten et al., 2002; Weijers et al., 2007). Application of such proxies (see *manuscript II* for application of the BIT-Index) can help to access additional data to aid in the interpretation of compound-specific radiocarbon data.

Pigment isolation for this thesis was conducted using an Agilent 1200 Series HPLC system equipped with a 1200 Series DAD. For GDGT analysis an Agilent 1200 Series HPLC system equipped with an Agilent 6120 Quadrupole APCI-MS was used.

### 1.2.7 ISOTOPE RATIO MASS SPECTROMETRY

Compound-specific stable isotope analysis (e.g.,  $\delta^{13}\text{C}$ ,  $\delta^{15}\text{N}$ ) provides powerful information on biomarkers used for compound-specific radiocarbon analysis. Assessment of  $\delta^{13}\text{C}$  values can help in estimating the sources of biomarkers, like marine vs. terrestrial, more specific characterization of plant type, for example the differentiation of  $\text{C}_3$ ,  $\text{C}_4$  of CAM plants (see *manuscript II*) (e.g., Collister et al., 1994; Lockheart et al., 1997; Rieley et al., 1991), or in identifying the substrates organisms feed on (Hinrichs et al., 1999; Hinrichs et al., 2000). Determination of  $\delta^{15}\text{N}$ , for example, allows the environmental conditions and nutrient species uptake to be characterized (see *manuscript III*) (e.g., Kashiyama et al., 2008a; Kashiyama et al., 2008b; Ohkouchi et al., 2006).

Systems used for stable isotope analysis of organic compounds are adapted for the specific chemical properties of the compounds measured. GC/IRMS can be used for lipid isotopic analysis, whereas EA/IRMS (Figure 1.10) is one alternative used for polar

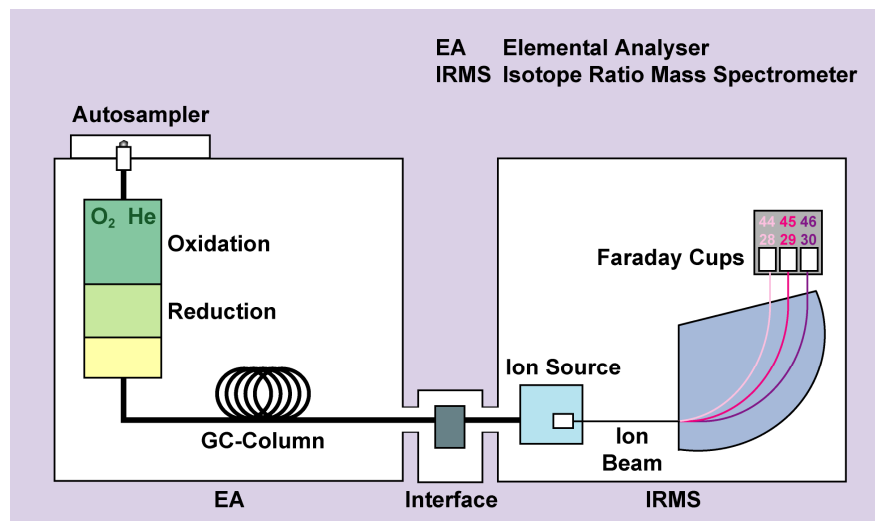


**Figure 1.10** Diagram of the EA/IRMS system used in this thesis to determine  $\delta^{13}\text{C}$  and  $\delta^{15}\text{N}$  of pigments.

molecules like pigments, since tetrapyrroles (intact pigments) are not amenable for a GC despite the fact that they are converted into their monopyrrole units (maleimides) (Chikaraishi et al., 2008). Another set-up for analysing stable isotopes of polar compounds is HPLC/IRMS.

Stable isotope analysis of lipid biomarkers in this thesis was performed using a Thermo Finnigan TRACE GC Ultra coupled to a Thermo Finnigan 252 IRMS system. The  $\delta^{13}\text{C}$  measurements on splits of CO<sub>2</sub> reported by NOSAMS were determined using a VG Optima IRMS. Pigment  $\delta^{13}\text{C}$  and  $\delta^{15}\text{N}$  values were analysed using a modified Thermo FlashEA1112 Automatic Elemental Analyser connected to a Thermo Finnigan Delta plus XP IRMS via a ConFlow IIIB Interface. Bulk sedimentary  $\delta^{13}\text{C}$  and  $\delta^{15}\text{N}$  values were analysed using a Finnigan Delta plus IRMS.

### 1.3 BIOMARKERS USED FOR COMPOUND-SPECIFIC RADIOCARBON ANALYSIS

Biomarkers are molecular fossils found in recent environmental and older geological samples with ages up to billions of years. They are taxonomically specific, which allows them to be unambiguously assigned to certain biological sources (for an overview of biomarkers see Killops and Killops, 2004; Peters et al., 2005). Biomarkers can record element cycling, sediment and water chemistry, redox conditions, and temperature histories and, consequently, they are used as proxies in Earth Sciences to provide information on early life as well as recent biogeochemical processes. Even if biomarkers become altered, they can still be linked to their precursor molecules, as first proposed by Treibs (1936). Biomarkers used for compound-specific radiocarbon dating in this thesis include alkenones, long chain *n*-alkanes, long chain *n*-alkanoic acids (*n*-fatty acids), as well as chloro- and pheopigments (Figure 1.11).

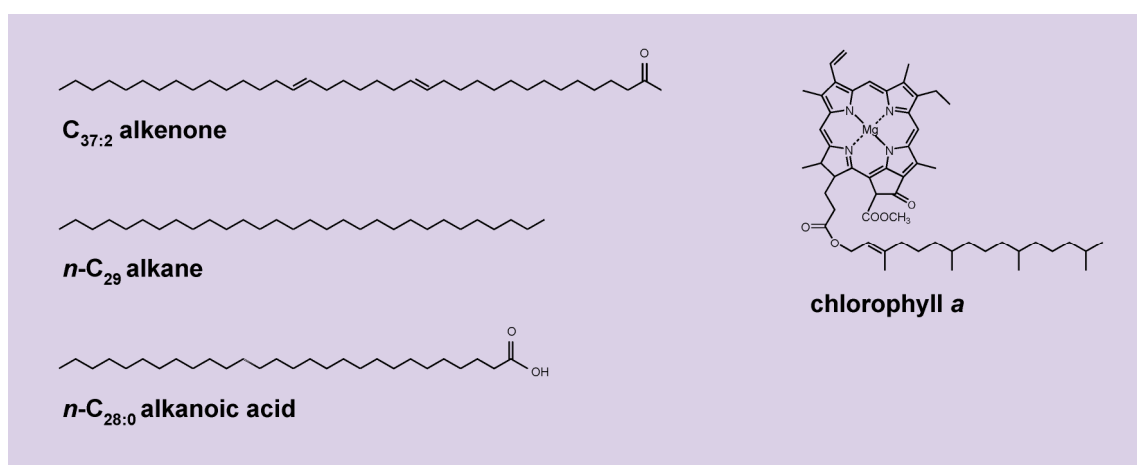


Figure 1.11 Example molecular structures of lipid and tetrapyrrole biomarkers discussed in this thesis.

Alkenones are long chain unsaturated methyl and ethyl ketones produced by a few species of haptophyte algae from the class Prymnesiophyceae, mainly the coccolithophorid *Emiliania huxleyi* (Volkman et al., 1980a). Alkenones are widely used in marine organic geochemical studies since their unsaturation changes according to the temperatures in which they grow. This relationship can be used to reconstruct paleo-sea surface temperature from marine sediments using the  $U_{37}^K$  (alkenone unsaturation) index (Brassell et al., 1986; Müller et al., 1998; Prahl and Wakeham, 1987). Furthermore, radiocarbon dating of alkenones has been shown to be a valuable tool in identifying lateral sediment transport processes (Mollenhauer et al., 2003; Mollenhauer et al., 2005a; Mollenhauer et al., 2006; Ohkouchi et al., 2002).

Long chain *n*-alkanes ( $>n\text{-C}_{27}$ ) and long chain *n*-fatty acids ( $>n\text{-C}_{26}$ ) are biomarkers that are overwhelmingly synthesized by terrestrial higher plants, where they serve as protective epicuticular waxes (Eglinton and Hamilton, 1967). These vascular plant biomarkers are commonly used in paleoenvironmental studies to reconstruct the distribution and composition of terrestrial vegetation on the continents. Their molecular and isotopic composition provides information on temperature, aridity and  $p\text{CO}_2$ , and, thus, continental climate at the time of biosynthesis (Eglinton and Eglinton, 2008).

Unlike alkenones, long chain *n*-alkanes, and long chain *n*-fatty acids, photosynthetic pigments are not restricted to either the marine or terrestrial realm, but are synthesized by virtually all photoautotrophs, since chlorophyll *a* is the major antenna pigment in the light harvesting system (Falkowski, 2003). Although these tetrapyrrole molecules cannot be directly linked to a single source, pigments found in marine sediments generally have a solely phytoplanktonic origin, since degradative processes, such as (autolytic) cell senescence, microbial or viral lysis, enzymatic or hydrolysis reactions, photo-oxidation and grazing, are too severe for terrigenous pigments to survive transport to the ocean in large quantities (Chikaraishi et al., 2007; Kashiyama et al., 2008b; Sanger, 1988). The great value of pigments, as well as their degradational products (e.g., porphyrins), is their potential as tracers of (paleo-) environmental conditions. Their stable carbon and nitrogen isotopic composition has been shown to reliably record surface ocean nutrient utilization and the respective carbon and nitrogen sources and uptake pathways (Kashiyama et al., 2008a; Kashiyama et al., 2008b; Ohkouchi et al., 2006; Ohkouchi et al., 2008).

## 1.4 MOTIVATION AND GOALS OF THIS THESIS

This thesis aims to contribute to the general understanding of the carbon cycle biogeochemistry. It focuses specifically on estimating the timescales of physicochemical and sedimentological processes affecting terrestrial and marine organic matter during exchange amongst carbon reservoirs until final burial in marine sediments. The detailed timescales of most of these carbon exchange processes are virtually unknown. Knowledge of these timescales is, however, crucial when mitigation strategies against anthropogenic perturbations of atmospheric chemistry and global climate are considered.

Compound-specific radiocarbon analysis of biomarkers from marine sediments has proven to be a powerful tool for the identification of processes that hamper immediate burial of organic matter in marine sediments, and the determination of their respective timescales. However, it requires the application of dedicated techniques that are currently performed in only a few laboratories worldwide. Hence, compound-specific radiocarbon data illuminating timescales of carbon cycle dynamics are limited. The overall goal of this thesis is to provide new insights into the temporal dynamics of carbon cycle processes within the ocean and from land to the ocean.

The specific topics addressed in the following chapters are:

### TRACING TIMESCALES OF LATERAL SEDIMENT TRANSPORT WITHIN THE OCEAN

Marine sediments represent one of the most important archives of past environmental conditions. Understanding the sedimentary record is therefore essential to gain information about past geochemical cycles. Compound-specific radiocarbon studies have revealed that organic matter in sediments is characterized by complex age structures controlled by sedimentological and diagenetic processes, which might lead to proxy decoupling and a distortion in the interpretation of paleoceanographic data. An important sedimentological process is lateral sediment transport occurring in the water column, both, prior to initial deposition and following advection and resuspension from surface sediments. Lateral sediment transport can be identified and quantified using  $^{230}\text{Th}$  normalization. However, this method does not provide insights into the temporal dynamics and, moreover, conclusions reached using it in studies on the Eastern Equatorial Pacific, one of the key areas on Earth for understanding the role of physical and biological interactions related to climate change, have recently been questioned. **Chapter 2** contributes to this on-going debate, using radiocarbon analysis of alkenones, total organic carbon and foraminifera to assess lateral sediment transport, determine its timescales, and estimate its effect on proxy records from the Panama Basin.

## TRACING TERRESTRIAL RESIDENCE TIMES FROM MARINE SEDIMENTS

Terrestrial organic matter transported to the ocean via riverine and aeolian mechanisms can contribute to marine sediments, thus, allowing past continental climate to be reconstructed. Before becoming delivered to the oceans, however, terrestrial organic matter can be retained in continental reservoirs such as soils on multi-annual to multi-millennial timescales. Accordingly, vascular plant biomarker-based climate reconstructions can be prone to temporal offsets, which are most critical when coupling continental and marine environmental histories or investigating rapid climatic changes. Deciphering average terrestrial residence times of certain biomarkers can be achieved using compound-specific radiocarbon analysis. Even so, the controlling factors determining terrestrial turnover still cannot be satisfactorily identified. Knowledge of these factors is essential to help evaluate the potential for temporal offsets in paleo-studies based on terrigenous biomarkers. Therefore, **Chapter 3** aims to identify the controlling parameters determining average terrestrial residence times for different river drainage areas of the Black Sea catchment using radiocarbon analysis of long chain *n*-alkanes, *n*-fatty acids and total organic carbon.

## TRACING PRESERVATIONAL TIMESCALES IN THE OCEAN

Only a minor amount of organic matter produced in surface waters or transported from land to the ocean is ultimately buried in marine sediments. Most of the organic matter is remineralized within the water column, the sediment-water interface, and the uppermost sediment layer. Prior to complete remineralisation, diagenetic processes can alter the chemical structure of a molecule through the preferential loss of functional groups, transforming it into a different compound. The timescales of such diagenetic degradation have been determined mostly via concentration-based assessments of degradation rate constants, from which the potential for preservation can be inferred. Such estimates, however, imply linear preservation and homogenous age structures and do not consider the true ages inherent to the compounds. These ages are likely to have been affected by preferential preservation or degradation, which are specific to local small-scale environmental conditions and varying input sources. To assess such influences and their effect on the sedimentary record, **Chapter 4** shows results from the first application of compound-specific radiocarbon analysis to tetrapyrrole molecules, which are diagenetically altered in multiple ways and temporal dimensions. Decompositional timescales are obtained from the preserved radiocarbon concentrations of chlorophyll *a* and its successive pheopigments under different environmental conditions (NW Black Sea shelf).



## 2. MANUSCRIPT I

### Timescales of lateral sediment transport in the Panama Basin as revealed by compound-specific radiocarbon ages of alkenones, total organic carbon and foraminifera

Stephanie KUSCH<sup>1,2</sup>, Timothy I. EGLINTON<sup>3</sup>, Alan C. MIX<sup>4</sup>, Gesine MOLLENHAUER<sup>1,2</sup>

1 Alfred-Wegener-Institut für Polar- und Meeresforschung, Am Handelshafen 12, 27570 Bremerhaven, Germany

2 Fachbereich Geowissenschaften, Universität Bremen, Klagenfurter Str., 28359 Bremen, Germany

3 Department of Marine Chemistry and Geochemistry, Woods Hole Oceanographic Institution, Woods Hole, Massachusetts 02543, USA

4 College of Ocean and Atmospheric Sciences, Oregon State University, Corvallis, Oregon 97331, USA

**published in Earth and Planetary Science Letters, 290, 340-350  
doi: 10.1016/j.epsl.2009.12.030**

---

#### Abstract

Paired radiocarbon measurements on haptophyte biomarkers (alkenones) and on co-occurring tests of planktic foraminifera (*Neogloboquadrina dutertrei* and *Globogerinoides sacculifer*) from late glacial to Holocene sediments at core locations ME0005-24JC, Y69-71P, and MC16 from the south-western and central Panama Basin indicate no significant addition of pre-aged alkenones by lateral advection. The strong temporal correspondence between alkenones, foraminifera and total organic carbon (TOC) also implies negligible contributions of aged terrigenous material. Considering controversial evidence for sediment redistribution in previous studies of these sites, our data imply that the laterally supplied material cannot stem from remobilization of substantially aged sediments. Transport, if any, requires syn-depositional nepheloid layer transport and redistribution of low-density or fine-grained components within decades of particle formation. Such rapid and local transport minimizes the potential for temporal decoupling of proxies residing in different grain size fractions and thus facilitates comparison of various proxies for paleoceanographic reconstructions in this study area. Anomalously old foraminiferal tests from a glacial depth interval of core Y69-71P may result from episodic spillover of fast bottom currents across the Carnegie Ridge transporting foraminiferal sands towards the north.

---

## 2.1 INTRODUCTION

The Equatorial Pacific plays a major role in the global carbon and nitrogen cycle via oceanic biological productivity and ocean-atmosphere gas exchange (Chavez and Barber, 1987; Pennington et al., 2006). Regionally high primary productivity is maintained by upwelling along the equatorial divergence (Kessler, 2006; Wyrtki, 1967), pumping organic carbon to the deep sea. However, the Equatorial Pacific is presently a net source of CO<sub>2</sub> to the atmosphere since its major nutrients are not fully consumed perhaps due to iron limitation (Behrenfeld et al. 1996; Kolber et al. 1994). Understanding the climate history of this region is important for understanding the interaction of physical and biological processes related to climate change.

The Panama Basin has been intensively studied for its climate and paleoproductivity history over glacial-interglacial timescales based on a wide range of proxies (Loubere, 1999; Loubere, 2000; Loubere et al., 2003; Loubere et al., 2004; Loubere and Richaud, 2007; Lyle et al., 2002; Lyle et al., 2005; Lyle et al., 2007; Martinez et al., 2006; Paytan et al., 1996; Pedersen, 1983; Pisias and Mix, 1997; Sarnthein et al., 1988). A conflict has emerged in terms of the past sedimentation dynamics of this region. Accumulation rates of sedimentary constituents related to marine productivity and vertical carbon export (e.g., organic carbon, calcium carbonate or barite) indicate higher glacial export rates compared to interglacials (Lyle et al., 2002; Paytan et al., 1996; Pedersen, 1983; Sarnthein et al., 1988), whereas proxies normalized to a “constant flux” proxy (i.e. <sup>230</sup>Thorium<sub>excess</sub>) (Loubere, 1999; Loubere, 2000; Loubere et al., 2003; Loubere et al., 2004) and faunal assemblages (Loubere, 1999; Martinez et al., 2006) imply constant or reduced glacial productivity. The latter findings imply lateral particle transport and sediment focusing processes play an important role in this region. Such transport might also account for conflicts among paleoceanographic proxies carried in different grain-size fractions (Mix, 2006).

Moore et al. (1973) demonstrated that the distribution of biogenic sediments (carbonate and opal) in the Panama Basin does not match the pattern which should be derived from the overlying primary productivity, and inferred winnowing and lateral transport of fine-grained material. Using textural analysis Van Andel (1973) estimated that winnowed fine-grained material from the surrounding volcanic ridges contributes at least 40-50% of total sediment accumulation in the Panama Basin. Honjo (1982) showed that the lithogenic fraction in sediment traps at 3560 m depth was several times higher than the corresponding fraction from 890 and 2590 m depth, implying that a major fraction of the lithogenic particles reaching the deep Panama Basin did not originate from overlying surface waters. A combined photo-optical and sediment trap approach reveals that marine snow abundances cannot account for the particle fluxes collected by traps, requiring resuspension from the sediment water interface and subsequent lateral transport (Asper et al., 1992).

Radiocarbon measurements of seawater dissolved inorganic carbon (DIC), particulate inorganic and organic carbon (PIC and POC) from different water depths as well as sediment fluff inorganic and organic carbon (SIC and SOC) require a source of old carbon in the deep water, which is at least partly derived from resuspended sediment (Druffel et al. 1998).

Using the  $^{230}\text{Th}$  normalization method, several authors suggested that the sediment accumulation maxima observed in glacial sediments from the Panama Basin might be an artifact resulting from lateral supply rather than paleoproductivity (Kienast et al., 2007; Loubere et al., 2004; Marcantonio et al., 2001). Kienast et al. (2007) report  $^{230}\text{Thorium}_{\text{excess}}$  ( $^{230}\text{Th}_{\text{xs}}$ ) derived focusing factors ( $\Psi$ ) for cores from the Panama Basin as high as  $\Psi=7.5$ , implying substantial contribution of laterally supplied sediment. Nevertheless, the applicability of  $^{230}\text{Th}$  method in the Equatorial Pacific and particularly in the Panama Basin remains a subject of debate (Broecker, 2008; Francois et al., 2007; Kienast et al., 2007; Lyle et al., 2005; Lyle et al., 2007; Siddall et al., 2008).

Comparison of radiocarbon ages of molecular fossils of marine phytoplankton such as the haptophyte-derived alkenones with those of co-occurring calcareous microfossils of planktic foraminifera can independently be used to identify aged allochthonous material supplied via lateral sediment transport processes (Mollenhauer et al., 2003; Ohkouchi et al., 2002). Organic matter is associated with the low-density fraction and is prone to resuspension. Critical shear velocities for resuspension of phytodetritus range from 0.4 to 0.9 cm/s (Beaulieu, 2002; Thomsen and Gust, 2000), considerably less than the critical shear velocities of >1.2 cm/s needed to resuspend foraminifera of ~200-400  $\mu\text{m}$  diameter (assuming the physical properties of sand) (Ziervogel and Bohling, 2003). Thus transport of particles by currents can lead to significant spatial and also temporal offsets between organic matter (alkenones and TOC) and co-occurring foraminifera.

Ohkouchi et al. (2002) reported radiocarbon age offsets of up to 7000  $^{14}\text{C}$  years between alkenones and planktic foraminifera from identical sediment depth intervals from the Bermuda Rise. They concluded that alkenones were originally deposited at the Canadian Margin where they had been resuspended and transported to the Bermuda Rise. Similar processes were identified by Mollenhauer et al. (2003) for the Benguela upwelling area. Alkenones were found to be approximately 2500  $^{14}\text{C}$  years older than co-occurring planktic foraminifera, which was interpreted as the result of continuous cycles of resuspension and redeposition of particles originating from the inner shelf off Namibia.

The lateral displacement of sediment constituents associated with different grain-size classes, however, does not necessarily lead to a temporal offset in their radiocarbon contents. Mollenhauer et al. (2006) showed combined  $^{14}\text{C}$  and  $^{230}\text{Th}_{\text{xs}}$  data for the Argentine Basin. In this region, independent evidence exists for lateral displacement of alkenone-bearing particles (Benthien and Müller, 2000; Röhleman and Butzin, 2006).

While  $^{230}\text{Th}_{\text{xs}}$  derived focusing factors indicate lateral transport, radiocarbon ages of alkenones and foraminifera were similar, implying that lateral advection in the Argentine Basin occurs rapidly after sedimentation, and moves essentially modern material (Mollenhauer et al., 2006).

Here we present radiocarbon data for planktic foraminiferal carbonate, total organic carbon (TOC) and alkenones for three cores in the Panama Basin. The good age agreement between most of these different sediment constituents suggest minimal supply of pre-aged organic material of either marine or terrigenous origin. Considering the multiple lines of evidence for occurrence of lateral sediment transport in the Panama Basin, we conclude that lateral transport of the easily-resuspendable, low-density sediment fraction occurs syn-depositionally.

## 2.2 STUDY AREA

The Panama Basin is located in the Eastern Equatorial Pacific off the coast of Central America and northwestern Southern America ([Figure 2.1](#)). It is relatively isolated from the (Central) Equatorial Pacific by the volcanic Cocos and Carnegie Ridges on the north and south, respectively, and the Galapagos Platform in the west. Underlying the equatorial divergence upwelling region, high rates of primary productivity result in high biogenic particle export from the surface waters to the seafloor. The productivity in the euphotic zone above the Southern Panama Basin is estimated at  $\sim 600 \text{mg C/m}^2/\text{day}$  with a biomass of approximately  $0.5 \text{ mg Chl/m}^3$ . The productivity in the Central Panama Basin is less pronounced at  $\sim 300-400 \text{mg C/m}^2/\text{day}$  and  $\sim 0.3 \text{mg Chl/m}^3$  biomass (Behrenfeld and Falkowski 1997; Moore et al., 1973; Pennington et al., 2006; <http://giovanni.gsfc.nasa.gov> (2002-2008)).

The Panama Basin area is influenced by bottom currents from the Peru Basin, entering through the Ecuador Trench with a sill depth of 2920 m. Water masses disperse north- and westward off northern Ecuador and penetrate into the SW Panama Basin south of the Malpelo Ridge where they spread to the north and the south (Laird, 1971; Lonsdale, 1977). An additional inflow-passage into the Panama Basin exists across the central saddle of the Carnegie Ridge located between  $85^\circ$  and  $86^\circ\text{W}$  with a sill depth of 2330 m. Here, an outcrop of the acoustic basement indicates erosion (or non-deposition) of sediment which is up to 400 m thick on the adjacent ridge flanks (Lonsdale, 1977; Malfait and Van Andel, 1980). Erosional valleys up to 400 m deep continue from the saddle incision down the northern flank of the Carnegie Ridge. Temperature profiles within the Panama Basin imply that episodic spillover is more likely than a constant flow across the Carnegie Ridge. The cause and frequency of these spillover events is unknown and reliable hydrographic data is lacking (Lonsdale, 1977).

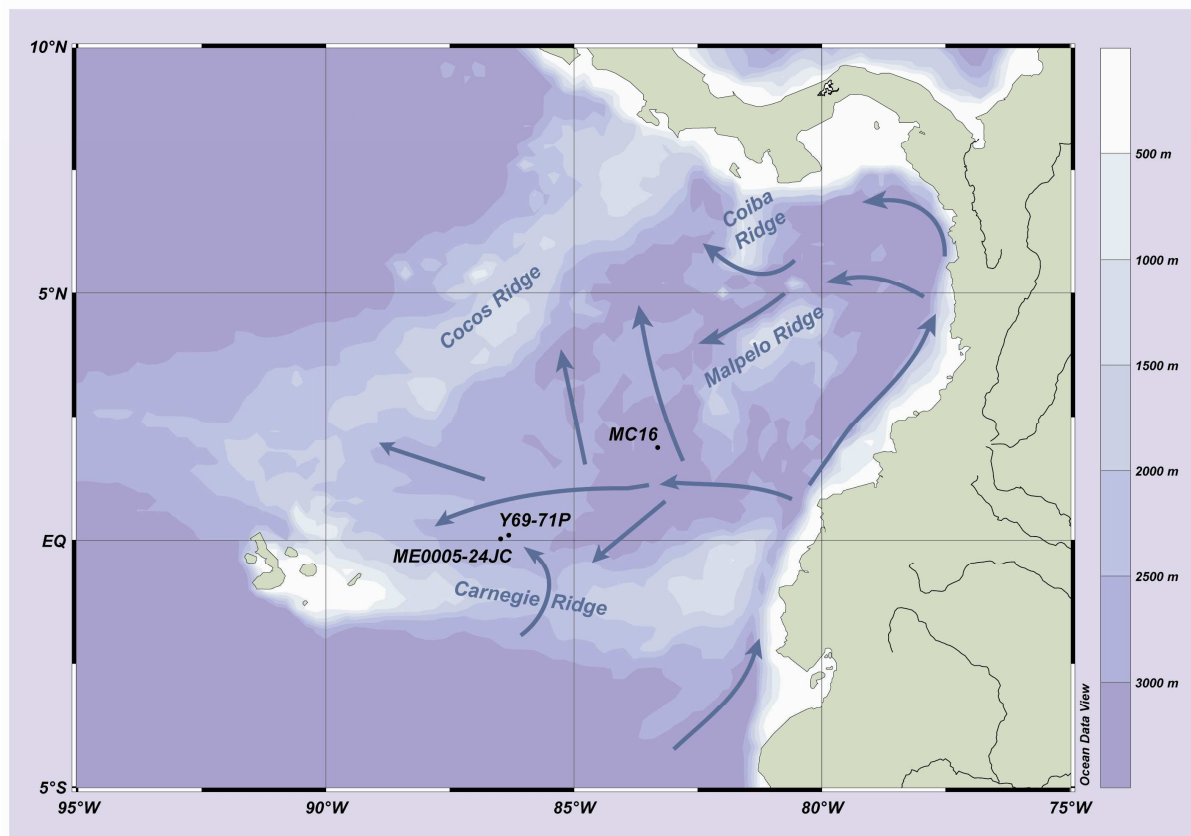


Figure 2.1 Study area and core locations. Grey arrows indicate flow directions of bottom currents.

### 2.3 MATERIALS AND METHODS

We used deep-sea sediment cores from three locations in the Panama Basin (Table 2.1). Core ME0005A-24JC was taken during R/V *Melville* cruise ME0005A in 2000, while the neighboring core Y69-71P was taken in 1969 on board R/V *Yaquina* during cruise YALOC69. Both cores were retrieved just north of the Carnegie Ridge in an area of abyssal hills, which is part of a narrow east-west trending trough (Figure 2.1). Y69-71P was collected mid-slope, while ME0005A-24JC was taken within an adjacent but separate abyssal valley about 10km south of Y69-71P. Samples of 110-136 g wet weight were taken from core intervals spanning approximately 5 cm and represented late glacial to Holocene sediments (Table 2.2). For both cores  $^{230}\text{Th}_{\text{xs}}$  data are available (Kienast et al. 2007).

Core	Latitude N	Longitude W	Water depth (m)
ME0005A-24JC	0°01.3'	86°27.8'	2941
Y69-71P	0°06'	86°29'	2740
MC16	1°51.6'	86°18.3'	2767

Table 2.1 Core locations.

Additionally multicorer core MC16 from the Central Panama Basin was chosen in order to reconstruct the age relationships of the different sediment constituents in an area with minor influence of lateral advection (Kienast et al. 2007). Core MC16 was taken during R/V *Knorr* campaign in 2005 (KNR 182-9), sampled in 1 cm slices on board ship and stored at -20 °C until further analysis. Core slices of 3 sub-cores were re-combined in order to obtain sufficient material for all analyses.

Samples were freeze-dried and homogenized prior to further treatment. Co-occurring alkenones and planktic foraminifer tests were isolated from each sample and radiocarbon dated. For TOC radiocarbon analyses, subsamples of the freeze-dried samples of 100 mg-500mg (equivalent to 1 mg organic carbon) were used.

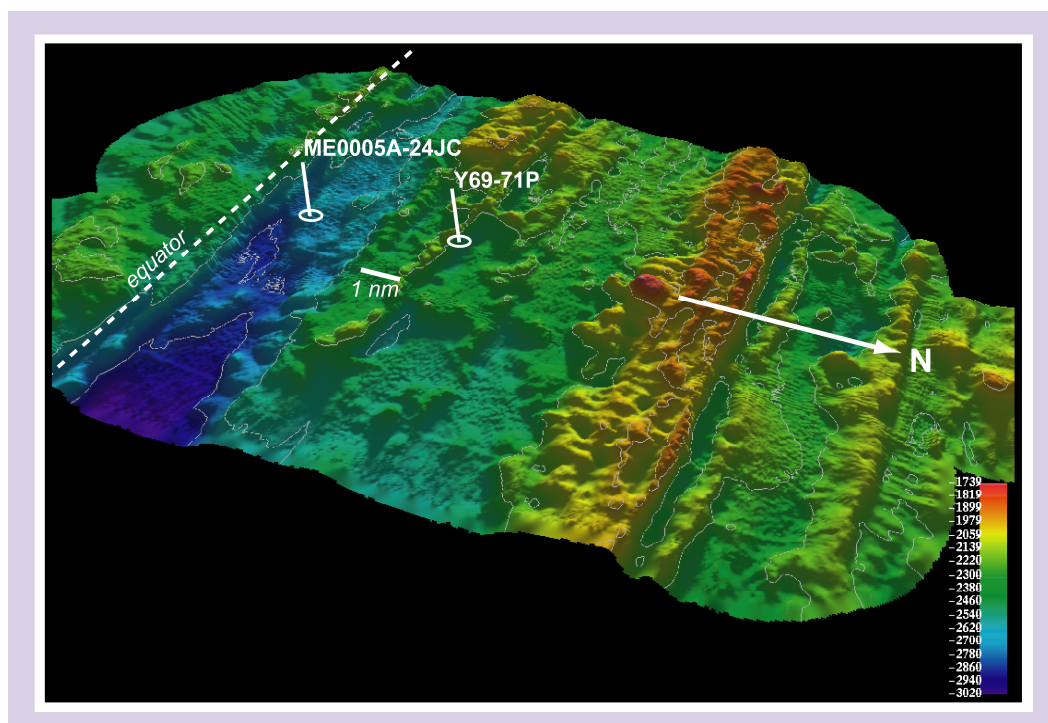


Figure 2.2 High resolution swath bathymetry image showing the abyssal hill topography around cores ME0005A-24JC and Y69-71P. Note east-west trending troughs.

### 2.3.1 Alkenone Purification

Alkenones were extracted from 30 to 40 g of freeze-dried and homogenized sediments using Soxhlet extraction or Accelerated Solvent Extraction (ASE) and purified following the analytical procedures of Ohkouchi et al. (2005b). Total lipid extracts were saponified with 0.5M solution of KOH in MeOH for 3 h at 85 °C. After cooling, up to 90% of the solvent was evaporated under a stream of nitrogen and neutral lipids were extracted into hexane five times. The neutral fraction was further separated into three polarity fractions by use of a silica gel column (1% de-activated SiO<sub>2</sub>, 0.063-0.2 mm mesh size, column: 6 mm i.d. x 4 cm) eluting hydrocarbons using 4 ml hexane, ketones and aldehydes using 4ml hexane:CH<sub>2</sub>Cl<sub>2</sub> (1:2 v:v), and alcohols using 4 ml MeOH.

Urea adduction (Marlowe et al., 1984) was performed on fraction 2 to separate straight-chain ketones/aldehydes from branched constituents. For this purpose, the samples were dissolved in a hexane:CH<sub>2</sub>Cl<sub>2</sub> (2:1 v:v, 4.5 ml) solution and a saturated urea solution (40 g/l in MeOH, 1.5 ml) was added dropwise. Samples were refrigerated for 15 min followed by removal of solvents under a stream of nitrogen. These steps were repeated twice. Afterwards urea crystals were rinsed with hexane five to seven times to recover non-adducted (branched and cyclic) components. Subsequently, urea crystals were dissolved in Seralpure water and extracted into hexane five to seven times. The straight-chain fraction was then applied to a column containing AgNO<sub>3</sub>-coated silica gel to separate saturated ketones (4 ml CH<sub>2</sub>Cl<sub>2</sub>) from unsaturated ketones (4 ml ethyl acetate or ether). To ensure maximum recovery, a third fraction using 4 ml MeOH was eluted. Resulting di-, tri- and tetra-unsaturated ketones were finally cleaned using a silica gel column (1% de-activated SiO<sub>2</sub>, mesh size 0.063-0.2 mm, column 6 mm i.d. x 4 mm) eluting with 4 ml hexane:CH<sub>2</sub>Cl<sub>2</sub> (1:2 v:v) to remove potential contamination introduced during the analytical procedures.

Following each analytical step, purification of the samples was monitored by analysis of subsamples (representing 0.1% of total sample) using an HP5890 series chromatograph equipped with a flame ionization detector.

### 2.3.2 Foraminifera

Tests of planktic foraminifera were hand-picked from the >125 µm fraction of sediments obtained by wet-sieving using tap water. A species with consistently high abundance, *Neogloboquadrina dutertrei*, was chosen in order to minimize differential abundance artifacts associated with bioturbation (Broecker et al., 1984). For the Eastern Equatorial Pacific the dominant foraminiferal species is *N. dutertrei* representing 60-70% of the Holocene and 45-65% of the last glacial foraminiferal assemblages (Martinez et al. 2006). This species prefers water depths of 60-150 m, but shows a pronounced abundance peak between 25 and 50 m in the Panama Basin (Fairbanks et al., 1982), and has δ<sup>18</sup>O consistent with calcification from 50 to 100 m depth (Benway et al., 2006). In sample 15-20 cm of core ME0005A-24JC and samples 11-18 cm and 25-30 cm of core Y69-71P, a second co-occurring species (*Globigerinoides sacculifer*) was analysed. The maximum concentrations of living *G. sacculifer* in the Panama Basin have been shown in 25-37 m water depth (Fairbanks et al., 1982), while tracer analyses on shells from the sea floor suggest calcification depths of 30-40 m (Benway et al., 2003).

For core ME0005A-24JC foraminiferal <sup>14</sup>C ages from 81 cm, 230 cm, 291 cm and 351 cm sediment depth used here are published in Kienast et al. (2007). The radiocarbon age from 120 cm core depth in core Y69-71P is from Kish (2003).

### 2.3.3 Radiocarbon measurements

Samples were radiocarbon-dated at National Ocean Sciences Accelerator Mass Spectrometry (NOSAMS) Facility at Woods Hole Oceanographic Institution, USA and Leibniz-Laboratory Kiel, Germany ([Table 2.3 in the Appendix](#)). Samples for TOC-dating were submitted unprocessed, while alkenone samples were submitted as CO<sub>2</sub>. For the conversion of purified alkenones into CO<sub>2</sub>, the samples were transferred into pre-combusted quartz tubes and 150 µg pre-combusted copper oxide (CuO) was added as an oxygen source. Using a vacuum line the samples were evacuated and flame-sealed. Afterwards the samples were combusted at 900 °C for 8 h, and resulting CO<sub>2</sub> was quantified and purified.

Foraminiferal samples measured at NOSAMS were submitted at dry shells, cleaned ultrasonically and with acid leaching of ~5-10% of the raw calcite. Foraminiferal samples measured at Leibniz-Laboratory were submitted as graphite. The foraminifera were cleaned with H<sub>2</sub>O<sub>2</sub> and converted to CO<sub>2</sub> using phosphoric acid. The gas samples were furthermore purified and reduced to graphite with H<sub>2</sub> and using iron powder as a catalyst. AMS measurements of carbonate and TOC samples at NOSAMS were carried out using standard methods (McNichol et al., 1994). AMS measurements of alkenone isolates were performed following the protocol for small samples (Pearson et al., 1998).

Radiocarbon ages are reported as conventional radiocarbon ages ( $\pm 1\sigma$  analytical error) referring to Stuiver and Polach (1977), which are corrected for carbon isotopic fractionation occurring during sample formation and processing. A conversion to calibrated (calendar) <sup>14</sup>C ages is not applied when discussing the age relationships of the samples. However, calibrated ages of foraminifera are used when sedimentation rates are calculated, or age models are developed. For calibration, the Marine04 calibration data set including a 400 years marine reservoir correction (Hughen et al., 2004b) was applied using the calibration software CALIB 5.0.2 (Stuiver et al. 2005).

## 2.4 RESULTS

### 2.4.1 ME0005A-24JC

The conventional <sup>14</sup>C ages of the dated sediment constituents ([Table 2.2, Figure 2.3](#)) range from the Holocene to the Last Glacial Maximum (LGM). Radiocarbon ages of all sediment fractions increase with core depth ([Figure 2.3](#)). Measured radiocarbon ages of the planktic foraminifera, alkenones, and TOC agree well, generally within  $400 \pm 100$  <sup>14</sup>C years. This age offset is not significant (within  $2\sigma$  analytical errors), especially considering the measurement uncertainties for small sample sizes (<300µg), which are related to sample preparation and combustion backgrounds as well as the analytical errors of AMS measurement. Here, we consider reported radiocarbon age offsets insignificant if they are within  $2\sigma$  analytical uncertainties.

Alkenones are only up to  $100 \pm 165$   $^{14}\text{C}$  years older than foraminifera, except for the depth interval from 226.5 to 231.5 cm where alkenones are  $250 \pm 155$   $^{14}\text{C}$  years younger than the foraminifera. Both values lie within  $1\sigma$  error margins. TOC and alkenones also agree within  $350 \pm 175$   $^{14}\text{C}$  years. For the intervals 46-51 cm and 76-81 cm, only foraminifera and TOC  $^{14}\text{C}$ -data were obtained as the alkenone yields were too small to perform radiocarbon AMS measurements.

Overall, we conclude that the alkenones are not significantly pre-aged relative to other sediment constituents. TOC and foraminiferal ages show a maximum age offset of only  $215 \pm 45$   $^{14}\text{C}$  years. The sample from core depth 345-350 cm represents an exception where TOC is  $400 \pm 100$   $^{14}\text{C}$  years younger than corresponding foraminifera. Taking into account that the foraminiferal age was measured from 351 cm core depth, the actual age offset between TOC and foraminifera should be less pronounced and not significant.

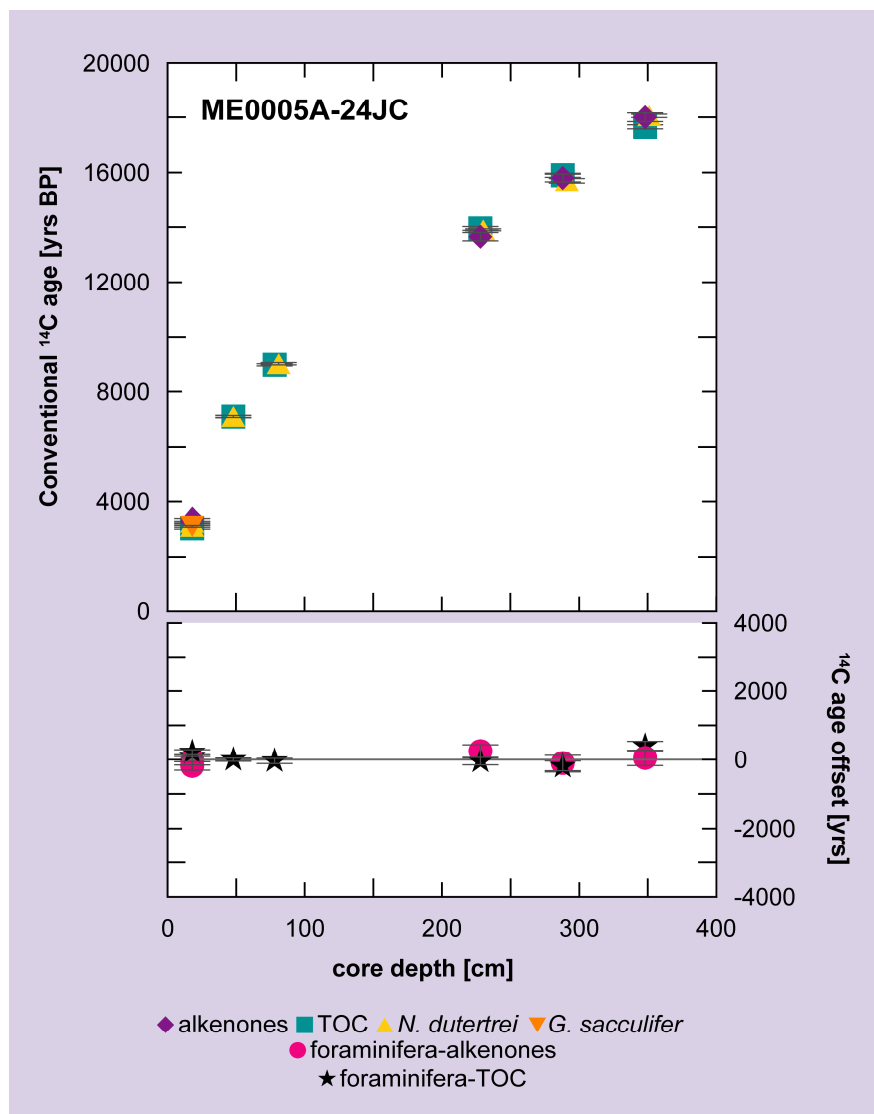


**Figure 2.3** Conventional radiocarbon ages of alkenones, foraminifera (*N. dutertrei*) and Total Organic Carbon (TOC) for core ME0005A-24JC and the age-offsets between alkenones and foraminifera (circles) and TOC and foraminifera (stars). Error bars indicate  $1\sigma$  analytical uncertainty (the propagated error is given in the lower panel).

Sample	Core depth (cm)	Foraminifera		TOC		Alkenones	
		Species	fMC	<sup>14</sup> C age (yrs BP)	fMC	<sup>14</sup> C age (yrs BP)	fMC
ME0005A-24JC	15-20	<i>N. dutertrei</i>	0.6670±0.0025	3 255±30	0.6849±0.0029	3 040±35	0.6635±0.0078
	15-20	<i>G. sacculifer</i>	0.6794±0.0025	3 105±30			3 290±95
	46-51	<i>N. dutertrei</i>	0.4129±0.0022	7 100±40	0.4130±0.0024	7 100±45	
	76-81 (81)	<i>N. dutertrei</i> <sup>a</sup>	0.3246±0.0016	9 040±40	0.3263±0.0017	9 000±40	
	226.5-231.5 (230)	<i>N. dutertrei</i> <sup>a</sup>	0.1772±0.0008	13 900±35	0.1764±0.0014	13 950±65	0.1822±0.0035
	285-290 (291)	<i>N. dutertrei</i> <sup>a</sup>	0.1416±0.0015	15 700±85	0.1382±0.0013	15 900±75	0.1402±0.0025
	345-351 (351)	<i>N. dutertrei</i> <sup>a</sup>	0.1057±0.0009	18 050±65	0.1114±0.0010	17 650±75	0.1061±0.0021
	11-18	<i>N. dutertrei</i>	0.6681±0.0022	3 240±25	0.6530±0.0024	3 420±30	0.4120±0.0168
	11-18	<i>G. sacculifer</i>	0.7247±0.0023	2 590±25			7 120±330
	25-30	<i>N. dutertrei</i>	0.4674±0.0019	6 110±30	0.4871±0.0024	5 780±40	0.4004±0.0136
Y69-71P	25-30	<i>G. sacculifer</i>	0.4864±0.0043	5 790±70			7 350±270
	31-39	<i>N. dutertrei</i> <sup>b</sup>	0.2968±0.0015	9 760±40	0.4194±0.0019	6 980±35	
	50	<i>N. dutertrei</i> <sup>b</sup>	0.2987±0.0022	9 705±60	0.3120±0.0019	9 350±45	0.3090±0.0052
	51-56	<i>N. dutertrei</i>	0.1604±0.0013	14 700±65	0.2377±0.0017	11 550±60	0.2183±0.0067
	81-89	<i>N. dutertrei</i> <sup>b</sup>	0.0920±0.0008	19 150±70	0.1678±0.0017	14 350±80	0.1567±0.0047
	117-123 (120)	<i>N. dutertrei</i> <sup>b</sup>	0.1106±0.0019	17 690±140	0.1328±0.0014	16 200±80	0.1208±0.0036
	163-167	<i>N. dutertrei</i> <sup>b</sup>	0.0350±0.0016	26 920±370	0.0979±0.0013	18 650±110	0.0998±0.0024
	180	<i>N. dutertrei</i> <sup>b</sup>	0.0305±0.0007	28 000±190	0.0521±0.0009	23 700±130	0.0531±0.0015
	183-188	<i>N. dutertrei</i>					18 500±200
	253-258	<i>N. dutertrei</i>					23 600±230
	260	<i>N. dutertrei</i> <sup>a</sup>					
MC16	0-4	<i>N. dutertrei</i>	0.7565±0.0034	2 240±35	0.7682±0.0033	2 120±35	0.7981±0.0085
	1-2	<i>N. dutertrei</i>	0.8076±0.0030	1 715±30	0.7644±0.0027	2 160±30	
	3-4	<i>N. dutertrei</i>	0.7792±0.0029	2 005±30	0.7768±0.0030	2 030±30	0.7630±0.0059
	11-12	<i>N. dutertrei</i>	0.3458±0.0022	8 530±50	0.3675±0.0021	8 040±45	2 170±60
	31-32	<i>N. dutertrei</i>					0.3760±0.0039
							7 860±80

<sup>a</sup> Data from Klenast et al. (2007).  
<sup>b</sup> Data from Clark et al. (2004).

**Table 2.2** Radiocarbon data (fMC; fraction modern carbon and conventional <sup>14</sup>C ages) of foraminifera, TOC and alkenones of cores ME0005A-24JC, Y69-71P and MC16. Depths in parentheses refer to foraminifera samples, if different from organic matter samples. Analytical uncertainties are given as 1 $\sigma$  analytical errors.

## 2.4.2 Y69-71P

The  $^{14}\text{C}$ -dated core depths for core Y69-71P cover marine oxygen isotope stages 1 and 2 (Table 2.2, Figure 2.4). All radiocarbon ages increase with core depth. Foraminifera and TOC ages agree within  $355\pm70$   $^{14}\text{C}$  years in most core depths. Exceptions are found at core depth 11-18 cm (*G. sacculifer*) and 183-188 cm (*N. dutertrei*) where TOC is  $830\pm40$  and  $960\pm180$   $^{14}\text{C}$  years older than foraminifera, respectively.

In most cases, we observe no systematic age offset between alkenones and TOC, which show age differences ranging from  $80\pm140$  to  $800\pm255$   $^{14}\text{C}$  years. Likewise, the age relationship between alkenones and foraminifera shows an inconsistent pattern with age offsets of  $200\pm250$  to  $810\pm245$   $^{14}\text{C}$  years.

Significant age offsets are evident for the depth interval 253-258 cm, where TOC ( $23,700\pm130$   $^{14}\text{C}$  yr BP) and alkenones ( $23,600\pm230$   $^{14}\text{C}$  yr BP) are  $3220\pm390$  and

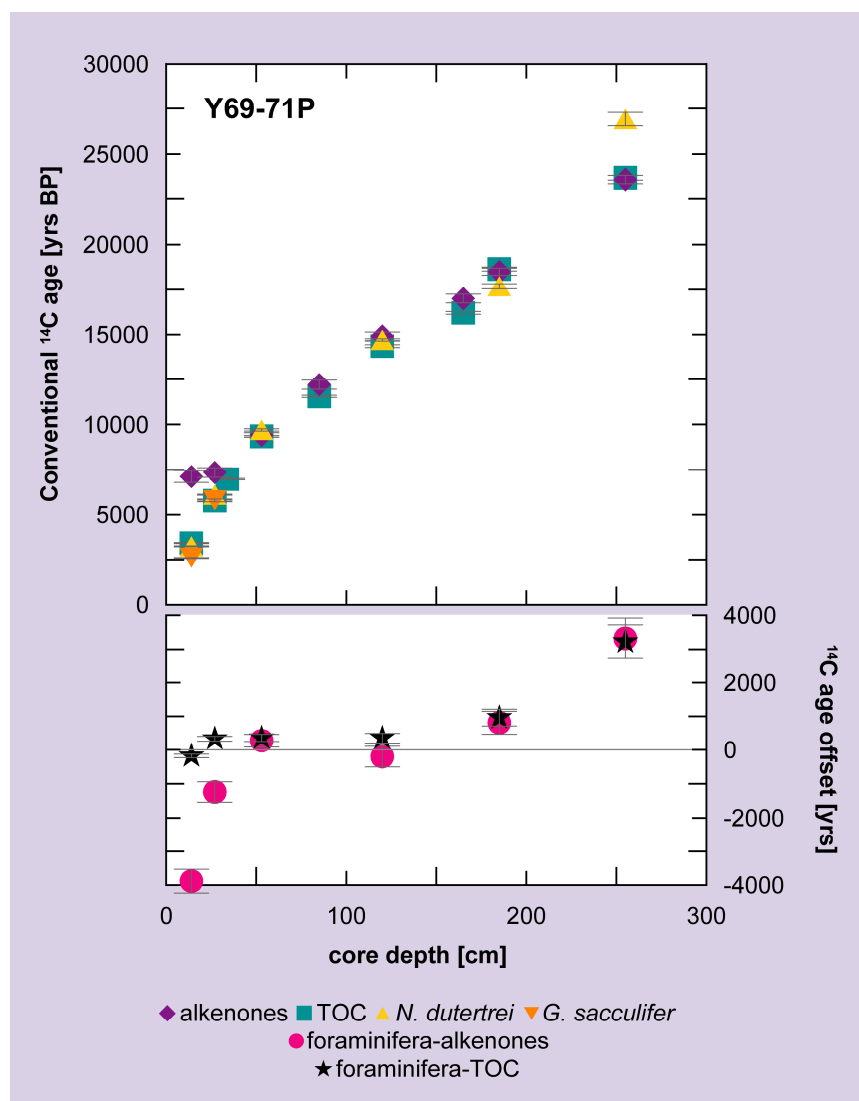


**Figure 2.4** Conventional radiocarbon ages of alkenones, foraminifera (*N. dutertrei* and *G. sacculifer*) and Total Organic Carbon (TOC) for core Y69-71P and the age-offsets between alkenones and foraminifera (circles) and TOC and foraminifera (stars). Error bars indicate  $1\sigma$  analytical uncertainty (the propagated error is given in the lower panel).

$3320 \pm 435$   $^{14}\text{C}$  years younger than corresponding foraminifera ( $26,920 \pm 370$   $^{14}\text{C}$  yr BP). Furthermore, alkenone dates from near the core top (11-18 cm and 25-30 cm) are much older (up to  $4530 \pm 330$   $^{14}\text{C}$  years) than those of the other dated sediment components. Alkenones and TOC differ by up to  $3700 \pm 330$   $^{14}\text{C}$  years for the two uppermost depth intervals, and the former are  $1240 \pm 270$  to  $4530 \pm 330$   $^{14}\text{C}$  years older than foraminifera for the 11-18 cm and 25-30 cm samples. The alkenones themselves show no significant age difference between 11-18 cm and 25-30 cm core depth. We consider these alkenone-radiocarbon ages to be less reliable due to very small sample sizes that were measured (<30 $\mu\text{g C}$ ).

#### 2.4.3 MC16

The dated core interval for core MC16 (Figure 2.5, Table 2.2) spans the Holocene (<9000a BP). Foraminifera, alkenone and TOC  $^{14}\text{C}$ -ages agree to within a few hundred

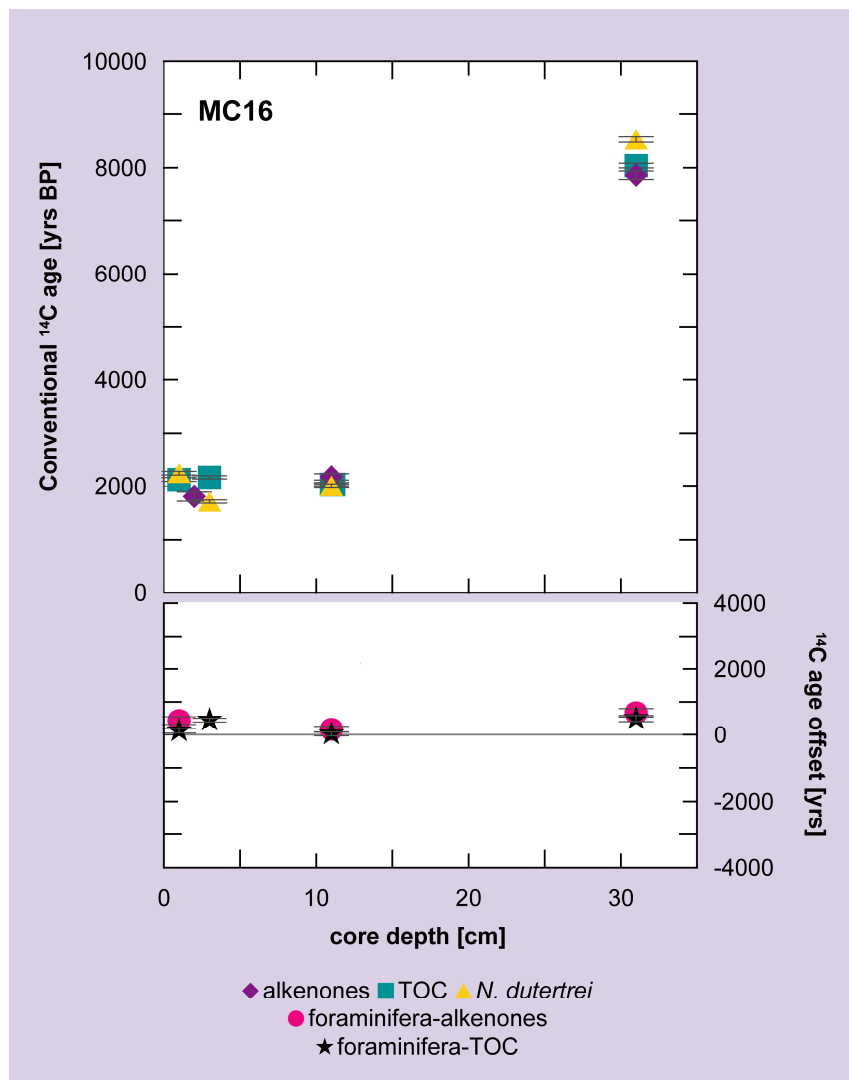


**Figure 2.5** Conventional radiocarbon ages of alkenones, foraminifera (*N. dutertrei* and *G. sacculifer*) and Total Organic Carbon (TOC) for core MC16 and the age-offsets between alkenones and foraminifera (circles) and TOC and foraminifera (stars). Error bars indicate  $1\sigma$  analytical uncertainty (the propagated error is given in the lower panel).

years, with a maximum age-offset of  $670 \pm 95$   $^{14}\text{C}$  years. The core-top radiocarbon ages for the depth intervals 1-2 cm and 3-4 cm have different age relationships between the different sediment constituents. For 1-2 cm, foraminifera ( $2240 \pm 35$   $^{14}\text{C}$  yr BP) are slightly older than TOC ( $2120 \pm 35$   $^{14}\text{C}$  years). In contrast, for 3-4 cm the foraminifera are younger ( $1715 \pm 30$   $^{14}\text{C}$  yr BP) than corresponding TOC ( $2160 \pm 30$   $^{14}\text{C}$  yr BP). The alkenones ( $1810 \pm 85$   $^{14}\text{C}$  yr BP) were combined for the depth interval 0-4 cm to yield enough material for radiocarbon dating. At 11-12 cm core depth, all three sediment fractions agree to within  $165 \pm 65$   $^{14}\text{C}$  years. The foraminifera at 31-32 cm ( $8530 \pm 50$   $^{14}\text{C}$  yr BP) are slightly older than co-occurring alkenones ( $7860 \pm 80$   $^{14}\text{C}$  yr BP) and TOC ( $8040 \pm 45$   $^{14}\text{C}$  yr BP).

## 2.5 DISCUSSION

Foraminifera are generally thought to most accurately represent the time of sediment deposition since their size and density are large enough to promote rapid sinking. This limits horizontal transport and lateral redistribution if bottom currents or tidal movements are weak. For the time intervals covered by our cores, these components are therefore in most cases considered the best estimate for the depositional age (uncorrected for reservoir or production effects).

In contrast, organic matter is associated with the fine grain-sized and low-density material, which may easily be incorporated into nepheloid layer aggregates, and become resuspended and laterally transported prior to final burial. Hence, age offsets between marine biomarkers or TOC and foraminifera can indicate supply of older organic material that has previously been stored elsewhere. One benefit of compound-specific radiocarbon dating of phytoplankton-derived biomarkers is that biases due to input of pre-aged terrigenous or ancient organic matter (e.g., from erosion of bedrock or fossil fuel derived contamination) can be excluded.

In most cases the reported  $^{14}\text{C}$  ages of the different sediment constituents, i.e. alkenones, foraminifera and TOC, agree well in all studied cores (Figures 2.3-2.5). Therefore, the alkenone radiocarbon ages do not indicate significant or systematic inputs of pre-aged organic matter supplied via lateral sediment transport and redistribution. Likewise, the good agreement between the ages of marine planktic components (foraminifera and alkenones) and TOC excludes aged terrigenous material as a significant source of organic matter. The data do not preclude redistribution and lateral sediment transport, which is suggested by bulk and component sedimentation rates and  $^{230}\text{Th}$  normalization. If redistribution is occurring, however, it must be dominated by resuspension of material from the benthic “fluff” layers of essentially zero age at the time of redeposition. This probably implies relatively local transport within the east-west trending troughs from which the cores were raised (Figure 2.2), if any occurs.

$^{14}\text{C}$  age differences within  $2\sigma$  error margins can in most cases be explained with measurement uncertainties. Sample preparation and chemical processing can introduce small amounts of carbon contaminant (carbon process blank) of unknown isotopic composition. This issue is especially critical for small sample sizes ( $<300\ \mu\text{g}$ ) and compounds needing several processing steps like organic material. Nevertheless, small size alkenone purification in connection with  $^{14}\text{C}$  dating at NOSAMS Facility is reliable within  $17\%$  or  $500\ ^{14}\text{C}$  years, respectively (Mollenhauer et al., 2005b, Ohkouchi et al., 2005b).

Some depth intervals show pronounced and significant age offsets. In core Y69-71P alkenones in the uppermost depth intervals (11-18 cm and 25-30 cm) are offset up to  $3880\pm330\ ^{14}\text{C}$  years to *N. dutertrei* and TOC, but notably, TOC and *N. dutertrei* ages agree within  $180\pm40\ ^{14}\text{C}$  years for depth interval 11-18 cm. TOC is even  $330\pm50\ ^{14}\text{C}$  years younger than *N. dutertrei* in 25-30 cm core depth. Conversely, in the oldest depth interval *N. dutertrei* is  $3320\pm435\ ^{14}\text{C}$  years older than alkenones and TOC. The same pattern is evident in core MC16 at depth interval 30-32 cm, where foraminiferal  $^{14}\text{C}$  ages are  $670\pm95$  and  $490\pm65\ ^{14}\text{C}$  years older than alkenones and TOC, respectively. These age relationships between foraminifera, TOC and alkenones are less consistent and more muted than previously found (Mollenhauer et al., 2003; Ohkouchi et al., 2002). Lateral supply of pre-aged organic matter to the uppermost core section of Y69-71 is regarded less likely because of the good agreement between TOC and foraminiferal ages. Since TOC, mostly of marine origin, and alkenones reside in the same size fraction, they are expected to be affected by the same sedimentation processes. Thus, if lateral sediment transport occurred it should have also supplied other pre-aged marine organic matter resulting in higher TOC ages. Potential causes for the discrepancies thus include analytical biases during sample processing, organic matter degradation during core storage, bioturbation, calcification depth, differential dissolution, and selective transport of either the foraminiferal or organic fractions.

## 2.5.1 Potential biases of alkenone radiocarbon ages

### 2.5.1.1 Large blank contribution to small samples

Age offsets of alkenones at 11-18 cm and 25-30 cm core depth in Y69-71P, which exceed  $4500\ ^{14}\text{C}$  years, were measured from alkenone samples containing only 24 and  $29\ \mu\text{g}$  carbon, respectively. Using isotopic mass balance equation we can calculate the amount of contamination required if the reported age offsets between alkenones and foraminifera were due to addition of blank carbon during sample processing alone. Assuming a contamination with  $^{14}\text{C}$ -dead material (fraction modern carbon  $fMC=0$ ), approximately 38% or 43% blank C for depth interval 11-18 cm would yield the observed age offset relative to co-occurring *N. dutertrei* or *G. sacculifer*, respectively. Assuming an

fMC=0.25, the blank carbon would account for 60% (*N. dutertrei*) or 61% (*G. sacculifer*) of the measured sample. For core depth 25-30 cm, the same calculation results in 14% or 39% (*N. dutertrei*) and 18% or 36% (*G. sacculifer*) blank C depending on whether an fMC value of 0 or 0.25 is used, respectively. This amount of contamination could have been introduced to the samples during any step of the sample preparation methodology. However, we consider addition of such large amounts of blank material unlikely, as CO<sub>2</sub> yields from combustion were close to the expected amount of carbon based on gas-chromatographic quantification of purified alkenones.

#### 2.5.1.2 Degradation of alkenones during storage

Core Y69-71P was retrieved in 1969 and had observed patches of surface mold when sampled. Selective bacterial degradation of alkenones can occur and the bacterial metabolic pathway includes isotopic fractionation during the degradation of alkenones to alkenols (Gong and Hollander, 1999; Rontani et al., 2005; Rontani et al., 2008; Sun et al., 2004). However, if bacterial activity occurred, it is not expected to influence the radiocarbon content of the alkenones, since radiocarbon data reported according to Stuiver and Polach (1977) are corrected for isotopic fractionation during sample formation, decay as well as processing.

At present, we are unable to provide a satisfactory explanation for the unexpectedly old alkenones in the uppermost samples of Y69-71P. Unfortunately, sample availability does not permit us to repeat these measurements.

#### 2.5.2 Potential biases on foraminiferal ages

For depth intervals 253-258 cm of core Y69-71P and 30-32 cm of core MC16 foraminiferal <sup>14</sup>C ages are significantly (>2σ analytical uncertainty) older than the other dated sediment constituents. If foraminiferal ages represent the best estimate of the time of deposition in locations affected by sediment transport we would not expect such an age relationship. Moreover, in previous studies, foraminifera were consistently reported to be the youngest sediment constituents (Mollenhauer et al., 2003; Mollenhauer et al., 2005a; Ohkouchi et al., 2002). Soxhlet and ASE extraction procedures seem not to introduce any significant uncertainties to the radiocarbon measurements of foraminiferal tests (Ohkouchi et al., 2005a). Likewise winnowing of the organic material, which is more susceptible to resuspension and transport, exposing relict foraminifera is unlikely. In addition to the above mentioned multiple lines of evidence for sediment focusing at the core sites, chirp subbottom profiler data for core Y69-71P (Lyle et al., 2005) show thick sediment coverage implying that the core was not taken at a location of sediment winnowing.

### 2.5.2.1 Bioturbation

For core MC16 core-top radiocarbon ages are elevated and essentially constant down to 12 cm sediment depth for all dated components. This pattern can be explained with bioturbation and is in agreement with the existing literature. Aller et al. (1998) report maximum bioturbation depths of up to 20 cm for cores from the Northern Panama Basin.

A potential explanation for age offsets between the different components is age-dependent or particle size induced differential bioturbation by benthic organisms (Smith et al., 1993; Thomson et al., 1995). Mixing depths may be greater for fine than coarse grain sizes or younger than older material. This process, when coupled to different input abundance histories can induce complex phasing and smoothing effects in different grain-size fractions, especially where sedimentation rates are <10 cm/kyr (Bard, 2001). However, differential bioturbation is an unlikely explanation for the age offsets observed at 253-258 cm core depth of core Y69-71 showing >3000  $^{14}\text{C}$  years older foraminiferal ages compared to co-occurring alkenones and TOC. The sedimentation rate of core Y69-71 ranges between 7 and 17 cm/kyr (for 400 cm core depth; Lyle et al., 2002). Lowest sedimentation rates are reconstructed for the interval from 8500 years to the core top, implying that those intervals may be more susceptible to bioturbation-induced offsets than glacial intervals. However, according to Bard (2001) bioturbation should in general not induce such a large age offset between different sediment constituents here.

For core MC16 with an estimated sedimentation rate of 2.7-3.1 cm/kyr (using calibrated radiocarbon ages) an age offset of up to 2500 years induced by differential bioturbation would be expected according to Bard (2001; equation 1) assuming bioturbation depths of 15 cm (fine fraction) and 5 cm (coarse fraction). This offset is much higher than the observed  $^{14}\text{C}$  age offset between foraminifera and organic matter ( $\leq 670 \pm 95$   $^{14}\text{C}$  years).

### 2.5.2.2 Calcification depth and differential dissolution of foraminiferal tests

In the topmost core sections of core Y69-71P (11-18 cm and 25-30 cm) and core ME0005A-24JC (15-20 cm) *G. sacculifer* is consistently younger than *N. dutertrei* by several hundred years. This finding is in line with the species-specific calcification depths in the euphotic zone, which are characterized by different DIC  $^{14}\text{C}$  contents. However, the differences in calcification depth are small (Fairbanks et al., 1982), so observed age offsets are greater than would be expected for pre-anthropogenic DIC  $^{14}\text{C}$  differences alone.

A possible explanation for  $^{14}\text{C}$  age offsets between foraminiferal species introducing a bias towards younger ages might be differential dissolution in the sediment mixed layer (Barker et al., 2007), which can occur under the influence of carbonate ion

undersaturated bottom waters, or as a result of respiratory CO<sub>2</sub> release in the sediment. In the Panama Basin, the lysocline depth was observed at around 2800 m (Thunell et al., 1981), which is equivalent to the depths of our core sites ME0005A-24JC, Y69-71P and MC16. *G. sacculifer* is one of the most soluble species, whereas *N. dutertrei* is highly resistant (Berger, 1970). Thus differential dissolution of the more susceptible *G. sacculifer* could explain the younger radiocarbon ages of this species. Alternatively, differences in the species seasonal or interannual fluxes may contribute to the <sup>14</sup>C differences. *G. sacculifer* contains algal symbionts and can survive oligotrophic conditions during intervals of low upwelling, while *N. dutertrei* thrives during upwelling events, which bring deeper, relatively <sup>14</sup>C-depleted, nutrient-rich water to the sea surface (Watkins et al., 1996). While there are no *G. sacculifer* ages for the core depth 253–258 cm of core Y69-71P, published alkenone SST data (Kienast et al., 2006; Prahl et al., 2006), faunal assemblage changes (Martinez et al., 2006) and coupled δ<sup>18</sup>O, δ<sup>13</sup>C and Mg/Ca SST data (Pena et al., 2008) do not suggest increased upwelling activity at our sites during the glacial interval, although stronger advection of cool waters upwelled into the eastern boundary current off Peru and Chile is probable (Feldberg and Mix, 2003). We therefore regard this process to be of minor importance for the explanation of old foraminiferal tests in 253–258 cm core depth.

#### 2.5.2.3 Addition of secondary calcite

Secondary calcification could be a possible cause for the foraminiferal <sup>14</sup>C age of 253–258 cm in Y69-71P. Secondary calcification within the sediment by precipitation of pore water DIC derived from old carbon from deeper sediments could be responsible for older <sup>14</sup>C ages of foraminifera (Barker et al., 2007). For an age offset of >3000 <sup>14</sup>C years, this requires the addition of large amounts of secondary calcite added to the foraminiferal tests. We can again use isotopic mass balance to calculate the amount of secondary calcite needed to cause the foraminiferal age offset. Assuming pore water DIC-addition from e.g. 15 cm or 30 cm deeper ( $fMC=0.046$  or 0.04 calculated with interpolated TOC-based sedimentation rate), the required additional amount of older calcite is 280% and 140%, respectively, which is implausible considering that only intact foraminifera without visual evidence of secondary calcite precipitation were handpicked for <sup>14</sup>C analysis.

#### 2.5.2.4 Downslope transport of foraminifera

Downslope transport from nearby abyssal hills or the Carnegie Ridge is considered a possible explanation for older foraminiferal ages. As described above, between 85° and 86°W the central saddle of Carnegie Ridge shows an erosional valley, where incision into the acoustic basement from bottom water spillover is evident (Lonsdale, 1977; Van Andel et al., 1971). The Sand Dune Valley, located on the eastern side of this erosional feature,

shows transverse dunes and barchans, which consist of sand-sized broken and intact Quaternary foraminiferal tests. The foraminiferal dunes are moved down-valley in a NW direction (towards our core locations) by the episodic spillover of bottom water across the central saddle of the Carnegie Ridge reaching velocities of >30 cm/s (Lonsdale and Malfait, 1974). The eroded material is likely accumulated in abyssal valleys like our core sites. Since the process is episodic in nature, we do not expect large additions of fossil foraminifera in all core depths (and thus no important contribution to mass accumulation rates), which could explain that only one of our studied depths intervals seems to be affected. If this is the case, however, the fact that we did not find the same offsets in core ME0005A-24JC (closest to Carnegie Ridge) as we did in Y69-71P (one basin to the north) would have to be random chance.

Anomalously old foraminiferal  $^{14}\text{C}$  ages of core MC16 (30-32 cm) might be explained by downslope transport from the Malpelo Ridge, which is predominantly covered with carbonate from intact and broken foraminiferal tests. But sediment winnowing from the Malpelo Ridge may be less extensive since the concentration of more readily mobilizable fine-grained carbonate on the Malpelo Ridge is higher than on the Carnegie Ridge (Moore et al., 1973).

### 2.5.3 Potential particle sources and timescales of lateral transport

Despite potential radiocarbon age biases related to the above mentioned processes, all sediment constituents agree well in age in most of the core depths of cores ME0005-24JC, Y69-71P and MC16 and thus sediment redistribution likely occurs syn-depositionally. For our study area, especially for cores ME0005A-24JC and Y69-71P, the syn-depositionally transported sedimentary material is probably derived from nearby abyssal hills by interaction with abyssal tidal flow (internal tides). Enhanced current velocities near the seafloor may enhance the small scale vertical shear and thereby increase the probability of sediment erosion and redistribution. The resuspended sediment is injected into the near-bottom water, where it is laterally displaced away from the topographical highs (Turnewitsch et al., 2008). This is in agreement with the  $^{230}\text{Th}_{\text{xs}}$  data from Kienast et al. (2007), as the supplied material is likely to have been transported by bottom currents, according to the basic assumptions of the  $^{230}\text{Th}$  normalization method (Francois et al., 2004). Based on modeling studies, Egbert et al. (2004) reconstructed the tidal kinetic energy and tidal dissipation in the deep ocean for the LGM. Their results show enhanced global tidal dissipation during the LGM compared to present day conditions, especially in the deep ocean. This way, enhanced lateral transport could explain high sediment focusing factors in the Panama Basin during the last glacial. Nevertheless, internal tides do also occur in the Holocene and could have contributed to the apparent sediment focusing, even though they were weaker than during the LGM (Kienast et al., 2007).

Honjo et al. (1992) present data for the northern Panama Basin, which give evidence for strongest deep currents in approximately 2000 m water depth. This is in good agreement with our assumption that the resuspended material derives from the topographic highs around our locations, which rise to approximately 2300-1800 m water depth (Fig. 1B). Likewise, the measured current velocities (on average 5-7 cm/s) are in the range needed to resuspend low-density material (organic matter), but too not affect denser material like foraminifera.

Considering the minor age offsets of the radiocarbon-dated sediment constituents in most of the samples of cores ME0005A-24JC, Y69-71P and MC16, the apparent lack of aged terrigenous organic matter, and the  $^{230}\text{Th}_{\text{xs}}$  derived focusing factors of Kienast et al. (2007), we suggest that laterally supplied material is rapidly transported and redistributed by bottom currents soon after particle formation or particle sedimentation. Using  $^{234}\text{Th}/^{238}\text{U}$  disequilibria, Turnewitsch et al. (2008) calculated residence times of laterally transported particulate matter resuspended from a sloping seafloor by internal tides. The residence time of those particles in near-bottom water traced by  $^{234}\text{Th}$  is <2-3 weeks. This is consistent with sediment redistribution on a local scale. However, this residence time might significantly increase by further interaction with the kilometer-scale topography, but the overall magnitude is most probably below the analytical uncertainties associated with radiocarbon dating.

Furthermore,  $U_{37}^{K'}$  (alkenone unsaturation index) derived sea surface temperatures (SST) of cores ME0005-24JC (Kienast et al., 2006) and Y69-71P (Prahl et al., 2006) and our own data (Appendix) agree in the topmost samples (late Holocene) with annual mean SSTs at this site (Locarnini et al., 2006). This argues against transport processes over long distances, since the  $U_{37}^{K'}$  index would reflect the SST signal of the region of the alkenone origin (Benthien and Müller, 2000; Mollenhauer et al., 2006; Ohkouchi et al., 2002).

Moreover, cores ME0005-24JC and Y69-71P (Figure 2.2) as well as core MC16 (not shown) are located in narrow east-west trending troughs, which are bordered by the Carnegie Ridge in the south and the Cocos-Nazca Rise in the north. This surrounding large-scale topography restricts the potential source regions for bottom current driven advection and supports the assumption that laterally transported material is mainly derived from nearby topographic highs within the east-west trending troughs. Contrary, the supply of pre-aged foraminifera from the Carnegie Ridge (at ~130 km from the core sites) might be triggered by a yet unknown but different mechanism than tidal dissipation. Since the sediments of its northern flank consist of relict foraminiferal sands, high concentrations of old alkenones are not expected at this erosional site. Modern alkenones from the overlying water column would, however, not affect the  $U_{37}^{K'}$  based SST estimate as they would reflect conditions similar to those alkenones synthesized at

our core sites ( $\Delta\text{SST} < 0.7^\circ\text{C}$ ; Locarnini et al., 2006). However, old foraminiferal tests would record Mg/Ca SST from the time of synthesis. Significant disagreements between the  $U_{37}^{K'}$  exist in early Holocene, deglacial and glacial intervals of these cores, however. The origin of these differences is not known, but is under consideration (Prahl and Kienast, personal communication 2009). Our radiocarbon data constrain these considerations and exclude the possibility that offsets in  $U_{37}^{K'}$  between these cores reflects differential input of older materials.

For core MC16 our  $^{14}\text{C}$  data do not necessarily imply resuspension and redistribution of organic matter. Nevertheless, this location is influenced by the bottom water circulation of the Panama Basin (Figure 2.1), and is situated just south of the Malpelo Ridge, which is mostly covered with fine-grained sediments that may serve as a source of advected sediment (Druffel et al., 1998; Moore et al., 1973; Van Andel, 1973). For core P7, which is located in the Central Panama Basin NW of core MC16 in a similar water depth, Kienast et al. (2007) measured slightly elevated recent  $^{230}\text{Th}_{\text{xs}}$  levels and calculated higher focusing for the glacial. If we assume that cores P7 and MC16 are influenced by a similar sediment depositional pattern, it is likely that MC16 is also influenced by lateral advection of sediments. Our  $^{14}\text{C}$  results, which mostly show insignificant age differences between alkenones, foraminifera and TOC, indicate that like for cores ME0005A-24JC and Y69-71P, the timescale for lateral transport is rapid and occurs syndepositionally, i.e. less than a few decades after particle formation and synchronous within the uncertainty associated with the radiocarbon method. As the  $U_{37}^{K'}$  derived SST (not shown) also matches the mean annual temperature at this site (Locarnini et al., 2006), we consider the advection processes to also occur on a local (trough-wide) scale.

#### 2.5.4 Implications for paleoceanographic studies in the southern Panama Basin

Paleoceanographic studies reconstructing marine productivity and vertical carbon export using accumulation rates of different sedimentary constituents have shown higher glacial export rates compared to interglacials (Lyle et al., 2002; Paytan et al., 1996; Sarnthein et al., 1988). Contrary results were obtained in studies using constant flux proxies (Kienast et al. 2007; Loubere, 1999; Loubere, 2000; Loubere et al., 2003; Loubere et al., 2004) and faunal assemblages (Loubere, 1999; Martinez et al., 2006) implying reduced glacial productivity and enhanced sediment focusing. In light of this paradox, the applicability of the  $^{230}\text{Th}$  method in the Panama Basin is controversial (Broecker, 2008; Francois et al., 2007; Kienast et al., 2007; Lyle et al., 2005; Lyle et al., 2007; Siddall et al., 2008).

Our results have important implications for these paleoceanographic studies. Since the age discrepancy between the different sediment components is small and the

transported material is likely to be advected from nearby topography the rapid sediment transport processes within the Panama Basin do not lead to a decoupling of proxy records residing in different grain size fractions. Therefore, combined records of paleoproxies from different grain-size fractions as presented by Kienast et al. (2006) and Prahl et al. (2006) can indeed be considered coeval in this region. For example, apparent offsets between paleotemperatures estimated from  $U_{37}^{K}$  and those estimated from Mg/Ca ratios in foraminifera cannot be dismissed as artifacts of local reworking, but must be explained based on environmental influences on the respective proxies (Mix, 2006). However, one aspect revealed by our study is the potential selective transport of foraminiferal sands washed downslope from the Carnegie Ridge, which might bias paleoceanographic reconstructions based on foraminiferal tests. Our results suggest the occurrence of episodic downslope transport particularly for the glacial time period. The unexpectedly old *N. dutertrei* in core depth 253-258 cm and the deviation of foraminiferal  $^{14}\text{C}$  ages from Clark et al. (2004) with our data of core Y69-71P furthermore suggests that the age model for this core used in Kienast et al. (2007) might need to be revised. This implies that  $^{230}\text{Th}$  derived focusing factors would even increase for marine oxygen isotope stage 2 time interval used in Kienast et al. (2007).

Irrespective of which of the mechanisms suggested to affect  $^{230}\text{Th}_{\text{xs}}$  inventories (i.e. lateral redistribution or water column scavenging, or any other yet unknown influence) is the true controlling process, our data give strong evidence for a local (trough-wide) source of all marine sediment constituents. Evidence for delivery of distant marine organic matter or addition of any pre-aged terrigenous components supplied from the continental margins or by dust is lacking.

## 2.6 SUMMARY AND CONCLUSION

Radiocarbon ages of alkenones, foraminifera and TOC in most core depths of cores ME0005A-24JC, Y69-71P and MC16 have insignificant  $^{14}\text{C}$  age offsets between the different sediment components, arguing against long-distance lateral supply and deposition of pre-aged allochthonous material from marine or terrestrial sources in the Panama Basin. This finding constrains mechanisms of sediment focusing inferred from  $^{230}\text{Th}_{\text{xs}}$  data (Kienast et al., 2007).

Allochthonous material in this region likely stems from local particle winnowing from kilometer-scale topographic highs within the east-west trending troughs by internal tidal activity or bottom currents that return recently sedimented particles to bottom waters. These tidal water movements or bottom currents locally transports and redistributes the particles within less than a few decades after particle formation, equal to the uncertainty of the radiocarbon method.

Spillover of fast bottom currents originating in the Peru Basin and crossing the Carnegie Ridge may occur episodically, transporting coarser-grained particles downslope to the Southern Panama Basin. A bias in paleoceanographic reconstructions based on foraminiferal tests for core Y69-71P might arise from this process, although it is not obvious why similar effects would not have been found in core ME0005A-24JC which is closer to Carnegie Ridge and in slightly deeper water.

The proximity and rapidity of transport precludes extensive alteration of the entrained pelagic organic matter. Enhanced tidally related current velocities in the abyssal ocean during lowstands of sea level may explain higher sediment focusing factors found in the Panama Basin during glacial time compared to the Holocene.

## Acknowledgments

This study was funded by the Helmholtz Young Investigators Group „Applications of molecular  $^{14}\text{C}$  analysis for the study of sedimentation processes and carbon cycling in marine sediments“. We kindly thank Ralph Kreutz and Daniel Montluçon for laboratory assistance, Birgit Meyer-Schack and Monika Segl for  $^{14}\text{C}$  processing guidance. G.M. acknowledges financial support from WHOI postdoctoral scholarship program. T.I.E. was supported by NSF grant OCE-0526268. A.C.M. was supported by NSF grant ATM0602395. We thank R. Turnewitsch, two anonymous reviewers, and M.L. Delaney (editor) for beneficial comments that improved this manuscript.

## 2.7 SUPPLEMENTARY DATA

### 2.7.1 Potential effects of sediment transport on $U_{37}^{K'}$ derived sea surface temperatures

Comparison of the  $U_{37}^{K'}$  derived SSTs of both cores ME0005-24JC and Y69-71P published by Kienast et al. (2006) and Prahl et al. (2006) (Figure 2.6) shows a general temperature offset of approximately 1 to 1.5 °C (with Y69-71P being colder) although both cores should reflect the same SST due to their proximity. If we use our  $^{14}\text{C}$  data to develop a new age model for core Y69-71P, the temperature offset is reduced for the deglacial and disappears for the early to middle Holocene. But for the uppermost core depths, reflecting the late Holocene, the temperature offset of ~1 °C remains. This offset prevails mainly in the core interval where our data show alkenones older than foraminifera and TOC (11-18 cm and 25-30 cm).

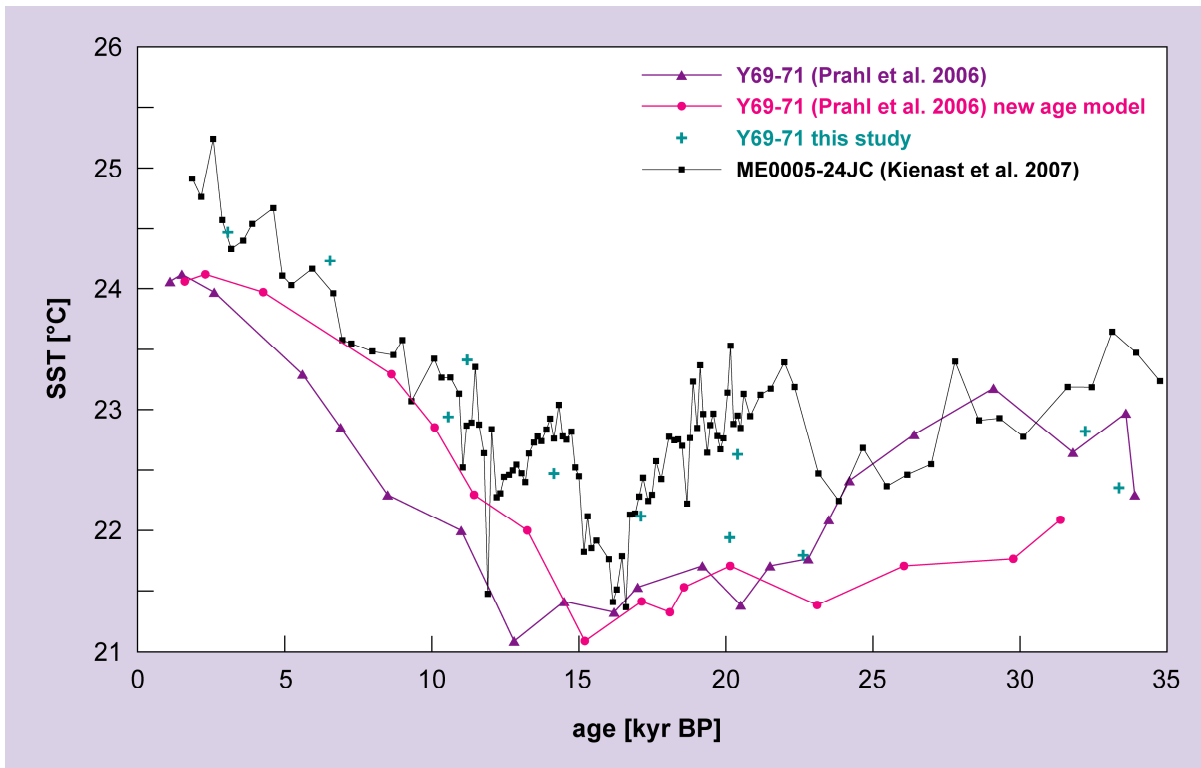


**Figure 2.6**  $U_{37}^{K'}$  derived SSTs for core ME0005-24JC (Kienast et al. 2007) and Y69-71P (Prahl et al. 2006; this study). For core Y69-71P SSTs are additionally plotted using a modified age model based on our foraminiferal  $^{14}\text{C}$  results.

We can calculate the potential contribution of alkenones reflecting colder temperatures (e.g. the time interval of Heinrich event 1 H1) and use isotopic mass balance to quantify the likely effect on the  $^{14}\text{C}$  age assuming that the  $U_{37}^{K'}$  derived SSTs estimated for core ME0005-24JC reflect the “true” SSTs. For depth interval 25-30 cm an H1 alkenone contribution of approximately 17% ( $f\text{MC}=0.1567$ ) alters the “true” alkenone depositional age ( $f\text{MC}=0.4674$ ; assumed to be reflected by the equivalent foraminiferal

age) to the actually measured age ( $fMC=0.4004$  measured;  $fMC=0.4140$  calculated). Therefore, if the observed age offset between alkenones and foraminifera and TOC for depth intervals 25-30 cm is real, contribution of older alkenones (H1) could be a potential explanation for that age offset. Contrary, the age offset evident for depth interval 11-18 cm cannot be explained by contribution of approximately 22% of H1 alkenones alone. Applying the same mass balance equation as above does not alter the alkenone age sufficiently ( $fMC=0.4120$  measured;  $fMC=0.5556$  calculated).

If, as discussed above, the alkenone contamination is radiocarbon dead ( $fMC=0$ ) we can quantify the  $U_{37}^{K'}$  derived SST signal of those advected alkenones. The mass balance derived potential contamination of 38% for depth interval 11-18 cm (5.1.1) would require alkenones synthesized in sea surface waters with approximately  $22.7\text{ }^{\circ}\text{C}$ . This temperature is well within the range of the temperatures for the time interval 50-150 kyr measured by Prahl et al. (2006). Again, if the observed age offset between alkenone and foraminiferal and TOC  $^{14}\text{C}$  ages is real, addition of  $^{14}\text{C}$ -free alkenones might be a possible explanation. As discussed above, the material is likely to be delivered from nearby topography. However, the potential source areas (surrounding abyssal hills) must have been different at the respective times to explain the different ages (H1 vs. >50 kyr) required for the advected alkenones to result in the measured age offsets to foraminifera and TOC.

## 2.7.2 Receipt numbers of radiocarbon analysis

Sample	Core depth (cm)	Foraminifera		TOC	Alkenones
		Species	receipt #	receipt #	receipt #
ME0005A-24JC	15-20	<i>N. dutertrei</i>	KIA 34472	58954	58950
	15-20	<i>G. sacculifer</i>	KIA 34471		
	46-51	<i>N. dutertrei</i>	66556	66554	
	76-81			66555	
	81	<i>N. dutertrei</i>	33431		
	226.5-231.5			58955	58951
	230	<i>N. dutertrei</i>	33432		
	285.5-290.5			58956	58952
	291	<i>N. dutertrei</i>	33433		
	345-350			58957	58953
Y69-71P	351	<i>N. dutertrei</i>	33434		
	11-18	<i>N. dutertrei</i>	43983	43167	43161
	11-18	<i>G. sacculifer</i>	43984		
	25-30	<i>N. dutertrei</i>	43985	43168	43162
	25-30	<i>G. sacculifer</i>	43986		
	31-39			40605	
	51-56	<i>N. dutertrei</i>	KIA 35966	63256	63250
	81-89			40607	40722
	117-123			40608	40723
	120	<i>N. dutertrei</i>	33428		
	163-167				
	183-188	<i>N. dutertrei</i>	KIA 35967	63257	63251
	253-258	<i>N. dutertrei</i>	KIA 35968	63258	63252
MC16	1-2	<i>N. dutertrei</i>	KIA 35969	63259	
	3-4	<i>N. dutertrei</i>	KIA 35970	63260	
	0-4				63253
	10-12				63254
	11-12	<i>N. dutertrei</i>	KIA 35971	63261	
	30-32				63255
	31-32	<i>N. dutertrei</i>	KIA 35972	63262	

Table 2.3 Receipt numbers from NOSAMS and Leibniz laboratory (KIA numbers, in italics).



### 3. MANUSCRIPT II

## Controls on the age of terrigenous organic matter in Black Sea sediments

Stephanie KUSCH<sup>1,2</sup>, Janet RETHEMEYER<sup>1,2,a</sup>, Enno SCHEFUß<sup>3</sup>, Gesine MOLLENHAUER<sup>1,2</sup>

1 Alfred Wegener Institute for Polar and Marine Research, Am Handelshafen 12, 27570 Bremerhaven, Germany

2 Faculty of Geosciences, University of Bremen, Klagenfurter Str., 28359 Bremen, Germany

3 MARUM Center for Marine Environmental Sciences, University of Bremen, Leobener Str., 28359 Bremen, Germany

<sup>a</sup> present address: University of Cologne, Institute for Geology and Mineralogy, Zülpicher Str. 49a, 50674 Cologne, Germany

**submitted to Geochimica et Cosmochimica Acta**

---

### Abstract

Transfer of organic carbon (OC) from the terrestrial to the oceanic carbon pool is largely driven by riverine and aeolian transport. Before transport, however, terrigenous organic matter can be retained in intermediate terrestrial reservoirs such as soils. The average terrestrial residence time can be evaluated using compound-specific radiocarbon dating of terrigenous biomarkers.

Here we show compound-specific radiocarbon ( $^{14}\text{C}$ ) ages of terrigenous biomarkers and bulk  $^{14}\text{C}$  ages accompanied by geochemical proxy data from core top samples collected along transects in front of several river mouths in the Black Sea.  $^{14}\text{C}$  ages of long chain *n*-alkanes, long chain *n*-fatty acids and total organic carbon (TOC) are highest in front of the river mouths, correlating well with BIT (branched and isoprenoid tetraether) indices, which indicates contribution of pre-aged, soil-derived terrigenous organic matter. The radiocarbon ages decrease further offshore towards locations where organic matter is dominated by marine production and aeolian input potentially contributes terrigenous organic matter. Average terrestrial residence times deduced from *n*-C<sub>29+31</sub> alkanes and *n*-C<sub>28+30</sub> fatty acids ages from stations directly in front of the river mouths range from 900±70 years to 4400±170 years. These average residence times correlate with size and topography in climatically similar catchments, whereas the climatic regime appears to control continental carbon turnover times in morphologically similar drainage areas. Along-transect data imply petrogenic contribution of *n*-C<sub>29+31</sub> alkanes and input via different terrigenous biomarker transport modes, i.e. riverine and aeolian, resulting in aged biomarkers at offshore core locations. Because *n*-C<sub>29+31</sub>

alkanes show contributions from petrogenic sources,  $n\text{-C}_{28+30}$  fatty acids likely provide better estimates of average terrestrial residence times.

---

### 3.1 INTRODUCTION

Actively cycling carbon stored as organic matter on land exceeds the amount of organic matter stored in the oceans by a factor of two and is an important player within the global carbon cycle. However, the origin and fate of terrigenous organic matter transported to the ocean is still poorly understood (Burdige, 2005; Hedges and Keil, 1995; Hedges et al., 1997). Rivers are the major source of terrigenous organic matter (OM) delivered to the ocean ( $\sim 0.4 \times 10^{15}$  g C/yr). Aeolian transport is considered to be smaller ( $\sim 0.1 \times 10^{15}$  g C/yr) but most important in open ocean settings (Hedges, 1992; Hedges and Keil, 1995; Hedges and Oades, 1997; Hedges et al., 1997; Schlünz and Schneider, 2000). Although most of the terrigenous organic matter supplied to the ocean is remineralized (>80%; Hedges and Oades, 1997) and escapes burial in oceanic sediments, it is thought to consist of rather refractory material, which survived microbial degradation in soils and aquifers as well as during transport (Keil et al., 1997). As an effect of this high refractivity pre-aged terrigenous organic matter previously stored on the continents can contribute to the OC of marine sediments leading to old sedimentary TOC radiocarbon ages (Eglinton et al., 1996; Goni et al., 1997; Jones and Gagnon, 1994; Sackett et al., 1974).

The contribution of terrigenous OC to riverine dissolved and particulate organic carbon (DOC and POC) and its effect on the apparent radiocarbon ages was investigated in several studies (e.g., Blair et al., 2003; Blair et al., 2004; Hedges et al., 1986; Kao and Liu, 1996; Raymond and Bauer, 2001a; Raymond and Bauer, 2001b). Variable radiocarbon ages were attributed to differences in morphology and geology of the respective catchments. Raymond and Bauer (2001b) suggested that the main controlling factor is the relief of the headwaters. Steep-relief catchments showed higher radiocarbon ages interpreted as the result of increased erosion of old soils and bedrock. Contrary, Blair et al. (2004) argued that OC storage in lowland soils controls the riverine POC age and overprints the headwater signals. However, they also showed that intermediate storage in soils may be bypassed in small mountainous rivers, where the POC age is determined by the bedrock and plant isotopic signal (Blair et al., 2003; Blair et al., 2004). Longworth et al. (2007) argued that particulate OM is older in headwater catchments draining both OM-rich lithology and agricultural land use areas. Moreover, Griffith et al. (2009) recently have shown that at least in densely populated catchments riverine DOC and POC radiocarbon ages are biased by sewage of wastewater contributing high

amounts (~25%) of fossil carbon. Accordingly, riverine DOC and POC may not be good indicators for the estimation of controlling factors determining the terrigenous OM age.

Vascular plants are the main producers of terrigenous organic matter and their recalcitrant organic matter found in marine sediments includes biomacromolecules (e.g., lignin or cellulose) as well as lipid epicuticular waxes (Burdige, 2005; Hedges and Keil, 1995; Hedges et al., 1997). Such leaf wax lipids comprise *inter alia* long-chain *n*-alkanes, *n*-alkanols and *n*-alkanoic acids which are thought to be relatively resistant to biodegradation and hence survive transport over long distances and timescales with the original, e.g., isotopic, information entrained (Eglinton and Eglinton, 2008; Eglinton and Hamilton, 1967; Hedges et al., 1997). The use of compound-specific radiocarbon analysis of these vascular plant biomarkers can provide important information on their average residence time in global reservoirs.

Pearson and Eglinton (2000) estimated mean terrigenous residence times for higher plant wax derived *n*-alkanes from Santa Monica Basin sediments to be less than 100 years. Their findings were corroborated by radiocarbon dates of long-chain *n*-fatty acids from Santa Monica and Santa Barbara Basins by Mollenhauer and Eglinton (2007). Likewise, Eglinton et al. (1997) demonstrated that terrigenous vascular plant *n*-alkanes from the Central Black Sea exhibit similar ages as marine autochthonous biomarkers, implying the relative freshness and short mean terrigenous residence time of the continental plant waxes. In contrast, in the Arabian Sea higher plant wax radiocarbon ages were up to 5000 years likely supplied from desiccated lake sediments or paleosols by dust plumes from the Arabian Peninsula or the Horn of Africa (Eglinton et al., 1997). Using marine sediments from the Beaufort Sea, a terrestrial residence time of 5000 to 10,000 years was estimated by Drenzek et al. (2007) for the North American Arctic by radiocarbon dating long chain *n*-fatty acids delivered by the Mackenzie River. Drenzek (2007) furthermore investigated vascular plant long-chain *n*-fatty acids in sediments from Cariaco Basin and Saanich Inlet to assess terrestrial residence times in detail, subdividing terrigenous organic matter into pools of decadal and millennial age. For the Cariaco Basin average terrestrial residence times of 10 years and 2570 years were found, where the millennial pool accounts for the majority (70–90%) of the continental biomarker supply. Residence times for the Saanich Inlet are significantly higher, with the respective pools averaging 20 years and 5170 years (>80%). Additionally, there is an annually delivered fraction of modern age, interpreted to be supplied by aeolian transport. These data imply significant differences in terrestrial residence time between different regions, which might again be controlled by climate, geology, or morphology.

Here we present compound-specific radiocarbon data of terrigenous long chain *n*-alkanes and *n*-alkanoic acids (*n*-fatty acids) derived from vascular plants and total organic carbon (TOC) as well as geochemical proxy data (Branched and Isoprenoid

Tetraether Index; Hopmans et al., 2004) for five core top sample transects reaching from river mouths to the deep basin of the Black Sea. These data are used to evaluate the timescales of terrestrial organic matter supply and intermediate storage, e.g., in soils (average residence time) of different hinterland regimes. The results are interpreted in context of climatic, topographic and geologic characteristics of the respective hinterlands to assess the controlling factors determining average terrestrial residence times.

### 3.2 STUDY AREA

The Black Sea is a large semi-enclosed basin, whose water body is strongly stratified with oxygenated surface waters and constantly anoxic conditions below about 120–150 m water depth (Sorokin, 1983). Its north-western part is dominated by a large shelf area (Figure 3.1), while in the south-western and eastern Black Sea steep slopes plunge into the anoxic zone at short distances from the shore (Simoneit, 1977a; Sorokin, 1983; Teodoru et al., 2007).

A number of major rivers as well as smaller rivers and creeks drain into the Black Sea including the Danube, Dniester, Kuban and Don, Çoruh, and Gülcü and Çatalağci Rivers. Among the respective drainage areas the size and discharge (Table 3.1), climate and ecology and the near-shore topography differ substantially. The northern Black Sea drainage area is dominated by the Danube River, accounting for approximately 58% of the basin's freshwater input (Table 3.1) (Jaoshvili, 2002; Panin and Jipa, 2002; Teodoru et al., 2007) discharged through the three major delta branches Chilia, Sulina and Sfântu Gheorghe. The catchment area of the Danube River and its tributaries includes the

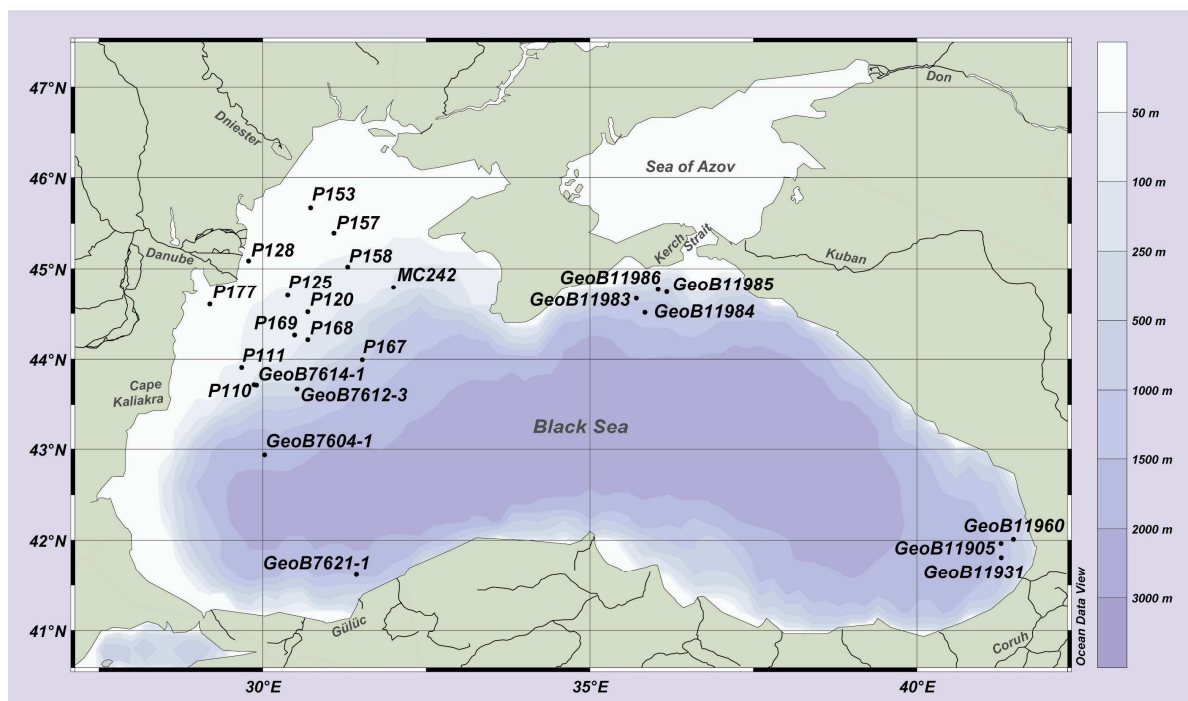


Figure 3.1 Study area with core locations.

river	drainage area [km <sup>2</sup> ]	water discharge [km <sup>3</sup> /yr]	sediment discharge [Mt/yr]
Danube <sup>a,b</sup>	817,000	200.0	51.7
Dniester <sup>a,b</sup>	72,100	9.1	2.5
Kuban <sup>b</sup>	57,900	13.4	8.4
Don <sup>b</sup>	442,500	29.5	6.4
Kerch Strait <sup>c</sup>	n.d. <sup>d</sup>	55.0	n.d. <sup>d</sup>
Çoruh <sup>a,e</sup>	22,100	8.7	8.4
Gülüç and Çatalağci <sup>a,f</sup>	<3600	1.2	n.d. <sup>d</sup>

<sup>a</sup> Data from Jaoshvili (2002).  
<sup>b</sup> Data from Panin and Jipa (2002).  
<sup>c</sup> Data from Sorokin (1983).  
<sup>d</sup> No data.  
<sup>e</sup> Data from Gulin et al. (2003).  
<sup>f</sup> Data from Bakan and Büyükgüngör (2000).

Table 3.1 Drainage area characteristics of the investigated river transects.

Bohemian Mountains and the Alps, the Hungarian Plain, the Dinaric Alps, the Transylvanian Alps, the Carpathian Mountains, the Balkan Mountains as well as the Romanian Plain and Bessarabia close to its delta. Several steep mountainous areas alternating with lowlands characterize the Danube catchment relief. To the north-east of the Danube drainage area, the catchment area of the Dniester River drains the northernmost Carpathian Mountains and discharges into a marshy delta system in its flood plain (Jaoshvili, 2002). Besides the steep headwater area, the Dniester drainage area is approximately evenly split in upland and lowland areas with less relief. The Sea of Azov, which is connected to the Black Sea via the Kerch Strait, receives freshwater largely from the Kuban and the Don Rivers draining the Caucasus Mountains, the Central Russian Hills and the Russian Plain. Very steep relief characterizes the Kuban River headwater region, whereas the lower Kuban and the Don River catchment relieves are low. Along the SW margin of the Black Sea the Çoruh River drains the very steep Eastern Pontic Mountains. In the South, the smaller Güllük and Çatalağci streams are draining a lower upland area of the Western Pontic Mountains characterized by intermediate relief.

Climatically, the Black Sea drainage area can be separated into two zones. In its northern part a temperate continental climate prevails, which is characterized by summer precipitation. In its southern part the Black Sea drainage area is influenced by Mediterranean climate with prevailing winter precipitation (Breckle et al., 1994). The entire catchment covers three vegetation zones. The northern Black Sea drainage area, ranging from the Danube delta to the Sea of Azov and the foothills of the Caucasus Mountains, belongs to the Pontic steppe characterized by grassland vegetation mainly growing on Chernozem soils (Bohn et al., 2003; Driessen et al., 2001). The western and eastern Black Sea drainage area, ranging from the Danube drainage area to the Bosphorus and from the Caucasus Mountains foothills to the Turkish border, is characterized by temperate coniferous, deciduous or mixed forests typically growing on Cambisol, Luvisol and also Leptosol soils (Bohn et al., 2003; Driessen et al., 2001). In

the South, ranging from the Bosphorus to the Georgian border, typical Mediterranean (maquis) vegetation grows on Cambisol, chromic Cambisol, and chromic Luvisol soils and Leptosol soils in the high mountainous regions (Driessen et al., 2001; Tavernier et al., 1963).

### 3.3 MATERIALS AND METHODS

In this study sediment cores from 24 locations in the Black Sea were used (Figure 3.1, Table 3.2). Core top samples were collected along shelf to basin transects from oxygenated shallow waters to the anoxic deep basin. The transects are located in front of the Danube and the Dniester river mouths in the NW Black Sea off Rumania and Ukraine, south of the Kerch Strait and in front of the Çoruh river mouth in the SE Black Sea off Georgia. An additional core location is situated north of the Gülc and Çatalağci river mouths in the SW Black Sea off Turkey. The cores were sampled during R/V Meteor campaigns M51/4, M72/1 and M72/3 and R/V Poseidon cruise P363. Multicore subcores were sampled in 1 cm slices on board and samples were frozen, stored and shipped in pre-combusted glass jars (plastic petri-dishes for material from M51/4 and M72/1) at

core	Longitude E	Latitude N	water depth [m]	campaign
<i>Danube River Sulina branch</i>				
P128	29°46.67'	45°04.67'	18	P363
P125	30°22.65'	44°42.01'	60	P363
P120	30°40.93'	44°30.66'	91	P363
P169	30°29.19'	44°15.48'	96	P363
P168	30°40.89'	44°12.36'	118	P363
P167	31°30.83'	43°58.88'	1336	P363
<i>Danube River Sfântu Gheorghe branch</i>				
P177	29°11.43'	44°35.76'	22	P363
P111	29°40.55'	43°53.78'	69	P363
P110	29°51.67'	43°42.61'	82	P363
GeoB7614-1	29°54.4'	43°42.8'	91	M51/4
GeoB7612-3	30°00.7'	43°40.2'	184	M51/4
GeoB7604-1	30°01.9'	42°56.2'	1988	M51/4
<i>Dniester River</i>				
P153	30°44.01'	45°39.69'	33	P363
P157	31°04.85'	45°23.22'	44	P363
P158	31°18.02'	45°01.05'	56	P363
MC242	31°59.65'	44°46.82'	227	M72/1
<i>Kerch Strait/Kuban and Don River</i>				
GeoB11985	36°09.99'	44°45.01'	95	M72/3
GeoB11986	36°01.99'	44°46.01'	173	M72/3
GeoB11983	35°42.52'	44°39.61'	747	M72/3
GeoB11984	35°49.99'	44°29.99'	1341	M72/3
<i>Çoruh River</i>				
GeoB11931	41°16.84'	41°47.84'	839	M72/3
GeoB11960	41°27.99'	42°00.35'	523	M72/3
GeoB11905	41°16.80'	41°57.43'	877	M72/3
<i>Gülc and Çatalağci River</i>				
GeoB7621-1	31°26.1'	41°36.9'	1714	M51/4

Table 3.2 Core locations along river-mouth to deep-basin transects.

–20 °C until further analysis. Core slices of up to 12 sub-cores of 0–1 cm or slices from 0–2 cm or 0–4 cm were re-combined in order to obtain sufficient material for compound-specific radiocarbon analyses.

The freeze-dried and homogenized samples were extracted in a Soxhlet-apparatus for 48 h using pre-extracted cellulose thimbles and a 9:1 (v:v) dichloromethane (DCM): methanol (MeOH) solvent mixture. The extracted total lipid extract was saponified with a 0.5M solution of potassium hydroxide (KOH) in MeOH at 85 °C for 3 h. After cooling, up to 90% of the solvent was evaporated under a stream of nitrogen. After addition of Seralpure water, neutral lipids were extracted into hexane 5 times. The residual extract was acidified to pH ~1 using 6N hydrochloric acid (HCl) and fatty acids were extracted into DCM. The neutral fraction was split into 2 equivalent halves. One half was further separated into hydrocarbons, ketones, and alcohols by use of a silica gel column (1% deactivated SiO<sub>2</sub>, 0.063–0.2 mm mesh size, column: 6 mm i.d. × 4 cm) using 4 ml of each hexane (hydrocarbons), DCM: hexane (2:1 v:v; ketones), and MeOH (alcohols). The other half was passed through an AlOx-coated SiO<sub>2</sub> column to separate apolar (eluted with 4 ml hexane: DCM 9:1 v:v) from polar compounds (eluted with 4 ml DCM: MeOH 1:1 v:v) containing glycerol dialkyl glycerol tetraethers (GDGTs). Prior to HPLC analysis of GDGTs, the polar fraction was filtered through a 0.45 µm PTFE membrane filter using a mixture of hexane: isopropanol (99:1).

For analysis of the GDGTs we used an Agilent HP1200 high performance liquid chromatography system coupled to a mass spectrometer equipped with an atmospheric pressure chemical ionization ion source (HPLC/APCI-MS) according to the method described in Hopmans et al. (2004).

The fatty acids were converted into fatty acid methyl esters (FAMEs) to allow gas chromatographic isolation. 3.5 ml MeOH of known δ<sup>13</sup>C and Δ<sup>14</sup>C and 175 µl concentrated HCl were added to the samples. After removal of air from the reaction tube by a stream of nitrogen, samples were methylated overnight at 80 °C. Afterwards 15 ml Seralpure water were added and FAMEs were extracted with hexane 5 times. Drying of extracts and separation from polar compounds was achieved by elution over a SiO<sub>2</sub> column (1% deactivated SiO<sub>2</sub>, 0.063–0.2 mm mesh size, column: 6 mm i.d. × 4 cm) covered with a 0.5 cm NaSO<sub>4</sub>-layer for removal of water, using 4 ml DCM: hexane 2:1 (v:v).

For isolation of long-chain *n*-fatty acid methyl esters (FAMEs) and long-chain *n*-alkanes, preparative capillary gas chromatography was used (Eglinton et al., 1996). Samples of 5 µl were repeatedly (about 60–80 times) injected into an Agilent HP6890N gas chromatograph equipped with a Gerstel CIS injection system and connected to a Gerstel preparative fraction collector (PFC). Separation was achieved on a Restek Rtx-XLB fused silica capillary column (30 m, 0.53 µm i.d., 0.5 µm). The CIS temperature program was 50°C (0.05 min), 12 °C/s to 320 °C (5 min), 12 °C/s to 340 °C (4 min). The *n*-alkane GC program was set 70 °C (0 min), 20 °C/min to 250 °C, 8 °C/min to

320 °C (25 min). For FAMEs, the GC oven was programmed 50 °C (1 min), 6 °C/min to 320 °C (20 min). Helium was used as carrier gas (4.8 ml/min). The transfer line and PFC were heated at 320 °C. The traps for collection of long-chain compounds (>24 carbon atoms chain-length) were maintained at 60 °C to avoid condensation of the compounds between the PFC capillary columns and the traps.

After isolation, single compounds were eluted over a SiO<sub>2</sub> column (1% deactivated SiO<sub>2</sub>, 0.063-0.2 mm mesh size, column: 6 mm i.d. x 4 cm) using 4 ml hexane: DCM (2:1 v:v) to remove potential contribution from column bleed. The isolation procedure was previously checked for blank carbon contribution and no significant contribution was detected (Mollenhauer and Rethemeyer, 2009). In order to obtain sample yields large enough for radiocarbon measurements some individual biomarker compounds (*n*-C<sub>29</sub> and *n*-C<sub>31</sub> alkanes; *n*-C<sub>28</sub> and *n*-C<sub>30</sub> FAMEs) had to be re-combined.

Samples larger than 20 µg C were radiocarbon-dated at the National Ocean Sciences Accelerator Mass Spectrometry (NOSAMS) Facility at Woods Hole Oceanographic Institution. Bulk sediment samples were submitted unprocessed, while biomarker samples were sent as CO<sub>2</sub>. For combustion purified *n*-alkanes and FAMEs were transferred into pre-combusted quartz tubes with 150 µg pre-combusted copper oxide for oxygen supply. The tubes were evacuated while immersed in dry ice, flame-sealed and subsequently combusted at 900 °C for 4 h. Resulting CO<sub>2</sub> was stripped of water and quantified. AMS measurements of TOC samples at NOSAMS were carried out using standard methods (McNichol et al., 1994). Compound-specific AMS radiocarbon measurements were performed following the protocol for small samples (Pearson et al., 1998). Samples containing less than 20 µg C were analysed at ETH Zürich using the MICADAS system equipped with a gas-ion source (Ruff et al., 2007).

Results are reported as conventional radiocarbon ages (yrs BP) and Δ<sup>14</sup>C referring to Stuiver and Polach (1977), which are corrected for isotopic fractionation by normalization to the standard δ<sup>13</sup>C value of -25‰ relative to the Vienna PeeDee Belemnite (VPDB). The radiocarbon ages of the individual *n*-fatty acids were corrected for the addition of one methyl group during derivatization using isotopic mass balance. For reporting mean terrestrial residence times calibration to calendar years (cal yrs BP) was achieved using the IntCal09 (terrigenous lipids) and Marine09 (total organic carbon) calibration data sets (Reimer et al., 2009) included in the calibration software CALIB 6.0 (Stuiver et al., 2010).

The stable carbon isotopic composition of the vascular plant biomarkers was determined using a TRACE GC Ultra coupled to a Thermo Finnigan MAT 252 IRMS system via a combustion interface. Additionally, δ<sup>13</sup>C on splits of the submitted CO<sub>2</sub> gas samples

measured at NOSAMS using a VG Optima IRMS is reported. Results are given in ‰ relative to VPDB.

### 3.4 RESULTS

#### 3.4.1 Branched and Isoprenoid Tetraether Index

The Branched and Isoprenoid Tetraether (BIT) Index (Hopmans et al., 2004) values reflect high terrigenous, soil-derived input in front of the river mouths and decreasing values further offshore along the sampled river mouth to deep basin transects (Figure 3.2A, Table 3.3). The highest BIT values are found in front of the Danube river mouth, where values as high as 0.64 (P128) and 0.40 (P177) were recorded. On these transects values decrease to 0.05 (P167) or 0.04 (GeoB7604-1) offshore. For the Dniester River transect the BIT value closest to the river mouth is 0.26 (P153) decreasing offshore to 0.04 (MC242). The same pattern is evident for the core locations off Georgia (Çoruh River) reflected by values of 0.27 (GeoB11931) decreasing to 0.04 further offshore (GeoB11960).

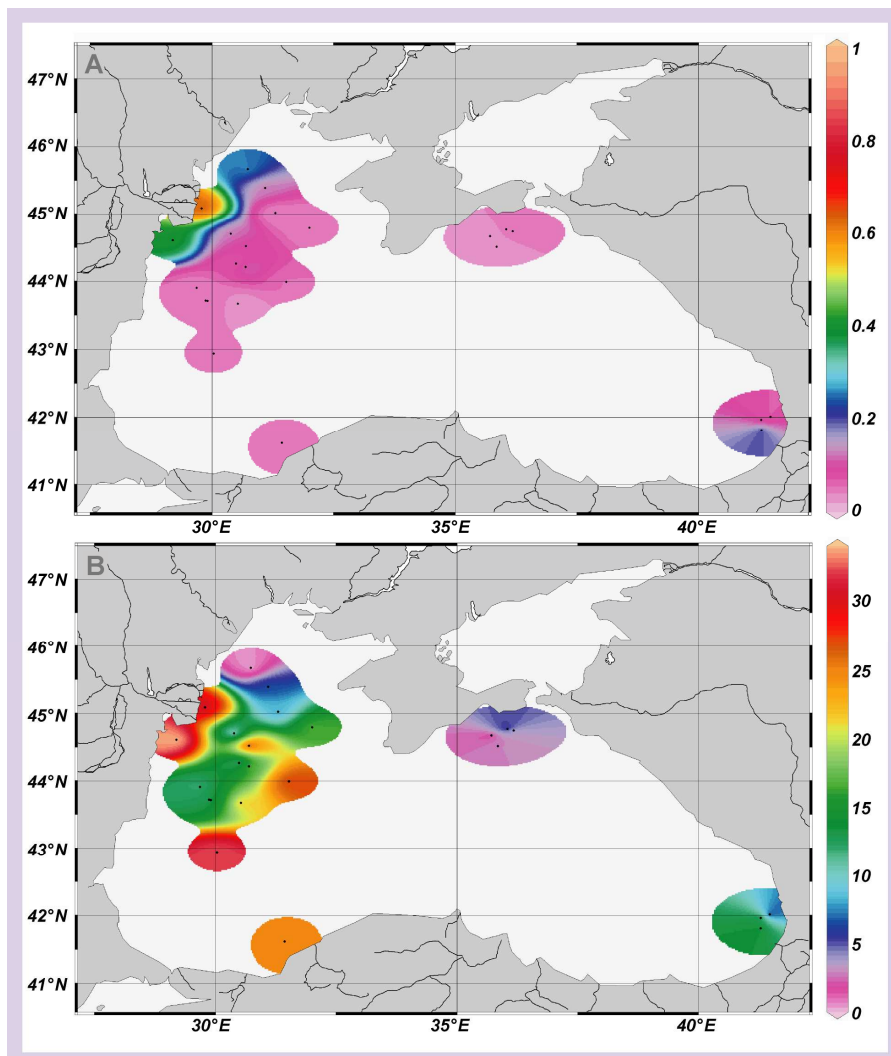


Figure 3.2 A) BIT-Index; B) Concentrations of  $C_{27+29+31+33}$  n-alkanes (mg/g TOC).

Sample	core depth [cm]	sedimentation rate [cm/kyr] <sup>a</sup>	sample age non-bioturbated [yrs] <sup>b</sup>	sample age bioturbated [yrs] <sup>c</sup>	BIT-Index <sup>d</sup>
<i>Danube River Sulina branch</i>					
P128	0-1	800	1	9	0.64
P125	0-1	350	3	21	0.12
P120	0-1	350	4	30	0.08
P169	0-1	150	7	50	0.04
P168	0-1	150	7	50	0.13
P167	0-1	60	17	anoxic	0.05
<i>Danube River Sfântu Gheorghe branch</i>					
P177	0-1	15	4	50	0.40
P111	0-1	90	11	83	0.04
P110	0-1	75	13	100	0.07
GeoB7614-1	2-4	75	53	100	0.03
GeoB7612-3	0-4	60	66	anoxic	0.02
GeoB7604-1	0-4	60	66	anoxic	0.04
<i>Dniester River</i>					
P153	0-1	400	2.5	19	0.26
P157	0-1	400	2.5	19	0.12
P158	0-1	350	3	21	0.03
MC242	0-2	100	10	anoxic	0.04
<i>Kerch Strait/ Kuban and Don River</i>					
GeoB11985	0-2	50	40	150	0.06
GeoB11986	0-2	35	58	anoxic	0.03
GeoB11983	0-2	30	66	anoxic	0.02
GeoB11984	0-2	35	58	anoxic	0.03
<i>Çoruh River</i>					
GeoB11931	0-2	100	20	anoxic	0.27
GeoB11960	0-2	100	20	anoxic	0.04
GeoB11905	0-2	100	20	anoxic	0.04
<i>Gülüç and Çatalağci River</i>					
GeoB7621-1	0-4	20	200	anoxic	0.04

<sup>a</sup> Extrapolated literature values (Calvert et al., 1987; Calvert et al., 1991; Jones and Gagnon, 1994; Arthur and Dean, 1998; Gulin, 2000; Gulin et al., 2002; Ayık et al., 2004; Giunta et al., 2007; Ivanova et al., 2007; Teodoru et al., 2007).

<sup>b</sup> Calculated using the respective sedimentation rate.

<sup>c</sup> Calculated using a mass balance model assuming a mixed layer depth of 15cm.

<sup>d</sup> Branched and Isoprenoid Tetraether Index calculated according to Hopmans et al. (2004).

**Table 3.3** Expected core top ages based on published sedimentation rates without and with the influence of bioturbation. Additionally shown is the Branched and Isoprenoid Tetraether Index at each station.

The sample transect south of the Kerch Strait as well as sample station GeoB7621-1 (Gülüç and Çatalağci River) show a much lower contribution of terrigenous GDGTs than observed along the other transects. In front of the Kerch Strait, the station closest to its mouth (GeoB11985) shows a value of only 0.06 and a further slight decrease to 0.03 (GeoB11984) is observed. For core location GeoB7621-1 the BIT value is 0.04.

### 3.4.2 Stable carbon isotope data of organic matter

#### 3.4.2.1 Total Organic Carbon (TOC)

TOC stable carbon isotopic values range from  $-22.9\text{\textperthousand}$  to  $-25.7\text{\textperthousand}$  (Table 3.4, Table 3.7 in the Appendix) for all stations. For the Dniester River transect  $\delta^{13}\text{C}$  values are increasing about  $1.1\text{\textperthousand}$  with distance offshore. However, the same spatial pattern is not apparent for both (Sulina and Sfântu Gheorghe) Danube River transects, where  $\delta^{13}\text{C}$

sample	$\Delta^{14}\text{C}$ [%]	$^{14}\text{C}$ age [yrs BP]	cal age [yrs BP]	$\delta^{13}\text{C}$ [%]	ID No. <sup>a</sup>
<i>Danube River Sulina branch</i>					
<i>P128 0-1 cm</i>					
<i>n-C<sub>29+31</sub> alkanes</i>	-599.87±3.1	7300±60	8110±60	-29.53	71672
<i>n-C<sub>26</sub> fatty acid</i>	-150.99±8.7	1260±85	1220±60	-30.08	74176
<i>n-C<sub>28+30</sub> fatty acids</i>	-216.08±5.1	1900±55	1850±50	-31.13	71676
TOC	-166.57±2.1	1410±20	950±30	-25.69	66558
<i>P168 0-1 cm</i>					
<i>n-C<sub>29+31</sub> alkanes</i>	-204.70±16.8	1780±170	1710±190	-31.23	71674
<i>n-C<sub>26</sub> fatty acid</i>	n.d. <sup>b</sup>	n.d. <sup>b</sup>	n.d. <sup>b</sup>	-28.85	74177
<i>n-C<sub>28+30</sub> fatty acids</i>	-26.76±5.4	160±45	200±30	-32.04	74178
TOC	-104.11±3.1	825±25	470±25	-24.21	66565
<i>P167 0-1 cm</i>					
<i>n-C<sub>29+31</sub> alkanes</i>	-134.60±17.8	1100±160	1040±140	-32.05	71673
TOC	44.45±2.5	bomb- <sup>14</sup> C		-24.56	66557
<i>Danube River Sfântu Gheorghe branch</i>					
<i>P177 0-1 cm</i>					
<i>n-C<sub>29+31</sub> alkanes</i>	-433.36±12.7	4500±180	5100±220	-32.56	71675
<i>n-C<sub>26</sub> fatty acid</i>	-254.62±10.0	2300±110	2310±160	n.d. <sup>b</sup>	74179
<i>n-C<sub>28+30</sub> fatty acids</i>	-395.78±8.8	3990±120	4450±170	-28.80	74180
TOC	-161.01±3.4	1350±30	900±40	-25.17	66564
<i>P110 0-1 cm</i>					
<i>n-C<sub>29+31</sub> alkanes</i>	-314.91±17.8	2980±210	750±230	-31.52	71671
<i>n-C<sub>28</sub> fatty acid<sup>c</sup></i>	-5.88±14.0	bomb- <sup>14</sup> C		-24.87	ETH37363
TOC	-36.29±2.5	240±20		-23.32	66559
<i>GeoB7614-1 2-4 cm</i>					
<i>n-C<sub>26+28</sub> fatty acids</i>	-127.18±6.0	1040±130	930±145	-29.55	ETH37361
TOC	-30.71±3.0	195±25		-23.33	58961
<i>GeoB7612-3 0-4 cm</i>					
<i>n-C<sub>24</sub> fatty acid</i>	-28.91±13.4	180±110	180±55	-27.09	60202
<i>n-C<sub>28</sub> fatty acid</i>	-103.13±15.5	820±120	740±65	n.d. <sup>b</sup>	60203
TOC	-97.35±3.6	765±30	420±45	-24.19	58960
<i>GeoB7604-1 0-4 cm</i>					
<i>n-C<sub>24</sub> fatty acid</i>	75.06±10.6	bomb- <sup>14</sup> C		-27.47	58965
TOC	34.84±5.3	bomb- <sup>14</sup> C		-24.59	58962
<i>Kerch Strait/ Kuban and Don River</i>					
<i>GeoB11985 0-2 cm</i>					
<i>n-C<sub>29+31</sub> alkanes</i>	-291.08±27	2710±220	2880±200	-31.30	ETH37367
<i>n-C<sub>24</sub> fatty acid</i>	13.92±10.7	bomb- <sup>14</sup> C		-26.56	67343
<i>n-C<sub>26</sub> fatty acid</i>	-97.12±12.5	765±110	720±80	-26.81	67344
<i>n-C<sub>28+30</sub> fatty acids</i>	-137.93±11.6	1140±110	1070±110	-30.08	67345
TOC	-134.59±3.5	1100±30	660±115	-23.41	66570
<i>GeoB11983 0-2 cm</i>					
<i>n-C<sub>29+31</sub> alkanes</i>	-162.63±12.9	1370±120	1290±120	-31.62	71669
<i>n-C<sub>24</sub> fatty acid</i>	-68.84±10.9	520±95	530±35	-27.02	67341
TOC	-71.93±3.4	540±30	190±55	-24.22	66569
<i>Çoruh River</i>					
<i>GeoB11960 0-2 cm</i>					
<i>n-C<sub>29+31</sub> alkanes</i>	-178.85±14.2	1530±140	1430±130	-32.90	71668
TOC	-77.40±3.4	590±30	250±30	-24.17	66571
<i>Gülüç and Çatalağci River</i>					
<i>GeoB7621-1 0-4 cm</i>					
<i>n-C<sub>24</sub> fatty acid</i>	30.06±0.5	bomb- <sup>14</sup> C		-26.07	60198
<i>n-C<sub>26</sub> fatty acid</i>	-119.73±14.8	970±140	860±125	-27.16	60199
<i>n-C<sub>28+30</sub> fatty acids<sup>d</sup></i>	-163.30±9.4	1370±90	1300±70	-27.93	67337
TOC	-123.27±3.2	1000±30	590±35	-23.77	58959

<sup>a</sup> NOSAMS or ETHZ ID number<sup>b</sup> No data.<sup>c</sup> Contamination of this sample with modern <sup>14</sup>C is considered likely.<sup>d</sup> 4-8 cm core depth.

Table 3.4 Radiocarbon and stable carbon isotopic data along river-mouth to deep-basin transects. Errors are given as  $1\sigma$  analytical uncertainty.

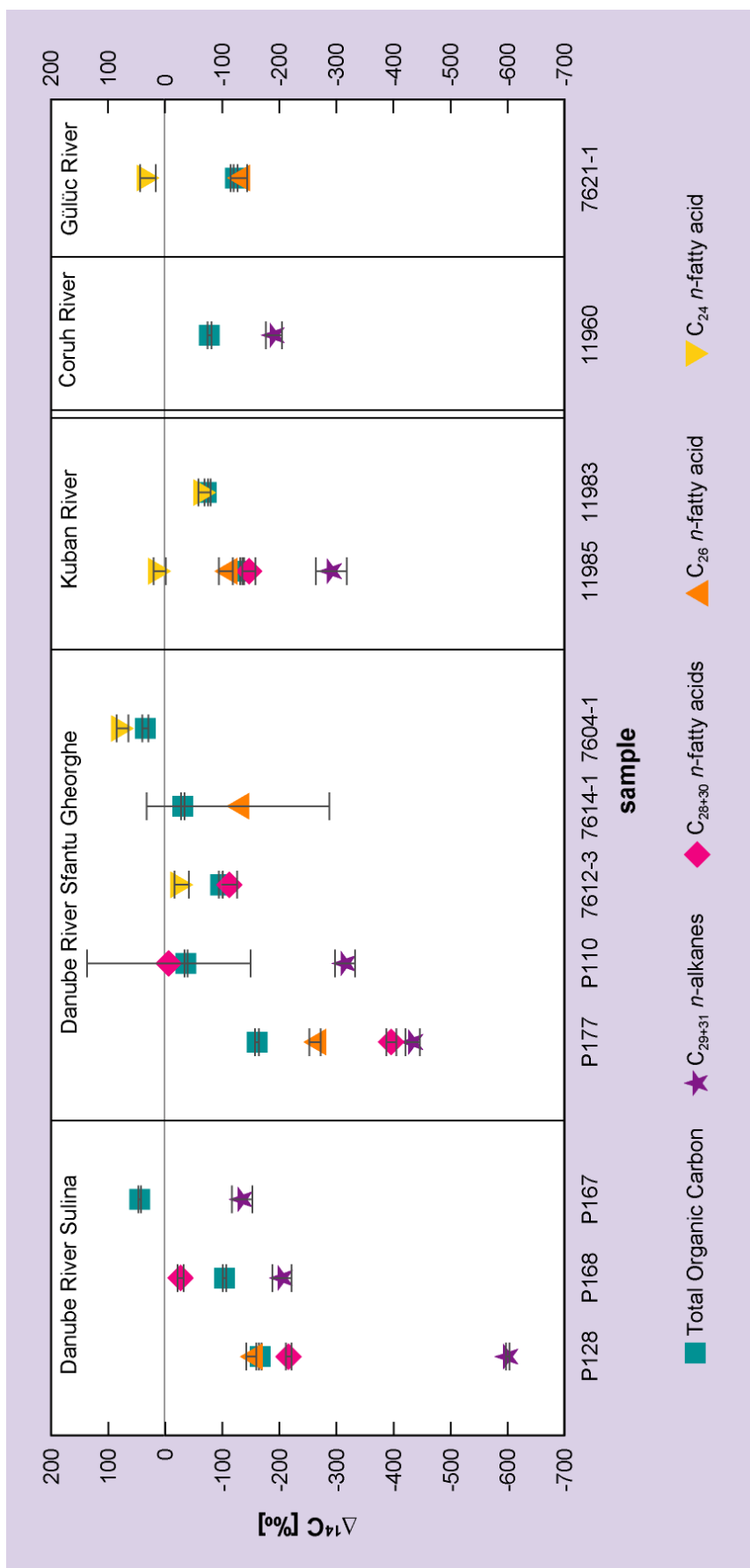


**Figure 3.3** Radiocarbon data ( $\Delta^{14}\text{C}$ ) for core locations along river-mouth to deep-basin transects. Doubled line indicates differentiation of northern and southern transects according to climatic regime. Error bars are given as  $1\sigma$  analytical error.

values are first increasing (P125 and P110) away from the river mouth (P128 and P177), but decreasing again further seawards (from P120 to P167 and GeoB7614-1 to 7604-1). Along the Kerch Strait transect TOC  $\delta^{13}\text{C}$  values are decreasing from  $-23.4\text{\textperthousand}$  (GeoB11985) to  $-24.2\text{\textperthousand}$  (GeoB11983).

### 3.4.2.2 Long chain *n*-alkanes and *n*-fatty acids

The  $\delta^{13}\text{C}$  values of long chain *n*-alkanes (Table 3.4) range from  $-29.5\text{\textperthousand}$  to  $-32.9\text{\textperthousand}$  for all stations where sample amounts were high enough to perform preparative gas-chromatographic isolation. No spatial distribution pattern is obvious. Stable carbon isotopic values of long chain *n*-fatty acids range from  $-26.1\text{\textperthousand}$  to  $-27.5\text{\textperthousand}$  for *n*-C<sub>24</sub> fatty acids, from  $-26.8\text{\textperthousand}$  to  $-30.1\text{\textperthousand}$  for *n*-C<sub>26</sub> fatty acids, and from  $-24.9\text{\textperthousand}$  to  $-32.0\text{\textperthousand}$  for *n*-C<sub>28</sub> or *n*-C<sub>28+30</sub> fatty acids, respectively. For samples with *n*-fatty acid homologues of different chain-lengths, i.e. P128, P168, GeoB11985, and GeoB7621-1, increasing  $\delta^{13}\text{C}$  depletion is evident with increasing chain-length. Analogous to the long chain *n*-alkanes a systematic spatial distribution pattern is missing.

### 3.4.3 Radiocarbon data of organic matter

#### 3.4.3.1 Total Organic Carbon (TOC)

In general, along all transects TOC ages decrease with distance from the coast (Table 3.4, Figure 3.3). The oldest radiocarbon ages are found in front of the Danube river mouth at stations P128 ( $1410\pm20$  yrs BP) and P177 ( $1350\pm30$  yrs BP). TOC conventional radiocarbon ages decrease with distance offshore reaching modern values at stations P167 and GeoB7604-1, indicated by presence of bomb-<sup>14</sup>C. On the Dniester transect, the radiocarbon age at near shore station P153 ( $400\pm30$  yrs BP; Appendix) is much younger compared to the Danube river mouth stations, but decreasing ages along the transect are likewise observed (bomb-<sup>14</sup>C at station P158). Closest to the Kerch Strait the TOC radiocarbon age is  $1100\pm30$  yrs BP (GeoB11985), becoming younger offshore ( $540\pm30$  yrs BP; GeoB11983). For the Çoruh River TOC <sup>14</sup>C data are only available for station GeoB11960 with a <sup>14</sup>C age of  $590\pm30$  yrs BP. In the SW Black Sea (GeoB7621-1) the TOC radiocarbon age is  $1000\pm30$  yrs BP.

#### 3.4.3.1 Long-chain *n*-alkanes

The radiocarbon age distribution of long-chain *n*-C<sub>29+31</sub> alkanes reflects the pattern observed for the TOC ages (Table 3.4, Figure 3.3). The *n*-alkanes are oldest in front of the Danube river mouth ( $7300\pm60$  yrs BP for P128 and  $4500\pm180$  yrs BP for P177) and show decreasing ages towards the offshore core locations with  $1780\pm170$  yrs BP (P168) and  $1100\pm160$  yrs BP (P167) on the Sulina transect as well as  $2980\pm210$  yrs BP (P110) on the Sfântu Gheorghe transect. In front of the Kerch Strait *n*-alkanes are  $2710\pm220$

yrs BP (GeoB11985) decreasing to  $1370 \pm 120$  yrs BP (GeoB11983). Off Georgia, core location GeoB11960 reflects  $n\text{-C}_{29+31}$  alkane radiocarbon ages of  $1530 \pm 140$  yrs BP.

Sediments from the stations along the Dniester transect (P153, P157, P158 and MC242) as well as station GeoB7621-1 did not yield sufficient  $n$ -alkanes for radiocarbon dating.

### 3.4.3.2 Long-chain $n$ -fatty acids

Like the  $n$ -alkane and TOC radiocarbon age distribution, the vascular plant  $n$ -fatty acids show decreasing ages towards offshore locations, but  $n$ -fatty acids are always younger than corresponding  $n$ -alkanes (Table 3.4, Figure 3.3). In front of the Danube River  $n\text{-C}_{28+30}$  fatty acids are  $1900 \pm 55$  yrs BP (P128) decreasing to  $160 \pm 45$  yrs BP (P168). At station P177  $n\text{-C}_{28+30}$  fatty acids are  $3990 \pm 120$  yrs BP. As an exception from the general pattern, the radiocarbon ages of  $n\text{-C}_{28}$  fatty acids along the Sfântu Gheorghe transect increase again with distance offshore. Whereas  $n\text{-C}_{28}$  fatty acid at station P110 contains bomb- $^{14}\text{C}$ , GeoB7612-3  $n\text{-C}_{28}$  fatty acid is  $820 \pm 120$  yrs BP and GeoB7614-1  $n\text{-C}_{26+28}$  fatty acids are even as old as  $1040 \pm 130$  yrs BP. However, considering the enriched  $\delta^{13}\text{C}$  value ( $-24.9\text{\textperthousand}$ ) of the  $n\text{-C}_{28}$  fatty acid at station P110, we suspect contamination of this sample.

In front of the Kerch Strait  $n\text{-C}_{28+30}$  fatty acids show an radiocarbon age of  $1140 \pm 110$  yrs BP (GeoB11985), decreasing to  $520 \pm 95$  yrs BP for  $n\text{-C}_{24}$  fatty acid at station GeoB11983. Off Turkey core location GeoB7621-1 yields an  $n\text{-C}_{28+30}$  fatty acids radiocarbon age of  $1370 \pm 90$  yrs BP.

In general, radiocarbon ages for  $n$ -fatty acid homologues increase with increasing chain-length (Table 3.4). As an example, for site GeoB11985  $n\text{-C}_{24}$  fatty acid contains bomb- $^{14}\text{C}$ ,  $n\text{-C}_{26}$  fatty acid is  $765 \pm 110$  yrs BP and  $n\text{-C}_{28+30}$  fatty acids are  $1140 \pm 110$  yrs BP. Again,  $n$ -fatty acid concentrations of samples from the Dniester and the Çoruh transects were too low for radiocarbon dating.

## 3.5. DISCUSSION

### 3.5.1 Input of terrigenous organic matter and its effect on TOC age

The BIT index can be used to estimate the riverine contribution of soil-derived organic matter to the total sedimentary organic matter (Hopmans et al., 2004). Here, the BIT Index reflects a seawards decreasing riverine terrigenous input to the sedimentary OC for all sample trajectories (Figure 3.2A) as would be expected for river-borne terrigenous input that gets diluted seawards where higher marine contribution controls the sedimentary OC.

The high terrigenous input in front of the Danube River is reflected by high TOC radiocarbon ages, which has been attributed to input of pre-aged or relict (reworked) OC

to the total sedimentary OC (Eglinton et al., 1996; Jones and Gagnon, 1994; Sackett et al., 1974). Pre-aged OC may derive from various sources including terrestrial vascular plant and soil OC or fossil,  $^{14}\text{C}$ -dead material from petrogenic sources like petroleum, petroleum source rocks or sedimentary rock weathering, leading to an increase of the bulk OC radiocarbon age (e.g., Dickens et al., 2004; Drenzek et al., 2007; Drenzek et al., 2009; Eglinton et al., 2002; Ohkouchi et al., 2003; Pearson and Eglinton, 2000; Pearson et al., 2001; Raymond and Bauer, 2001a). An additional source of pre-aged OC may be black carbon derived from incomplete combustion of, e.g., fossil fuel ( $^{14}\text{C}$ -free) or biomass (contemporary  $^{14}\text{C}$  concentration), which is mainly supplied to oceanic sediments by aerosol deposition (Eglinton et al., 2002; Masiello and Druffel, 1998). Therefore, bulk TOC ages are unspecific indicators of input of pre-aged or fossil OM, which can be derived from a multitude of different sources.

### 3.5.2 Radiocarbon ages of leaf-wax derived lipids

Long chain *n*-alkanes and *n*-fatty acids, which, according to their stable carbon isotopic composition derive mainly from C<sub>3</sub> plant leaf waxes (Table 3.4; Chikaraishi et al., 2004; Collister et al., 1994; Conte et al., 2003; Lockheart et al., 1997; Rieley et al., 1993), are significantly pre-aged (up to 7300 yrs BP; P128) upon deposition in core top sediments (Table 3.4). This may be due to their resistance to degradation caused by low reactivity or their stabilization by, for instance, absorption on mineral surfaces (Canuel and Martens, 1996; Eglinton and Eglinton, 2008; Eglinton and Hamilton, 1967; Sun and Wakeham, 1994). Accordingly, individual long chain *n*-alkanes and *n*-fatty acids can resist environmental decomposition resulting in old radiocarbon ages determined by the respective average residence time of the compounds in active carbon reservoirs such as soils or riverine sediments.

It is evident that *n*-fatty acids in our study are significantly younger (up to 5400 yrs) than corresponding *n*-alkanes. This was also reported for the Santa Monica Basin by Pearson et al. (2001), for the Beaufort Sea by Drenzek et al. (2007) and for the Bermuda Rise by Eglinton and Repeta (2003). Younger *n*-fatty acids could be caused by their higher reactivity compared to *n*-alkanes as shown by Sun and Wakeham (1994) and Canuel and Martens (1996), making them more prone to degradation. Furthermore, sedimentary long-chain *n*-alkanes might be contaminated by *n*-alkanes derived from petrogenic sources (Pearson and Eglinton, 2000).

For the *n*-fatty acids an increasing age (375 to 1690 yrs per C<sub>2</sub> group) with increasing chain-length is observed. This pattern has previously been reported by several authors (Drenzek, 2007; Drenzek et al., 2007; Drenzek et al., 2009; Eglinton and Repeta, 2003; Mollenhauer and Eglinton, 2007; Ohkouchi et al., 2003; Pearson et al., 2001; Uchida et al., 2001; Uchida et al., 2005) and might be caused by several effects or a combination of these, including mixing between allochthonous and autochthonous

sources or different chemical resistance. A likely cause is the higher resistance to degradation of long-chain *n*-fatty acids compared to their shorter chain-length homologues, caused by different reactivity, molecular structure and association with mineral surfaces (Camacho-Ibar et al., 2003; Canuel and Martens, 1996; Haddad et al., 1991). Contrary, mixing from autochthonous and allochthonous sources is rather unlikely. Although fatty acids up to *n*-C<sub>28</sub> have been found to be synthesized by some algae, such sources are exceptional (Schouten et al., 1998; Volkman et al., 1980b) and should not cause the radiocarbon age differences between *n*-C<sub>26</sub>, *n*-C<sub>28</sub>, and *n*-C<sub>28+30</sub> fatty acids. However, autochthonous contribution may indeed be a reason for the younger ages of the *n*-C<sub>24</sub> fatty acid (Sun and Wakeham, 1994). In this study we show isotopic data for *n*-C<sub>24</sub> fatty acid only because quantities of *n*-C<sub>26</sub>, *n*-C<sub>28</sub> or *n*-C<sub>28+30</sub> fatty acids were not high enough to obtain <sup>14</sup>C analysis for every sample.

### 3.5.3 Estimate of residence times in terrestrial reservoirs

Since vascular plants fix CO<sub>2</sub> from the ambient air incorporating the atmospheric <sup>14</sup>C signature, any deviation from this atmospheric signature can be attributed to retention in intermediate (terrigenous or marine) reservoirs. In a first approach we can use the vascular plant *n*-C<sub>29+31</sub> alkanes and *n*-C<sub>28+30</sub> fatty acids radiocarbon ages to estimate mean terrestrial residence times in the continental reservoir prior to delivery to the Black Sea. For the purpose of assessing the controlling factors for average terrestrial residence time, we will consider only the youngest measured age of a terrigenous lipid, mostly *n*-C<sub>28+30</sub> fatty acids. This approach furthermore requires the assumption that all leaf-wax lipids are supplied from one uniform reservoir and by the same delivery mechanism (e.g., riverine transport). To account for the influence of each sedimentological setting, the respective "true" surface sediment ages as expected without any contribution of pre-aged organic matter are subtracted from the calibrated biomarker ages. Surface sediment ages (Table 3.3) are calculated using published sedimentation rates (Arthur and Dean, 1998; Ayçik et al., 2004; Barnes and Cochran, 1991; Calvert et al., 1987; Calvert et al., 1991; Eckert et al., 2009; Giunta et al., 2007; Gulin, 2000; Gulin et al., 2002; Ivanova et al., 2007; Jones and Gagnon, 1994; Teodoru et al., 2007) including mass balance correction for bioturbation assuming a 15 cm mixed layer depth for those stations influenced by oxic bottom waters (Table 3.3). This calculation reveals that with exception of GeoB7621, the core-tops were expected to reflect only a few decades up to a century.

For the Danube River Sulina branch the long chain *n*-C<sub>29+31</sub> alkanes immediately deposited in front of the delta (station P128) translate to an average terrestrial residence time of 8100±60 yrs (Table 3.5). The more labile *n*-C<sub>28+30</sub> fatty acids at the same station represent a younger pool with a mean residence time of 1840±50 yrs. At the Sfântu

sample	<i>n</i> -C <sub>29+31</sub> alkanes cal age [yrs BP]	<i>n</i> -C <sub>29+31</sub> alkanes terrestrial residence time [yrs] <sup>a</sup>	<i>n</i> -C <sub>28+30</sub> fatty acids cal age [yrs BP]	<i>n</i> -C <sub>28+30</sub> fatty acids terrestrial residence time [yrs]
<i>Danube River</i>				
P128	8110±60	8100±60	1850±50	1840±50
P177	5100±220	5050±220	4450±170	4400±170
<i>Kerch Strait/ Kuban and Don River</i>				
GeoB11985	2880±200	2730±200	1070±110	920±110
<i>Çoruh River</i>				
GeoB11960	1430±130	1420±130	n.d. <sup>b</sup>	n.d.
<i>Gülüç and Çatalağci River</i>				
GeoB7621-1	950±60 <sup>c</sup>	850±60	1300±70 <sup>d</sup>	1000±70 <sup>e</sup>

<sup>a</sup> Calculated subtracting the respective sediment core top ages (Table 3) from the calibrated ages (Table 4).  
<sup>b</sup> No data.  
<sup>c</sup> *n*-C<sub>29</sub> alkane (42°N, 32°E); data from Wakeham (2006).  
<sup>d</sup> Calibrated age for 4–8 cm core depth.  
<sup>e</sup> Mean terrestrial residence time calculated subtracting the sediment age for 4–8cm.

**Table 3.5** Average terrestrial residence times for the investigated river catchments deduced from the core locations closest to the river mouths.

Gheorghe branch (P177) *n*-C<sub>29+31</sub> alkanes exhibit a mean terrestrial residence time of 5050±220 yrs with corresponding *n*-C<sub>28+30</sub> fatty acids of 4400±170 yrs. The difference in residence times of the two investigated delta branches is probably caused by different morphological characteristics. While the Sulina branch is channelized and constantly dredged for shipping, the Sfântu Gheorghe branch represents a less regulated, comparatively natural meandering river landscape (Panin and Jipa, 2002; Popa, 1997). Along the channels increased water discharge inhibits intermediate sediment retention, whereas increased sedimentation in the cut off meanders may foster enhanced retention (Popa, 1997). The high fatty acid radiocarbon ages imply that anthropogenic perturbations of the natural river bed morphology reduce the capability of retaining old riverine sedimentary organic carbon.

The terrigenous biomarkers delivered through the Kerch Strait (GeoB11985) reveal average terrestrial residence times of 2730±200 yrs and 920±110 yrs for the *n*-C<sub>29+31</sub> *n*-alkanes and *n*-C<sub>28+30</sub> fatty acids, respectively. This residence time, however, may include intermediate storage in the Sea of Azov prior to delivery to the Black Sea via the Kerch Strait (Panin and Jipa, 2002). Delivery of fine grain-sized particles (containing mineral-associated biomarkers) through the Kerch Strait to the Black Sea might be associated with high discharge events from the Don and Kuban Rivers, which potentially resuspend and redistribute previously deposited fine particles. In addition, a different transport mode, e.g., aeolian supply as implied by low BIT indices, might be more important at those stations in front of the Kerch Strait. For the Gülüç and Çatalağci River (GeoB7621-1) *n*-C<sub>28+30</sub> fatty acid radiocarbon ages suggest a mean terrestrial residence time of 1000±70 yrs. The average terrestrial residence time for *n*-C<sub>29+31</sub> alkanes in the Çoruh River catchment in Georgia (GeoB11960) amounts to 1420±130 yrs.

### 3.5.3.1 Effect of drainage area type on terrestrial residence time

Terrigenous residence time is presumably a function of the compounds' physicochemical properties such as structure, molecular size, polarity, polymeric nature, reactivity, mineral association and environmental properties like aridity, temperature, topography, soil type, wind stress, size and topography of the catchment area as well as changes caused by anthropogenic influence (Drenzek, 2007; Hedges and Oades, 1997; Oades, 1988; Post et al., 1985; Raymond and Bauer, 2001b; Trumbore, 1997; Trumbore, 2009). Hence, the mean terrestrial residence times should be different in the different river catchments of the Black Sea. To assess the influence of different morphological or climatic hinterland characteristics on average terrestrial residence times, the radiocarbon ages of  $n\text{-C}_{29+31}$  alkanes and  $n\text{-C}_{28+30}$  fatty acids of those stations immediately in front of the respective river mouths (P128, P177, GeoB11985, GeoB11960, and GeoB7621-1) are compared. By grouping climatically comparable drainage areas we attempt to identify morphological control parameters determining average terrestrial residence times. Likewise, grouping comparable catchment morphology aims at the evaluation of climatic controls. In this discussion, we will always consider the youngest measured age, typically that of an  $n$ -fatty acid, the best estimate of mean terrestrial residence time.

Considering the morphological properties of the entire drainage area of climatically comparable catchments, its size and relief appear to influence biomarker turnover. The greater Danube River catchment is characterized by a higher average terrestrial residence time (Table 3.5) compared to the smaller catchment area of the Kuban and Don Rivers, as would be expected by prolonged duration of terrigenous OM delivery due to transport over longer distances. This is particularly pronounced when considering only the estimate of average terrestrial residence time of 4400 yrs derived from the sample in front of the Sfântu Gheorghe branch, which supposedly reflects the natural situation better than the channelized Sulina branch. The average terrestrial residence time is also higher for the larger Çoruh River catchment compared to the Güllük and Çatalağci drainage area (Table 3.5). Moreover, high relief appears to correlate with higher residence times as observed for the turnover in the Çoruh and Danube drainage areas, which is apparently higher compared to the catchments of the Güllük/Çatalağci and Kuban/Don, respectively. Although the highest peaks of the Caucasus Mountains in the Kuban catchment exceed those in the Danube catchment, we consider the larger proportion of high relief area in the Danube catchment the more important relief factor controlling turnover times.

This observation is consistent with the results of Raymond and Bauer (2001b), who found the same correlation for riverine DOC and POC, which are older in rivers draining high relief headwater areas. The authors argue that accumulation of fresh OC might be substantially reduced in the high relief hinterlands and erosion of older soil OC and sedimentary rock is more likely than in the lower relief catchment areas, where

ongoing build-up of soil allows erosion of more recent OC (Raymond and Bauer, 2001b). Contrary, Blair et al. (2004) state that lowland areas contribute aged terrestrial soil OC to the riverine POC overprinting the upstream (steep relief) signals. Accordingly, if only the lower drainage area is considered, no apparent morphological difference of the Danube and Kuban is obvious. Both lowlands are arable land and both river deltas include wetlands, lakes, and ponds being periodically flooded, but the Danube's flowpath through the lowland portion of the drainage area is longer and its spatial extent is larger. This indicates that the average residence time of organic matter increases with size and length of the flowpath through the lowlands in large river catchments. Accordingly, when assessing the role of morphology in determining average terrestrial residence time, catchment size is the critical morphological control rather than relief as proposed by Raymond and Bauer (2001b).

Soil organic carbon turnover exhibits a strong climatic latitudinal and altitudinal dependence being lowest in warm deserts and greatest in cool, wet environments (Post et al., 1985; Trumbore, 1993). As the storage capacity rises, the potential of organic matter aging should rise as well. The storage of soil OM is controlled by inputs from plant production and outputs through heterotrophic decomposition. Generally, under humid climates, plant production and decomposition rate increase with increasing temperature, but the relative increase in decomposition rate is greater than the increase in plant production. In humid climates, the average age of soil OM should therefore decrease with increasing temperature. In arid to sub-humid areas where precipitation is the controlling parameter of plant production and decomposition, the relative increase of plant production is higher when precipitation increases (Jobbágy and Jackson, 2000). The average soil OM age in arid areas should therefore increase with increasing precipitation. Accordingly, rivers draining different climatic catchments should carry soil OM that differs in age as a function of climate. Overall, the soil OM age under humid in comparison to Mediterranean climate was reported to be younger (Becker-Heidmann et al., 1996). A higher average terrestrial residence time would therefore be expected for the southern river catchments of the Black Sea based on the soil inventories. However, if moisture is not a limiting factor higher soil carbon ages were reported for cooler temperatures (Trumbore et al., 1996; Trumbore, 2009). Since moisture is not a limiting factor in the Çoruh and Gülcük/Çatalağci River catchments, which indeed have higher annual precipitation compared to the Danube and Kuban/Don River drainage areas, their respective mean terrestrial residence time might be smaller than in arid Mediterranean catchments.

Neglecting any sedimentological differences, the best assessment of the influence of climate on average terrestrial residence time would be achieved by comparison of the morphologically and spatially most similar Kuban and Çoruh Rivers. Major differences

between these two river drainage areas include precipitation, temperature, and soil as well as vegetation type. However, the terrigenous organic matter from the stations in front of the Kerch Strait is a mixture of organic matter delivered by both the Kuban and Don River, which themselves are very different in catchment size and morphology (and, by inference, in residence time) and cannot be disentangled in the sediments. Therefore, a comparison of the Kuban and Çoruh River catchment residence times is not feasible. This comparison is even further complicated by the fact that BIT indices at the Kerch Strait indicate very low contribution of fluvially transported terrigenous organic matter.

A general comparison of the average terrestrial residence times of the northern and southern river catchments shows that they are higher for the Danube than for the southern catchments. The lowest measured ages for the Kuban/Don drainage areas are not significantly different from those for the Gülcü/Çatalağci catchments (Table 3.5). In the above discussion the size of the catchment was identified as a strong control on the age of organic matter delivered to adjacent marine sediments. The northern drainage areas are substantially (up to ~23 times) larger than the southern catchments. Therefore, a climatically induced difference in residence time may be overridden by the effect of catchment size. In spite of the large difference in catchment size between the Kuban/Don drainage areas versus those of the Gülcü/Çatalağci Rivers, the average residence time for terrigenous OM seems to be comparable. This may imply that indeed the Mediterranean climate in the southern region leads to longer retention of terrestrial organic matter in the soils. However, like for the Kerch Strait sample, the BIT index of the Gülcü/Çatalağci site implies very low contributions of fluvially supplied terrigenous organic matter. Therefore, our data do not allow the identification of an unambiguous climate dependency of average terrestrial residence time.

### *3.5.3.2 Spatial distribution of biomarker radiocarbon ages: the effect of origin and transport mode on average terrestrial residence time*

Surface sediments from river mouth core locations are most useful to estimate average terrestrial residence times for material delivered by the rivers, since potential sedimentological or hydrodynamic effects on radiocarbon ages are minimized. Along-transect data provide additional information by allowing the identification of further sources of long chain *n*-alkanes and *n*-fatty acids contributing to the sedimentary OM and the assessment of their influence on average terrestrial residence times. Sources include potential petrogenic contribution of *n*-alkanes and catchment-unspecific areas delivering biomarkers via aeolian transport modes. As an example, the Danube Sulina transect will be discussed in detail.

Fluvial delivery along the Danube Sulina transect, including potentially biomarker-rich fine-grained suspended material, is spatially limited to a depositional area in front of the river mouth (Figure 3.2A). This sedimentological pattern is caused by the Black Sea's

cyclonic wind-stress-driven rim current. The rim current deflects the river plume southwards, inhibits dispersal of terrigenous material towards the central basin, and induces a sediment starved area between the delta front area and the continental slope (Panin and Jipa, 2002). Nevertheless, the station furthest offshore (P167) also shows contribution of pre-aged *n*-alkanes although riverine supply is negligible as corroborated by a BIT index value of 0.05. Comparison of the spatial *n*-alkane concentration with the BIT index (Figure 3.2A) implies a further source of *n*-alkanes to the stations offshore. Sedimentation rates range from 30 to 70 cm/kyr in this area (Eckert et al., 2009; Gulin et al., 2002; Teodoru et al., 2007) indicating that high core top radiocarbon ages are not the result of non-deposition. As a consequence, additional sources of long-chain *n*-alkanes at the seaward core locations, e.g., aeolian supply or petrogenic contribution, have to be considered. Unlike long chain *n*-alkanes, sedimentary long chain *n*-fatty acids are expected to be free of any contribution derived from petrogenic sources (Eglinton et al., 2002).

Wakeham (1996) showed that highest amounts of petrogenic hydrocarbons are found on the shelves of the Black Sea. Therefore, a contribution of fossil hydrocarbons to our core locations is likely. To evaluate the maturity of long-chain homologues of *n*-alkanes in sediments the carbon preference index (CPI) can be used. For all *n*-alkane samples in this study the CPI ranges from 4 to 7 (Table 3.8 in the Appendix), which does not imply a significant contribution of fossil hydrocarbons (CPI ~1; Tissot and Welte, 1978). However, an unresolved complex mixture (UCM) was observed in chromatograms of the hydrocarbon fractions, which indeed indicates petrogenic hydrocarbon contribution.

We estimate the petrogenic fractional contribution to the *n*-C<sub>29+31</sub> alkanes using a mass balance defined as,

$$f_{p,s} = (R_{\Sigma,s} - R_{t,s}) / (R_p - R_{t,s}) \quad (3.1)$$

where  $f_{p,s}$  is the fractional petrogenic contribution of the C<sub>29+31</sub> *n*-alkanes at station s,  $R_{\Sigma}$  is the measured ratio of δ<sup>13</sup>C/CPI,  $R_t$  is the δ<sup>13</sup>C/CPI ratio of the terrigenous end member and  $R_p$  is the δ<sup>13</sup>C/CPI ratio of the petrogenic end member. Assuming the petrogenic contribution to be <sup>14</sup>C-free, an isotopic mass balance calculation can be used to correct *n*-alkane <sup>14</sup>C ages for petrogenic contribution (cf. Pearson and Eglinton, 2000). For the vascular plant end member we use an average δ<sup>13</sup>C value of -35‰ (Collister et al., 1994; Lockheart et al., 1997; Rieley et al., 1993) and a CPI of 10 (Pearson and Eglinton, 2000) and for the petroleum end member we define δ<sup>13</sup>C=-27.5‰ (Reddy et al., 2002) and a CPI of 1 (Tissot and Welte, 1978). This mass balance accounts for all sources of petrogenic *n*-alkanes including natural petroleum-seepage from the seafloor and anthropogenic petroleum-spilling from shipping or coastal sewage. The resulting petrogenic contribution (%C<sub>petro</sub>) and corrected radiocarbon ages are shown in Table 3.6.

sample	$\Delta^{14}\text{C}$ [% $\text{\textperthousand}$ ] corrected <sup>a</sup>	$^{14}\text{C}$ age [yrs BP] corrected <sup>a</sup>	%C <sub>petro</sub>
P128	-554.42±3.1	6440±60	10.2
P168	-175.10±16.8	1490±170	3.6
P167	-72.45±17.8	550±160	6.7
P177	-347.19±12.7	3370±180	13.6
P110	-173.59±17.8	1480±210	17.1
GeoB11985	-116.06±27	940±220	19.8
GeoB11983	44.10±12.9	bomb- $^{14}\text{C}$	19.8
GeoB11960	6.31±14.2	10±140	18.4

<sup>a</sup> Corrected for petrogenic contamination using equation (1).

**Table 3.6** Radiocarbon contents and conventional radiocarbon ages of *n*-C<sub>29+31</sub> alkanes corrected for petrogenic contribution.

It has to be noted that these values might be an over- or underestimation of the real petrogenic contribution considering the intensity of the UCM apparent in some of the samples, which cannot easily be quantified. This difficulty becomes obvious, e.g., at station P177 in front of the Danube River mouth where corrected *n*-C<sub>29+31</sub> alkanes are younger than *n*-C<sub>28+30</sub> fatty acids or station GeoB11960 off the Çoruh River where corrected *n*-C<sub>29+31</sub> alkanes are almost modern.

Aeolian supply over long distances driven by wind dynamics has been shown to be the major transport mechanism of organic matter to open marine settings (Gagosian and Peltzer, 1986; Gagosian et al., 1981; Ohkouchi et al., 1997; Simoneit, 1977b). This was confirmed for the central Black Sea by Wakeham (1996). Furthermore, Eglinton et al. (1997) report vascular plant derived long-chain *n*-alkane  $^{14}\text{C}$  ages equivalent to those of TOC and co-occurring marine markers in Black Sea sediments of the central western basin. This indicates aeolian supply of fresh terrigenous OC most likely derived from recent vegetation. Such aeolian *n*-alkanes abraded from the leaves' surfaces have a modern radiocarbon age reflecting atmospheric values. Nevertheless, it has to be considered that aeolian biomarkers can also contain a pre-aged OC fraction when blown out of desiccated lakes, swamps or soils. Matsumoto et al. (2001) report long chain vascular plant *n*-fatty acids (*n*-C<sub>24+26</sub> fatty acids) from a continental aerosol sample to be up to 5860 yrs BP old, likely aged as a consequence of storage in an intermediate reservoir and subsequent transport over long distances. Likewise, Eglinton et al. (2002) found old *n*-alkanol (~650 yrs BP) ages for dust off NW Africa interpreted as reflecting a mixture of *n*-alkanols derived from abraded modern leaf waxes and Holocene dusts and soils.

The most recent aeolian activity strong enough to foster sand dune development in the Danube delta occurred approximately from AD1770 to AD1940 (Preoteasa et al., 2009). Strong winds emitting soil dust from dried-out, erodible farmland in southern Ukraine have recently been reported (Birmili et al., 2008). Strong wind erosion is known from agriculturally used Chernozem soils from the North Caucasus, Lower Don, and eastern and southern Ukraine steppe regions, occurring 3 to 5 times per year (Birmili et

al., 2008; Dolgilevich, 1997; Larionov et al., 1997). According to the annual mean wind stress pattern above the Black Sea, the primary wind direction is from the north (Oguz et al., 1995; Schrum et al., 2001). Therefore, aeolian supply of *n*-alkanes and *n*-fatty acids from these degraded and erodible Chernozem soils around the northern Black Sea catchment to our study sites is very likely. The radiocarbon ages of the offshore *n*-alkanes and *n*-fatty acids might as a result consist of a modern fraction directly abraded from plant leaves and a pre-aged fraction derived from the soils, which would provide an explanation for the old radiocarbon ages ( $550 \pm 160$  years; corrected for  $\%C_{\text{petro}}$ ) at offshore location P167.

Unlike the petrogenic contribution, however, a correction for aeolian supply of *n*-alkanes and *n*-fatty acids cannot reliably be made since the respective mass balance is underdetermined missing the riverine and aeolian fractional contributions or the respective radiocarbon ages. Such a mass balance can only be solved making various assumptions, e.g., using the BIT index defining the riverine fractional contribution or the definition of core locations receiving organic matter exclusively through riverine or aeolian supply. These assumptions, however, cannot be verified and, if used, result in unsupported aeolian and riverine biomarker radiocarbon ages. We therefore refrain from calculation of aeolian contributions and the respective age corrections.

It is apparent that different modes of transport and different sources contribute to the sedimentary vascular plant  $n\text{-C}_{29+31}$  alkanes and  $n\text{-C}_{28+30}$  fatty acids determining an average terrestrial residence time of terrigenous material from marine sediments. The respective residence times of those biomarkers delivered by riverine and aeolian transport processes can, however, not be fully disentangled due to missing information, e.g., compound-specific aerosol or riverine biomarker radiocarbon data. Nevertheless, given the substantially older biomarker ages in front of the river mouths compared to those offshore it appears that the biomarker OC pool eroded and delivered by rivers is considerably older than the biomarker OC pool transported by winds. For the Black Sea a relative estimate of the average residence time of long chain *n*-alkanes and *n*-fatty acids supplied by rivers would yield approximately 1000 to 4500 years (river mouth stations P128, P177, GeoB11985, GeoB11960, and GeoB7621-1), whereas long chain *n*-alkanes and *n*-fatty acids from atmospheric deposition are estimated at maximum ages of 700 to 1000 years (offshore locations P167, GeoB7614-1, and GeoB7612-3). The latter is explained by a contribution of pre-aged *n*-alkanes and *n*-fatty acids from wind erosion of degraded agriculturally used soils of the northern Black Sea catchment.

A fossil petrogenic component contributing to total long chain *n*-alkanes results in significantly older radiocarbon ages compared to long chain *n*-fatty acids. Although a correction for this contribution can be achieved (equation 3.1), it might over- or underestimate the real petrogenic contribution and corrected radiocarbon age.

Considering this difficulty, long chain *n*-fatty acids, which have no petrogenic sources, apparently reflect average terrestrial residence times more reliably.

### 3.6. SUMMARY AND CONCLUSION

Our data reflect the importance of terrigenous input from various rivers to the Black Sea supplying pre-aged organic matter. BIT indices reflect high soil-derived organic matter input to marine surface sediments in front of the river mouths decreasing further offshore. Accordingly, where terrestrial input is high, increased total organic carbon core-top radiocarbon ages reflect contribution of pre-aged terrestrial OC admixing to recent marine sedimentary OC. Further offshore, where autochthonous production is dominant, TOC radiocarbon ages reach modern values showing bomb-<sup>14</sup>C contribution. Long chain *n*-C<sub>29+31</sub> alkanes, *n*-C<sub>26</sub> fatty acid, and *n*-C<sub>28+30</sub> fatty acids, derived from vascular plants utilizing C<sub>3</sub> metabolism, are pre-aged at most stations. According to their different reactivities and petrogenic *n*-alkane contribution radiocarbon ages of *n*-C<sub>29+31</sub> alkanes are older than corresponding, more labile *n*-C<sub>28+30</sub> fatty acids. Likewise, fatty acid radiocarbon ages increase with increasing chain length as a result of, e.g., decreasing reactivity or admixture from terrigenous and marine sources (*n*-C<sub>24</sub> fatty acid).

The *n*-C<sub>29+31</sub> alkanes and *n*-C<sub>28+30</sub> fatty acids radiocarbon ages from stations in front of the river mouths range from 900±70 years to 4400±170 years. Evaluation of the decisive controlling parameters determining the age of these terrigenous compounds revealed that catchment size is the major morphological control. A climatic controlling factor cannot unambiguously be determined. It appears drainage areas under Mediterranean climate were found to more strongly increase mean terrestrial residence times than cooler, humid areas under continental climate.

Along-transect radiocarbon data reveal that terrestrial *n*-C<sub>29+31</sub> alkanes show contribution from a petrogenic component and that both *n*-C<sub>29+31</sub> alkanes and *n*-C<sub>28+30</sub> fatty acids are supplied via two differing transport modes, namely riverine and aeolian. Aeolian transport of leaf wax lipids likely also delivers an aged fraction consisting of a mixture of lipids directly abraded from leaves and those blown out of degraded agricultural soils of the northern Black Sea catchment. As the result of petrogenic contribution of long chain *n*-C<sub>29+31</sub> alkanes, which can be corrected via mass balance but may result in over- or underestimation, average terrestrial residence times are more reliably represented by *n*-C<sub>28+30</sub> fatty acids.

Besides natural processes, anthropogenic perturbations seem to liberate old terrigenous carbon. Channel-dredging in the Danube Delta presumably causes reduction of the delta's ability to retain old organic carbon, which instead is delivered to the NW Black Sea shelf. Additionally, wind erosion transports organic matter from agriculturally degraded soils of the northern catchment to the central Black Sea.

**Acknowledgments**

The authors gratefully thank Birgit Meyer-Schack for help during  $^{14}\text{C}$  sample processing. We acknowledge Ralph Kreutz for support with processing PCGC samples and Konstanze Schipper for laboratory assistance. We appreciate the help of Florian Rommerskirchen with  $\delta^{13}\text{C}$  measurements.

We thank the Crews of R/V Meteor and R/V Poseidon for good collaboration during cruises and the NOSAMS and ETHZ staff for  $^{14}\text{C}$  measurements.

This work was funded by the Helmholtz Young Investigator Group „Applications of molecular  $^{14}\text{C}$  analysis for the study of sedimentation processes and carbon cycling in marine sediments“. Additional funding was provided by the Bremen International Graduate School for Marine Sciences (GLOMAR).

### 3.7 SUPPLEMENTARY DATA

#### 3.7.1 TOC radiocarbon and stable isotopic data

Sample	$\Delta^{14}\text{C}$ [%‰]	$^{14}\text{C}$ age [yrs BP]	$\delta^{13}\text{C}$ [%‰]	ID No. <sup>a</sup>
<i>Danube River Sulina branch</i>				
P125 TOC 0-1cm	-7.98±2.8	5±20	-22.92	66561
P120 TOC 0-1cm	-64.20±3.2	475±25	-23.67	70734
P169 TOC 0-1cm	-51.20±3.2	365±25	-23.36	70735
<i>Dniester River</i>				
P153 TOC 0-1cm	-54.95±3.8	400±30	-24.41	66566
P157 TOC 0-1cm	27.47±3.9	bomb $^{14}\text{C}$	-24.05	66562
P158 TOC 0-1cm	-1.93±3.3	bomb $^{14}\text{C}$	-23.26	66563

<sup>a</sup> NOSAMS ID number.

Table 3.7 TOC radiocarbon and stable carbon isotopic data for stations without compound-specific radiocarbon data. Errors are given as  $1\sigma$  analytical uncertainty.

### 3.7.2 Geochemical proxy data

sample	% C <sub>org</sub>	C/N ratio	ACL <i>n</i> -alkanes <sup>a</sup>	CPI <i>n</i> -alkanes <sup>b</sup>	ACL <i>n</i> -fatty acids <sup>a</sup>	CPI <i>n</i> -fatty acids <sup>b</sup>
<i>Danube River Sulina branch</i>						
P128 0-1 cm	2.44	9.12	29.24	4.96	26.56	7.52
P125 0-1 cm	2.30	7.54	29.70	3.83	26.71	9.99
P120 0-1 cm	3.72	8.82	29.52	5.87	26.74	4.71
P169 0-1 cm	3.97	13.22	29.41	4.45	26.89	6.71
P168 0-1 cm	2.99	8.43	29.55	7.14	25.78	7.31
P167 0-1 cm	4.61	10.52	29.06	6.26	25.04	13.75
<i>Danube River Sfântu Gheorghe branch</i>						
P177 0-1 cm	2.04	9.41	29.30	4.81	25.92	6.27
P111 0-1 cm	3.40	8.84	29.77	3.94	26.65	9.17
P110 0-1 cm	2.72	8.84	29.79	4.14	25.71	7.93
GeoB7614-1 2-4 cm	2.67	8.07	29.67	4.25	25.61	7.07
GeoB7612-3 0-4 cm	3.51	9.29	29.67	6.66	25.71	6.37
GeoB7604-1 0-4 cm	10.23	13.61	29.16	5.22	24.97	10.80
<i>Dniester River</i>						
P153 0-1 cm	3.74	8.67	29.68	5.31	25.53	4.53
P157 0-1 cm	3.33	7.75	29.54	6.00	27.50	8.94
P158 0-1 cm	3.45	8.26	29.67	5.33	26.29	6.15
MC242 0-1 cm	2.73	8.72	29.35	4.19	26.85	9.16
<i>Kerch Strait/ Kuban and Don River</i>						
GeoB11985 0-2 cm	2.13	7.82	29.51	3.79	26.74	7.12
GeoB11986 0-2 cm	2.12	8.28	29.36	4.03	26.72	6.41
GeoB11983 0-2 cm	2.79	9.36	29.20	3.83	26.01	7.24
GeoB11984 0-2 cm	2.80	8.31	29.31	4.54	25.38	11.22
<i>Çoruh River</i>						
GeoB11931 0-2 cm	3.22	10.13	29.08	4.37	25.48	6.76
GeoB11960 0-2 cm	2.11	9.61	29.45	4.16	26.05	7.08
GeoB11905 0-2 cm	3.32	9.95	29.09	4.14	25.90	8.39
<i>Gülüç and Çatalağci Rivers</i>						
GeoB7621-1 0-4 cm	3.52	9.13	29.89	4.36	25.84	7.66

<sup>a</sup> ACL (Average Chain Length) calculated as  $\Sigma(iX_i)/\Sigma X_i$ , where X= abundance and i= 25, 27, 29, 31 and 33 carbon atoms for *n*-alkanes, and i= 24, 26, 28, 30 and 32 carbon atoms for *n*-fatty acids.

<sup>b</sup> CPI (Carbon Preference Index) defined as  $0.5 * [\Sigma (X_i + X_{i+2} + \dots + X_n) / \Sigma (X_{i-1} + X_{i+1} + \dots + X_{n-1}) + \Sigma (X_i + X_{i+2} + \dots + X_n) / \Sigma (X_{i+1} + X_{i+3} + \dots + X_{n+1})]$ , where X= abundance, i= 25 and n= 33 for *n*-alkanes, and i= 24 and n= 32 for *n*-fatty acids.

Table 3.8 Geochemical proxy data along river-mouth to deep-basin transects.



## 4. MANUSCRIPT III

### Implications for chloro- and pheopigments synthesis and preservation from combined compound-specific $\delta^{13}\text{C}$ , $\delta^{15}\text{N}$ , and $\Delta^{14}\text{C}$ analysis

Stephanie KUSCH<sup>1,2</sup>, Yuichiro KASHIYAMA<sup>3</sup>, Nanako O. OGAWA<sup>3</sup>, Mark ALTABET<sup>4</sup>, Martin BUTZIN<sup>5,1</sup>, Jana FRIEDRICH<sup>1</sup>, Naohiko OHKOUCHI<sup>3</sup>, Gesine MOLLENHAUER<sup>1,2</sup>

1 Alfred Wegener Institute for Polar and Marine Research, Am Handelshafen 12, 27570 Bremerhaven

2 Fachbereich Geowissenschaften, Universität Bremen, Klagenfurter Str., 28359 Bremen

3 Institute for Research on Earth Evolution, Japan Agency for Marine-Earth Science and Technology, 2-15 Natsushima-cho, Yokosuka 237-0061, Japan

4 School for Marine Science and Technology, University of Massachusetts Dartmouth, 706 S Rodney French Blvd, New Bedford, MA 02744, USA

5 MARUM Center for Marine Environmental Research, Leobener Strasse, 28359 Bremen, Germany

***to be submitted to Proceedings of the National Academy of Science of the USA***

---

#### **Abstract**

Chloropigments and their derivative pheopigments, which can be preserved in sediments, can directly be linked to photosynthesis. Their carbon and nitrogen stable isotopic composition has been shown to be a good recorder of recent and past surface ocean environmental conditions tracing the carbon and nitrogen sources and utilization pathways of the phytoplanktonic community. In this study compound-specific radiocarbon and stable carbon and nitrogen isotopic analysis was applied to examine the temporal dimensions of synthesis and fate of chlorophyll *a* and its degradational products pheophytin *a*, pyropheophytin *a*, and cyclopheophorbide *a* enol until burial in Black Sea surface sediments. The pigments are mainly of marine phytoplanktonic origin as implied by their stable  $^{13}\text{C}$  and  $^{15}\text{N}$  isotopic composition. Pigment  $\delta^{15}\text{N}$  values indicate nitrate utilization as the major nutrient uptake pathway but isotopic depletion with distance offshore indicates contribution from  $\text{N}_2$ -fixation towards the open marine setting. Radiocarbon concentrations of pigments are much lower than expected translating into minimum and maximum pigment ages of approximately 40 to 1200 years. This implies protective mechanisms against decomposition such as association with minerals or eutrophication-induced hypoxia and light limitation are much more efficient than previously thought. However, seasonal variations of

nutrient source, growth period, and habitat and their associated isotopic variability are likely at least as strong as long-term trends.

---

#### 4.1 INTRUDUCTION

Primary production is the basis for sustaining life on earth. Photosynthesis by autotrophic organisms accounts for virtually all of the primary production (chemosynthesis <1%) and can thus be called the ultimate source of metabolic energy building organic biomass (Falkowski, 2003; Field et al., 1998). In aerobic photoautotrophic organisms the light harvesting systems are based on the tetrapyrrole molecule chlorophyll *a* being the major antenna pigment, both in the marine as well as the terrestrial environment. Accordingly, chlorophyll *a* is ubiquitously found in the marine surface waters either produced in situ or transported from the continents via riverine or aeolian processes. Ultimately, chlorophyll *a* may be buried in marine sediments. However, in both the marine and terrestrial environment chlorophyll *a* undergoes several pre- and post-depositional processes altering its original chemical structure by loosing functional groups for the residual chlorin or porphin macrocycle. Transformation pathways include, e.g., (autolytic) cell senescence, microbial or viral lysis, enzymatic or hydrolysis reactions, photo-oxidation and grazing (Carpenter et al., 1986; Chen et al., 2003; Gossauer and Engel, 1996; King, 1993; Louda et al., 1998; Moreth and Yentsch, 1970; Owens and Falkowski, 1982; Repeta and Simpson, 1991; SooHoo and Kiefer, 1982b; Spooner et al., 1995; Sun et al., 1993b). In particular, chlorophyll *a* of higher plants is decomposed enzymatically during senescence of the leaves (Matile et al., 1996; Oberhuber et al., 2003), by bacterial breakdown and meso- and micro-faunal grazing in soils (Chamberlain et al., 2006; Hoyt, 1966), and by oxidation and photo-degradation during transport (Sanger, 1988). Consequently, marine sedimentary pigments are overwhelmingly derived from marine photoautotrophs.

Primary degradation products of chlorophyll *a* include pheophytin *a* and pyropheophytin *a*, formed by loss of functional groups via demetallation and demethoxycarbonylation by either of the above mentioned pathways (Chen et al., 2003).  $13^2$ ,  $17^3$ -cyclopheophorbide *a* enol is considered an exclusively biologically mediated (grazing) degradation product (Goericke et al., 2000). In general, chloro- and pheopigments have been shown to be extremely labile, whereas their macrocycles can be preserved over very long timescales (Rho et al., 1973). Various studies have demonstrated rapid decrease of chlorophyll *a* and pheophytin *a* concentrations over time periods on the order of hours to days or few weeks (Bianchi and Findlay, 1991; Goericke et al., 2000; Owens and Falkowski, 1982; SooHoo and Kiefer, 1982a; Spooner et al., 1995; Sun et al., 1993b). Overall, degradation rates were enhanced under oxic compared to anoxic

conditions (Sun et al., 1993a; Sun et al., 1993b). Particularly  $13^2,17^3$ -cyclopheophorbide *a* enol is reported to be extremely unstable under oxic conditions with the result that it can only be found in anoxic sediments (Chen et al., 2003; Goericke et al., 2000; Ma and Dolphin, 1996; Ocampo et al., 1999). Although the various transformation processes alter the molecule's chemical structure, the original isotopic composition remains fairly unchanged (Hayes et al., 1987). It has been shown that the stable carbon and nitrogen isotopic composition of tetrapyrrole molecules can be used to determine the nutrient conditions of the surface water environment the photoautotrophs lived in and, thus, to characterize the photoautotrophic community (Chicarelli et al., 1993; Chikaraishi et al., 2008; Kashiyama et al., 2008a; Ohkouchi et al., 2008; Ohkouchi et al., 2005; Sachs et al., 1999). Here, we determine the timescales of synthesis and fate of chlorophyll *a* and its degradation products pheophytin *a*, pyropheophytin *a*, and cyclopheophorbide *a* enol under natural marine oxic and anoxic conditions as found in marine sediments using combined  $\delta^{13}\text{C}$ ,  $\delta^{15}\text{N}$ , and  $\Delta^{14}\text{C}$ .

## 4.2 MATERIALS AND METHODS

### 4.2.1 Sampling

Core-top sediments from stations P128 ( $45^{\circ}04.69'\text{N}$ ,  $29^{\circ}46.64'\text{E}$ ; 17 mbsl), P177 ( $44^{\circ}35.76'\text{N}$ ,  $29^{\circ}11.43'\text{E}$ ; 22 mbsl), P120 ( $44^{\circ}30.66'\text{N}$ ,  $30^{\circ}40.93'\text{E}$ ; 91 mbsl), P169 ( $44^{\circ}15.48'\text{N}$ ,  $30^{\circ}29.19'\text{E}$ , 96 mbsl), and P167 ( $43^{\circ}58.88'\text{N}$ ,  $31^{\circ}30.83'\text{E}$ ; 1336 mbsl) from the NW Black Sea (Figure 4.1) were taken using a multicorer on RV Poseidon Cruise P363

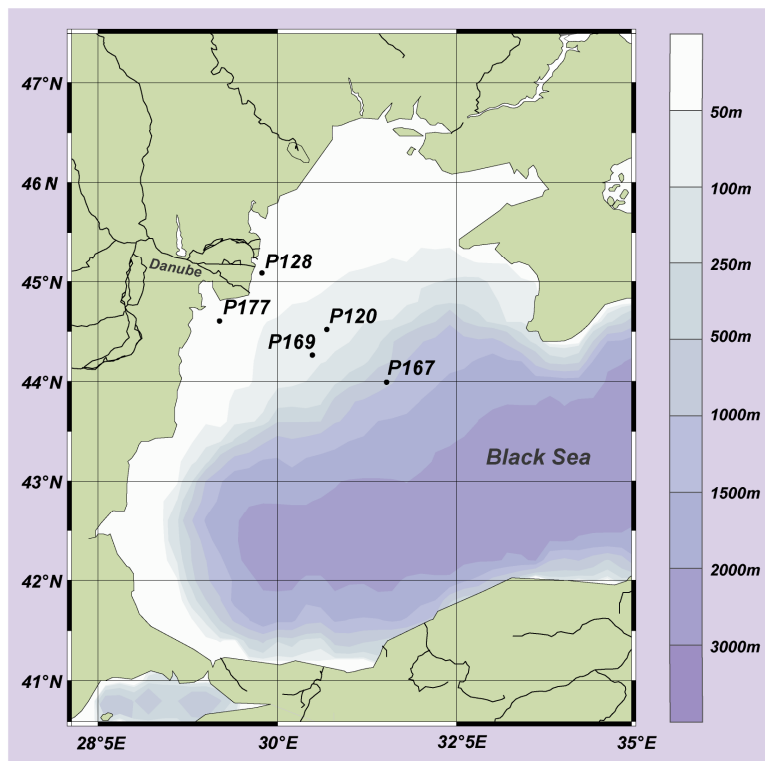


Figure 4.1 Study area showing core locations.

in 2008. The samples were sliced into 1 cm slices and stored frozen at -20 °C in glass jars until analysis. The uppermost 0-2 cm or 0-3 cm slices were recombined for analysis in order to yield enough chloropigment molecules for radiocarbon measurements. If available, co-occurring bivalve shells (*Scapharca* sp., *Modiolus* sp., *Abra fragilis*) were isolated from each sample and radiocarbon dated as well. For TOC radiocarbon analyses, subsamples of 100 to 500 mg of the freeze-dried samples were separated according to their organic carbon contents. Seawater samples at the respective stations were taken using a CTD rosette equipped with 30 l Niskin bottles. The seawater samples were poisoned with HgCl<sub>2</sub> to avoid bacterial activity.

#### **4.2.2 Pigment Extraction and Purification**

For the extraction of chloro- and pheopigments the freeze-dried sediment was ground and homogenized. Afterwards, dehydrated acetone was added (2x volume of the sediment) and samples were ultrasonicated for 15 min cooled in ice water. After ultrasonication samples were centrifuged at 2000 rpm for 5 min. The acetone-layer was removed and the extraction was repeated three times. After reduction of the volume under a cold stream of N<sub>2</sub>, the acetone-fraction was further transferred into a hexane-MilliQ bilayer (1:3), homogenized using vortex and centrifuged at 1500 rpm for 1 min. The hexane-layer was transferred and the extraction procedure was repeated until the hexane-fraction was colourless. The hexane-fraction was then reduced in volume under cold N<sub>2</sub> and rinsed through a column of pre-combusted sodium sulphate for dehydration. Afterwards dehydrated dimethylformamide (DMF) was added and solvents were homogenized by vortex before storing at -30 °C. After 10 min the sample was homogenized again and stored at -30 °C overnight. For HPLC analysis, the DMF layer was dried under a cold stream of N<sub>2</sub> for approximately 5 min to evaporate any hexane left in the solvent phase.

The HPLC-analysis was performed using an Agilent 1200 Series HPLC/DAD System applying two reversed-phase liquid chromatography modes for high sample capacity purification. For isolation of the chloro- and pheopigments from the extract, a semi-preparative Agilent Zorbax Eclipse XDB C18 column (9.4x250 mm; 5 µm) with a XDB C18 guard column (4.6x12.5 mm; 5 µm) were used. The chloro- and pheopigments were eluted isocratically with 75% acetonitrile/pyridine (100:0.5) and 25% ethyl acetate/pyridine (100:0.5) for 5 min, followed by a linear gradient of ethyl acetate/pyridine to 50% in 50 min. The flow rate was set to 4.2 ml/min and the oven temperature to 30 °C. Detection of the chloro- and pheopigments was achieved by Diode Array Detector. To achieve high single pigment purities, a second purification step was applied using an analytical Agilent Zorbax Eclipse PAH column (4.6x250 mm; 5 µm) equipped with a PAH guard column (4.6x12.5 mm; 5 µm). Isocratic elution of the pigments was achieved using 80% acetonitrile/pyridine (100:0.5) and 20%

2-butanone/pyridine (100:0.5) for 5 min, followed by two linear gradients of 2-butanone/pyridine (100:0.5), first to 60% in 25 min and second to 100% in 10 min. The flow rate was 1 ml/min. The oven temperature was 10 °C for chlorophyll *a* and pheophytin *a* and 30 °C for pyropheophytin *a* and cyclopheophorbide *a* enol.

HPLC processing blanks for each pigment methodology were determined by collection of the respective effluent volume. The solvent was dried using N<sub>2</sub> and the blank size and its respective <sup>13</sup>C (-29.6‰), <sup>15</sup>N (5.1‰), and <sup>14</sup>C (-1000‰) isotopic composition was determined. The blank size was 2.5 µg C and 0.1 µg N per run for chlorophyll *a*, 0.8 µg C and 0.02 µg N per run for pheophytin *a* and pyropheophytin *a*, and 1.9 µg C and 0.05 µg N per run for cyclopheophorbide *a* enol. For sample P128 14, 22, and 25 runs were performed for chlorophyll *a*, pheophytin *a*, and pyropheophytin *a*, respectively. For sample P177 4 runs were performed for chlorophyll *a*, 9 runs for pheophytin *a*, and 7 runs for pyropheophytin *a*. For samples P120 and P169 4 runs were performed for both chlorophyll *a* and pheophytin *a*, and 5 runs for pyropheophytin *a*. For sample P167 17, 23, 12, and 25 runs were performed for chlorophyll *a*, pheophytin *a*, pyropheophytin *a*, and cyclopheophorbide *a* enol, respectively.

#### 4.2.3 Isotope measurements

The stable carbon and nitrogen isotopic composition of chloro- and pheopigments were measured on a modified FlashEA1112 Automatic Elemental Analyser connected to a Thermo Finnigan Delta plus XP isotope ratio mass spectrometer (IRMS) via a ConFlow IIIB Interface. Seawater nitrate, chemically converted to N<sub>2</sub>O (McIlvin and Altabet, 2005), was measured for its δ<sup>15</sup>N composition using an automated purge-and-trap system connected to a Finnigan MAT 251. The stable carbon and nitrogen isotopic composition of bulk sediment was analysed using a Finnigan Delta plus IRMS. The isotopic compositions are expressed as conventional δ<sup>13</sup>C relative to Vienna PeeDee Belemnite (VPDB) and δ<sup>15</sup>N relative to atmospheric N<sub>2</sub>.

For radiocarbon measurements, chloro- and pheopigments, and bivalve shells were converted into CO<sub>2</sub>. Cleaned bivalves were acid-hydrolyzed. Pigment samples were transferred into pre-combusted quartz tubes and 150 µg pre-combusted copper oxide (CuO) was added as oxygen source. The samples were evacuated and flame-sealed under vacuum. Afterwards, the samples were combusted to CO<sub>2</sub> at 900 °C for 8 h. The resulting CO<sub>2</sub> gas was stripped of water and quantified under vacuum.

TOC was submitted as unprocessed samples and AMS measurements were performed using standard methods (McNichol et al., 1994). AMS measurements of chloropigment isolates were performed following the protocol for small samples (Pearson et al., 1998). Where sample sizes were sufficient dual measurements were obtained. Radiocarbon ages are reported as Δ<sup>14</sup>C (Stuiver and Polach, 1977), which is corrected for isotopic fractionation associated with sample formation and processing as well as for the decay

between sample formation and AMS measurement. Blank-correction of stable and radiocarbon isotope data was achieved using an isotopic mass balance calculation and using blank values determined for HPLC isolation protocol. Additionally, calibrated radiocarbon ages are given for pigments for determination of their “true” age and calculation of degradation timescales. Calibration of pre-bomb samples was achieved using the calibration software CALIB 6.0 (Stuiver et al., 2010) applying a reservoir correction of 400 years (Siani et al., 2000). The “true” age of bomb- $^{14}\text{C}$  containing pigments was determined using a modeled surface water  $\Delta^{14}\text{C}$  curve.

#### 4.2.4 Black Sea bomb surface water DIC Model

The history of Black Sea surface water  $^{14}\text{C}$  concentrations is poorly constrained by observations. For this reason the temporal evolution of surface water  $\Delta^{14}\text{C}$  was estimated by means of a heuristic one-dimensional model. Following (Butzin and Roether, 2004), the input of  $^{14}\text{C}$  via air-sea exchange and river runoff is balanced by radioactive decay, downward mixing, and by an additional first-order apparent loss or gain term which parameterizes up- or downwelling and net horizontal exchange. The temporal evolution of surface water  $\Delta^{14}\text{C}$  is then given by

$$\frac{\partial^{14}\text{R}_{\text{wat}}}{\partial t} = K \frac{\partial^2 {}^{14}\text{R}_{\text{wat}}}{\partial z^2} - (\lambda + \mu) {}^{14}\text{R}_{\text{wat}} \quad (4.1)$$

where  ${}^{14}\text{R}_{\text{wat}}$  is the scaled surface water  $^{14}\text{C}/^{12}\text{C}$  ratio at a given time  $t$  (following Toggweiler et al., 1989),  $K$  is an apparent vertical diffusivity,  $z$  is depth,  $\lambda$  is the decay rate of  $^{14}\text{C}$  ( $=1.2096 \times 10^{-4} \text{ yr}^{-1}$ ) (Godwin, 1962) and  $\mu$  is the time constant of the first-order loss and gain term. The model input are  $^{14}\text{C}$  fluxes representing air-sea exchange ( ${}^{14}\text{F}_{\text{air}}$ ) and continental river runoff ( ${}^{14}\text{F}_{\text{riv}}$ ). Air-sea exchange is estimated as

$${}^{14}\text{F}_{\text{air}} = \Phi p\text{CO}_2 / \Sigma\text{CO}_2 ({}^{14}\text{R}_{\text{atm}} - {}^{14}\text{R}_{\text{wat}}) \quad (4.2)$$

where  $\Phi$  is the average invasion rate of  $\text{CO}_2$  ( $=20 \text{ mol m}^{-2} \text{ yr}^{-1}/330 \text{ ppm}$ ) (Broecker et al., 1985),  $p\text{CO}_2$  is the partial pressure of atmospheric  $\text{CO}_2$  (Enting et al., 1994),  $\Sigma\text{CO}_2$  is the average concentration of dissolved inorganic carbon in surface water ( $=2 \text{ mol m}^{-3}$ ), and  ${}^{14}\text{R}_{\text{atm}}$  is the atmospheric  $^{14}\text{C}/^{12}\text{C}$  ratio in the northern hemisphere (Enting et al., 1994; Levin et al., 2008). The  $^{14}\text{C}$  delivery due to river runoff is crudely estimated as

$${}^{14}\text{F}_{\text{riv}} = V_{\text{run}} / A {}^{14}\text{R}_{\text{riv}} \quad (4.3)$$

where  $V_{\text{run}}$  is the runoff to the Black Sea ( $=350 \text{ km}^3 \text{ yr}^{-1}$ ) (e.g., Tolmazin, 1985),  $A$  is the surface area of the Black Sea ( $=420,000 \text{ km}^2$ ), and  $^{14}\text{R}_{\text{riv}}$  is the fluvial  $^{14}\text{C}/^{12}\text{C}$  ratio. As observations of  $^{14}\text{R}_{\text{riv}}$  were not available,  $^{14}\text{R}_{\text{riv}} = ^{14}\text{R}_{\text{atm}}$  was assumed, i.e., atmospheric  $^{14}\text{C}$  deposited in catchment areas enters the Black Sea instantaneously and without dilution. While this is clearly an overestimation, the contribution of  $^{14}\text{F}_{\text{riv}}$  amounts only about 1‰ of the atmospheric input flux. Equation (4.1) is numerically integrated from AD1810 to AD2010 and evaluated at 20 m depth since highest chlorophyll a concentrations have been found between 10 m and 30 m water depth (Chu et al., 2005; Krupatkina et al., 1991; Repeta and Simpson, 1991). The solution is fitted to scattered observations (Jones and Gagnon, 1994; Ostlund and Dryssen, 1986; Siani et al., 2000; this study) using  $K$  and  $\mu$  as fit coefficients. Values of  $K$  and  $\mu$  are about  $7 \times 10^3 \text{ m}^2 \text{ yr}^{-1}$  ( $\sim 2 \text{ cm}^2 \text{ s}^{-1}$ ) and  $\sim 1 \times 10^{-3} \text{ yr}^{-1}$ , respectively.

### 4.3 RESULTS

**Table 4.1** reports the isotopic data for each station. Bulk sedimentary  $\delta^{13}\text{C}$  values increase from  $-26.1 \pm 0.1\text{\textperthousand}$  (P128) to  $-23.2 \pm 0.1\text{\textperthousand}$  (P167) with distance seawards, which is in agreement with an increasing contribution of marine production at the offshore locations (**Figure 4.2**). Contrary,  $\delta^{13}\text{C}$  values of chloro- and pheopigments range from  $-24.5 \pm 0.1\text{\textperthousand}$  to  $-26.7 \pm 0.1\text{\textperthousand}$  without a distinct spatial pattern. Heterogeneous isotopic values within a range of  $\sim 2\text{\textperthousand}$  consistently occur within each sample except for P128, where all pigments have virtually identical  $\delta^{13}\text{C}$  values. The stable carbon isotopic values are in the range previously reported for marine phytoplankton (Sachs et al., 1999). The pigment  $\delta^{15}\text{N}$ -values range from  $4.0 \pm 0.4\text{\textperthousand}$  to  $-2.8 \pm 0.4\text{\textperthousand}$ . Generally, chlorophyll a is the most enriched whereas pyropheophytin a is the most depleted pigment within each sample. Along-transect data reveal a gradual isotopic depletion ( $\sim 4\text{\textperthousand}$ ) with increasing distance from the river mouth. Only chlorophyll a  $\delta^{15}\text{N}$  values at stations P120 and P169 deviate from this trend. The general trend is, moreover, consistent with a steady depletion of bulk sedimentary  $\delta^{15}\text{N}$  values (ranging from  $8.5 \pm 0.5\text{\textperthousand}$  to  $4.2 \pm 0.5\text{\textperthousand}$ ) with distance offshore, which is in agreement with previously reported data (Reschke et al., 2002). Seawater nitrate ( $\text{NO}_3^-$ )  $\delta^{15}\text{N}$  values from 0 m to 92 m water depth range between  $4.9 \pm 0.2\text{\textperthousand}$  and  $8.4 \pm 0.2\text{\textperthousand}$  (**Table 4.2** in the Appendix), consistent with estimates for global oxygenic open ocean seawater (Brandes et al., 1998; Cline and Kaplan, 1975; Liu and Kaplan, 1989; Sigman et al., 2000; Sigman et al., 2005; Voss et al., 2001).

TOC radiocarbon concentrations (Kusch et al., submitted; **Table 4.1**, **Figure 4.3**) are lowest at stations P128 and P177 in front of the Danube river mouth with  $\Delta^{14}\text{C}$  values of  $-166.6 \pm 2.1\text{\textperthousand}$  and  $-161.0 \pm 3.4\text{\textperthousand}$ , respectively. At these stations contribution of pre-aged terrigenous organic matter is likely (Kusch et al., submitted). With further distance offshore  $\Delta^{14}\text{C}$  values increase to  $-64.2 \pm 3.2\text{\textperthousand}$  (P120) and  $51.2 \pm 3.2\text{\textperthousand}$  (P169) and show bomb- $^{14}\text{C}$  contribution ( $44.5 \pm 2.5\text{\textperthousand}$ ) at anoxic core location P167. All radiocarbon dated

sample	$\delta^{13}\text{C}$ [%‰] <sup>a</sup>	$\delta^{15}\text{N}$ [%‰] <sup>a</sup>	$\Delta^{14}\text{C}$ [%‰] <sup>a</sup>	cal year AD <sup>b</sup>	ID No. <sup>c</sup>
<b>P128 0-2cm</b>					
chlorophyll a	-25.8±0.1	2.1±0.4	n.d.		
pheophytin a	-26.1±0.1	2.5±0.4	-127.88±11.9	1230±105	70736
pheophytin a	-26.1±0.1	2.5±0.4	-109.32±11.6	1380±70	70737
pyropheophytin a	-25.8±0.1	1.5±0.4	32.85±12.8	1963±1/2009±6	70738
<i>Scapharca</i> sp.	-1.10±0.1		56.14±3.3		70752
TOC 0-1cm <sup>d</sup>	-25.69±0.1		-166.57±2.1		66558
bulk sediment	-26.10±0.1	8.54±0.5			
<b>P177 0-3cm</b>					
chlorophyll a	-26.3±0.1	2.0±0.4	-183.16±15.3	690±160	71683
pheophytin a	-24.6±0.1	2.6±0.4	-6.64±18.1	1962±2	70746
pyropheophytin a	-24.8±0.1	1.9±0.4	-55.77±12.9	1950±1	70747
<i>Abra fragilis</i>	-0.57±0.1		53.95±3.3		70754
TOC 0-1cm <sup>d</sup>	-25.17±0.1		-161.01±3.4		66564
TOC 2-3cm	-24.68±0.1		-103.42±4.2		71682
bulk sediment	-25.67±0.1	8.39±0.5			--
<b>P120 0-3cm</b>					
chlorophyll a	-26.0±0.1	3.1±0.4	-36.67±15.5	1959±2	71685
pheophytin a	-25.3±0.1	-0.5±0.4	-50.60±7.6	1956±2	70748
pyropheophytin a	-24.5±0.1	-0.2±0.4	6.19±12.4	1962±1	70749
TOC 0-1cm <sup>d</sup>	-23.67±0.1		-64.20±3.2		70734
TOC 2-3cm	-23.58±0.1		-209.66±3.2		71681
bulk sediment	-23.97±0.1	6.73±0.5			
<b>P169 0-3cm</b>					
chlorophyll a	-26.4±0.1	4.0±0.4	181.12±17.1	n.d.	71684
pheophytin a	-24.7±0.1	-0.9±0.4	21.66±14.3	1963±1	70750
pyropheophytin a	-25.0±0.1	-0.9±0.4	n.d.		
<i>Modiolus</i> sp.	0.87±0.1		9.87±3.8		70753
TOC 0-1cm <sup>d</sup>	-23.36±0.1		51.20±3.2		70735
bulk sediment	-25.41±0.1	6.73±0.5			
<b>P167 0-2cm</b>					
chlorophyll a	-26.7±0.1	-0.1±0.4	-34.10±16.5	1959±3	70743
chlorophyll a	-26.7±0.1	-0.1±0.4	19.92±13.2	1963±1	70751
pheophytin a	-26.3±0.1	-1.2±0.4	13.64±12.2	1963±1	70740
pheophytin a	-26.3±0.1	-1.2±0.4	1.67±9.2	1962±1	70741
pyropheophytin a	-24.7±0.1	-2.8±0.4	105.47±18.0	1969±3/1981±6	70742
cyclopheophorbide a enol	-25.5±0.1	-0.7±0.4	48.34±12.2	1964±1/2002±6	70744
cyclopheophorbide a enol	-25.5±0.1	-0.7±0.4	-7.07±8.3	1962±1	70745
TOC 0-1cm <sup>d</sup>	-24.56±0.1		44.45±2.5		66557
bulk sediment	-23.21±0.1	4.23±0.5			

<sup>a</sup> Blank-corrected.<sup>b</sup> Calendar year AD calibrated using CALIB 6.0 for years <AD1950 and modelled surface DI<sup>14</sup>C values for years ≥AD1950.<sup>c</sup> NOSAMS laboratory ID numbers.<sup>d</sup> Data from (Kusch et al., submitted).

n.d. Not determined.

**Table 4.1** Blank-corrected radiocarbon ( $\Delta^{14}\text{C}$ ) and stable isotopic composition ( $\delta^{13}\text{C}$  and  $\delta^{15}\text{N}$ ) of purified chloro- and pheopigments, bivalve shells, total organic carbon (TOC), and bulk sediment. Where sample sizes were sufficient, samples were split prior to  $^{14}\text{C}$  analysis. Errors are given as  $1\sigma$  analytical uncertainties.

bivalve shells (Table 4.1, Figure 4.3) show contribution of bomb- $^{14}\text{C}$ . Shell  $\Delta^{14}\text{C}$  values range from  $56.1\pm3.3\text{‰}$  at the shallowest nearshore station (P128, *Scapharca* sp.) to  $9.9\pm3.8\text{‰}$  further offshore (P169, *Modiolus* sp.), which is consistent with utilization of more depleted DI $^{14}\text{C}$  with increasing water depth.

Chloro- and pheopigment  $\Delta^{14}\text{C}$  values (Table 4.1, Figure 4.3) vary over a range of  $\sim290\text{‰}$ . Lowest pigment  $\Delta^{14}\text{C}$  values are evident for pheophytin a at station P128 ( $-127.9\pm11.9\text{‰}$  and  $-109.3\pm11.6\text{‰}$ ) and chlorophyll a at station P177 ( $-183.2\pm15.3\text{‰}$ ) in front of the Danube River. However, in both samples the other pigments are significantly less depleted in  $^{14}\text{C}$ . Pyropheophytin a from station P128 is enriched with bomb- $^{14}\text{C}$  ( $32.9\pm12.8$ ). Likewise,  $\Delta^{14}\text{C}$  values of pheophytin a

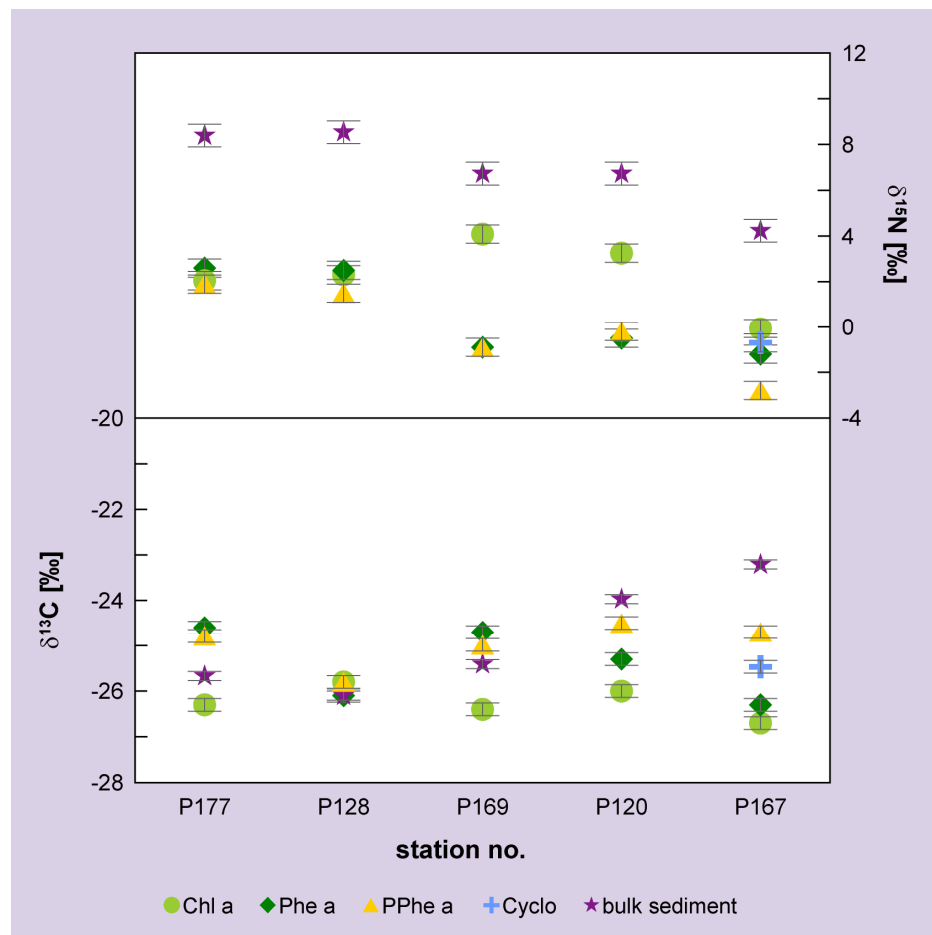


**Figure 4.2** Stable nitrogen and carbon isotopic composition ( $\delta^{13}\text{C}$  and  $\delta^{15}\text{N}$ ) of purified chloro- and pheo-pigments along a cross-shelf transect of the NW Black Sea. For reference, simplified bathymetry is shown on the bottom panel. Error bars give  $1\sigma$ -analytical uncertainty.  
 Chl a: chlorophyll a, Phe a: pheophytin a, PPhe a: pyropheophytin a,  
 Cyclo: cyclopheophorbide a enol.

( $-6.6 \pm 18.1\text{\textperthousand}$ ) and pyropheophytin a ( $-55.8 \pm 12.9\text{\textperthousand}$ ) from station P177 are notably increased. At intermediate station P120 pheophytin a ( $-50.6 \pm 7.6\text{\textperthousand}$ ) and chlorophyll a ( $-36.7 \pm 15.5\text{\textperthousand}$ ) agree within  $1\sigma$ -analytical uncertainty. Pyropheophytin a from the same sample, however, shows bomb- $^{14}\text{C}$  contribution ( $32.9 \pm 12.8\text{\textperthousand}$ ). Chlorophyll a at station P169, which is located in approximately the same water depth as P120, shows the most enriched  $\Delta^{14}\text{C}$  value of the data set ( $181.1 \pm 17.1\text{\textperthousand}$ ). Co-occurring pyropheophytin a ( $21.7 \pm 14.3\text{\textperthousand}$ ) is significantly less enriched in  $^{14}\text{C}$ . At anoxic station P167 dual measurements of pheophytin a ( $13.6 \pm 12.2\text{\textperthousand}$  and  $1.7 \pm 9.2\text{\textperthousand}$ ) are within  $1\sigma$ -analytical uncertainty. Chlorophyll a from this station yields  $\Delta^{14}\text{C}$  values of  $19.9 \pm 13.2\text{\textperthousand}$  and  $-34.1 \pm 16.5\text{\textperthousand}$ , agreeing within  $2\sigma$ -analytical uncertainty. Contrary,  $\Delta^{14}\text{C}$  values of cyclopheophorbide a enol ( $48.3 \pm 12.2\text{\textperthousand}$  and  $-7.1 \pm 8.3\text{\textperthousand}$ ) are significantly different ( $>2\sigma$ -uncertainty). Pyropheophytin a shows the highest incorporation of bomb- $^{14}\text{C}$  ( $105.5 \pm 18.0\text{\textperthousand}$ ) at this station.

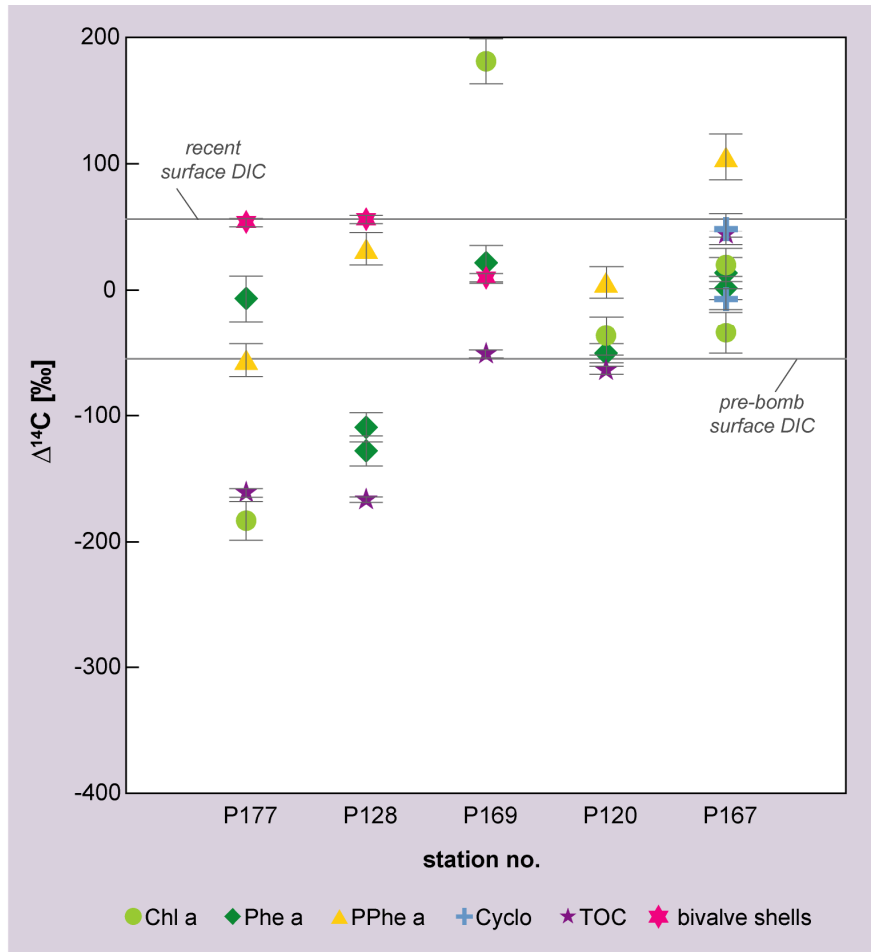


**Figure 4.3** Radiocarbon concentrations ( $\Delta^{14}\text{C}$ ) of purified chloro- and pheo-pigments. Error bars denote  $1\sigma$  analytical uncertainties. Chl a: chlorophyll *a*, Phe a: pheophytin *a*, PPhe a: pyropheophytin *a*, Cyclo: cyclopheophorbide *a* enol.

#### 4.4 DISCUSSION

The stable carbon and nitrogen isotopic composition of primary pigments reflects the isotopic composition of the nutrients according to the utilization pathway of the photoautotrophic community (Chicarelli et al., 1993; Chikaraishi et al., 2008; Kashiyama et al., 2008a; Ohkouchi et al., 2008; Ohkouchi et al., 2005; Sachs et al., 1999). Empirically it has been shown that chlorophyll *a* is enriched in  $^{13}\text{C}$  and depleted in  $^{15}\text{N}$  relative to total cellular carbon and nitrogen by approximately  $1.8 \pm 0.8\text{\textperthousand}$  and  $4.8 \pm 1.4\text{\textperthousand}$ , respectively (Ohkouchi et al., 2006; Ohkouchi et al., 2008; Sachs et al., 1999). Therefore, after accounting for the fractionation our data imply that cellular  $\delta^{13}\text{C}_{\text{cell}}$  values of the phytoplanktonic community range from  $-26.3 \pm 0.8\text{\textperthousand}$  to  $-28.5 \pm 0.8\text{\textperthousand}$ . These  $\delta^{13}\text{C}$  values reflect a marine phytoplanktonic origin of the chloro- and pheopigments (Sachs et al., 1999) considering that degradative mechanisms are considered too efficient to allow for a significant contribution of terrigenous chloro- and pheopigments to oceanic sediments (Chikaraishi et al., 2007; Kashiyama et al., 2008b; Sanger, 1988). The observed  $\sim 2\text{\textperthousand}$  scatter among the pigment  $\delta^{13}\text{C}$  values might be due

to growth season effects (Sachs et al., 1999). Seasonal variations in  $\delta^{13}\text{C}_{\text{DIC}}$ , e.g., driven by decreasing carbon isotopic fractionation during times of high productivity and low surface water  $\text{CO}_{2(\text{aq})}$  concentrations (Gislefoss et al., 1998; Gruber et al., 2002; Lehmann et al., 2004) or admixture with seasonally varying riverine  $\delta^{13}\text{C}_{\text{DIC}}$  (Hélie et al., 2002; Kanduč et al., 2007), could cause the observed  $\delta^{13}\text{C}$  variations since the seasonal particle fluxes through the water column of the Black Sea are coupled with spatially and temporarily varying pigment fluxes (King, 1995). In case of cyclophophorbide *a* enol an additional potential small isotopic effect could be the cleavage of the phytol side chain since the lipid is normally more depleted than the tetrapyrrole macro cycle (Ohkouchi et al., 2008; Sachs et al., 1999). Fractionation-corrected  $\delta^{15}\text{N}_{\text{cell}}$  values range from approximately  $8.8 \pm 1.5\text{\textperthousand}$  to  $2.0 \pm 1.5\text{\textperthousand}$  in good agreement with bulk sedimentary  $\delta^{15}\text{N}$  ( $8.5 \pm 0.5\text{\textperthousand}$  to  $4.2 \pm 0.5\text{\textperthousand}$ ). Nitrogen isotopic variations within each sample and especially the noticeable  $^{15}\text{N}$  enrichment of chlorophyll *a* at stations P120 and P169 could be caused by seasonal variations of the nitrogenous nutrient source. The nitrogen isotopic composition of a substrate becomes enriched in the heavy isotope when the nitrogen source becomes depleted (Altabet and Francois, 1994; Fuchsman et al., 2008; Murray et al., 2005; Velinsky et al., 1991). Chlorophyll *a* produced at the end of a phytoplanktonic bloom limited by nitrogen would be reflected in heavy  $\delta^{15}\text{N}$  values. Since chlorophyll *a*  $\delta^{15}\text{N}_{\text{cell}}$  values ( $8.8 \pm 1.5\text{\textperthousand}$  to  $4.7 \pm 1.5\text{\textperthousand}$ ) at all stations show good agreement with the respective seawater nitrate  $\delta^{15}\text{N}$  values, which are within the range reported for global seawater  $\text{NO}_3^-$  (Brandes et al., 1998; Cline and Kaplan, 1975; Liu and Kaplan, 1989; Sigman et al., 2000; Sigman et al., 2005; Voss et al., 2001), nitrate utilization must be the major nitrogen assimilation process of the apparent phytoplanktonic community (presuming a high  $\text{NO}_3^-$  uptake/availability ratio). However, an overall pigment  $\delta^{15}\text{N}$  depletion with distance offshore indicates that distinct groups of phytoplankton using several nitrogen assimilation processes occur in the surface waters of the study sites. Heavier  $\delta^{15}\text{N}$  values in front of the Danube river mouth indicate predominance of  $\text{NO}_3^-$  utilization, whereas lighter values towards the central basin may result from contribution of pigments derived from diazotrophs. Since nitrogen-fixing organisms utilize  $\text{N}_2$  with an isotopic composition close to ambient air, the respective stable nitrogen isotopic composition reflects values in the characteristic range of  $-3\text{\textperthousand}$  to  $0\text{\textperthousand}$  (Minagawa and Wada, 1986; Montoya et al., 2002). Such contribution from  $\text{N}_2$ -fixing biomass is consistent with the nutrient availability observed during the sampling campaign P363. In front of the Danube delta observed nitrogenous nutrient supply was high enough (P128 N:P>80) to maintain nitrate utilization; here phosphorus is the limiting nutrient (Cauwet et al., 2002). Contrary, further offshore towards station P167 nitrogen became limiting over phosphorus (P167 N:P<10). Since the Black Sea is strongly stratified, the permanent pycnocline prevents upward-mixing of nutrients from deeper waters. Thus,  $\text{N}_2$ -fixation by proteobacteria (Sorokin, 1983) might account for a

significant fraction of total nitrogen assimilation (McCarthy et al., 2007). The contributions from both nitrogen species assimilation pathways can be estimated applying isotopic mass balance defined as,

$$\delta_{c,s} = f_{n,s} \cdot \delta_{c,n,s} + f_{d,s} \cdot \delta_{c,d,s} \quad (4.4)$$

where  $\delta_c$  is the measured and fractionation-corrected cellular  $\delta^{15}\text{N}_{\text{cell}}$  value at station s,  $\delta_{c,n}$  is the  $\delta^{15}\text{N}_{\text{cell}}$  value for nitrate utilization (assumed to be 6‰) (Brandes et al., 1998; Cline and Kaplan, 1975; Liu and Kaplan, 1989; Sigman et al., 2000; Sigman et al., 2005; Voss et al., 2001),  $\delta_{c,d}$  is the  $\delta^{15}\text{N}_{\text{cell}}$  value for diazotrophic N<sub>2</sub>-fixation (assumed to be -1.5‰) (Minagawa and Wada, 1986; Montoya et al., 2002), and  $f_n$  and  $f_d$  are the respective fractional contributions where  $f_n + f_d = 1$ . Using averaged pigment  $\delta^{15}\text{N}$  values to avoid a seasonality effect the contribution of N<sub>2</sub>-fixation would account for ~35% of the  $\delta^{15}\text{N}$  inventory at station P167. At stations P120 and P169 N<sub>2</sub>-fixation would account for ~5% and ~6%, respectively. Our data, thus, suggest that the majority of the phytoplanktonic community along the investigated transect on the NW Black Sea shelf utilizes nitrate as primary nitrogenous nutrient source with nitrogen fixation becoming an important additional nitrogen source in more offshore waters.

Chlorophyll is generally expected to decompose within hours to days or weeks after cell death (Bianchi and Findlay, 1991; Goericke et al., 2000; Owens and Falkowski, 1982; SooHoo and Kiefer, 1982a; Spooner et al., 1995; Sun et al., 1993b). A sediment trap study in the Black Sea showed that the flux of chlorophyll *a* to a water depth of 100 m is only 0.2% of the production in 0-55 m water depth (Repeta and Simpson, 1991). Due to this instability of primary pigments, the  $\Delta^{14}\text{C}$  concentrations of pigments deposited in surface sediments would be expected to mirror recent surface water DIC  $^{14}\text{C}$  concentrations. Instead,  $^{14}\text{C}$  concentrations of chlorophyll *a* (-183.2±15.3‰) and pheophytin *a* (-127.9±11.9‰ and -109.3±11.6‰) at stations P177 and P128, respectively, are much lower than DIC  $\Delta^{14}\text{C}$  values represented by bivalve data from 17 m (56.14±3.3‰) to 96 m water depth (9.87±3.8‰) and reported values (Jones and Gagnon, 1994). Potential reasons for the low  $\Delta^{14}\text{C}$  concentrations include utilization of a different DIC pool, protective mechanisms associated with sedimentary matrices or faecal pellets, and contribution of terrestrial biomass. Although the Danube River catchment is geologically characterized by large areas of carbonaceous rocks, the old pigment ages at stations P177 and P128 are unlikely an artefact of riverine hardwater DIC utilization by marine phytoplankton since corresponding bivalve shells at both stations show bomb- $^{14}\text{C}$  concentrations, thus, unambiguously reflecting a modern DIC pool. We cannot exclude pigment contribution from riverine freshwater organisms, which lyse when encountering the more saline Black Sea water (Cauwet et al., 2002; Saliot et al., 2002) and might indeed be influenced by hardwater DIC. However, quantitatively riverine pigment

contribution should not be noticeably high considering that the riverine nutrient input favours marine phytoplanktonic blooms in the near-shore area contributing large biomass (Banaru et al., 2007; Cociasu et al., 1996). Aggregation with humic substances or protection by sediment matrices in general has previously been proposed as a protective mechanism preventing pigments from quick degradation (Bianchi et al., 1993). Association with a matrix reduces the reactivity of the pigments (Furlong and Carpenter, 1988), thus, improving their preservation potential. Adsorption might occur both as surface monolayer and inside mineral pores large enough for pigments protecting them from hydrolytic enzymes (Mayer, 1994a; Mayer, 1994b; Zimmerman et al., 2004), the latter process may be likely because of very high organic carbon/surface area ratios found for sediment water interface samples of the Black Sea (Mayer, 1994a). Such mineral adsorption would have to occur either during water column transit or immediately after initial sedimentation. The enormous (~51 million t/yr) and heterogeneous sediment discharge from the Danube River (Jaoshvili, 2002) should provide minerals appropriate for this process. A similar protective mechanism might be the packaging of pigments into fecal pellets after grazing by zooplankton. If the fecal pellets are not excreted in loose aggregates but as rather dense particles with high sinking velocities (Taguchi et al., 1993), they can quickly be exported from the photic zone and escape photo-oxidation. Such a process, however, would only account for the preservation of digestive pigments like pheophytin *a*, pyropheophytin *a*, and cyclopheophorbide *a* enol but not for the original chlorophyll *a*. Old chloro- and pheopigments adsorbed to minerals or incorporated into fecal pellets may afterwards be carried into younger sediments by bioturbation. Contribution of terrestrial biomass as indicated by low TOC and leaf-wax lipid (Kusch et al., submitted) radiocarbon concentrations, could account for older chloro- and pheopigments, if intact leaf fragments have been sequestered on land before delivery to the Black Sea. The Danube Delta is a periodically flooded wetland area characterized by lakes and ponds. A flood event or dredging processes may release leaves from plants previously preserved in anoxic lake sediments preventing degradation. Contribution from intact terrestrial leaves could also explain why only chlorophyll *a* and pheophytin *a* are noticeably depleted in  $\Delta^{14}\text{C}$  whereas pyropheophytin *a* is enriched in most samples and why only those stations immediately in front of the river mouth are affected. Both chlorophyll *a* and pheophytin *a* are primary pigments in the photosystem II and, thus, would be the only pigments in preserved intact leaves or leaf fragments. Furthermore, the southward deflection of Danube River sediments inhibits large scale dispersal of terrigenous organic matter across the NW Black Sea shelf (Panin and Jipa, 2002).

Except for chlorophyll *a* and pheophytin *a* at stations P177 and P128, respectively, all investigated pigments contain bomb- $^{14}\text{C}$ , i.e., they are enriched relative to the pre-bomb surface water DIC  $^{14}\text{C}$  concentration of -54.8‰ (Jones and Gagnon, 1994). Thus, they

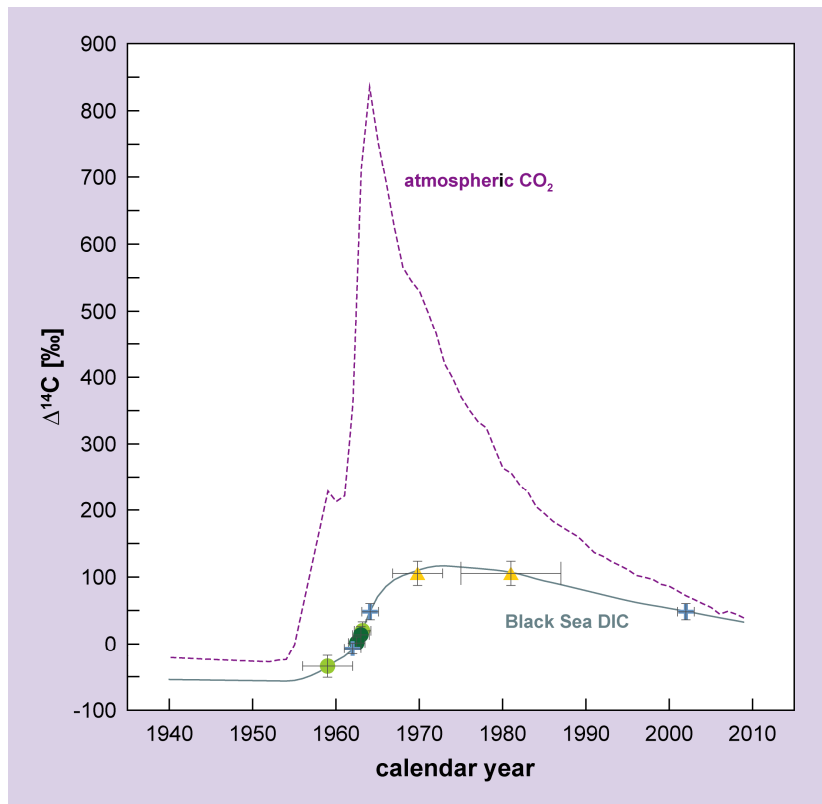


**Figure 4.4** Modelled Black Sea surface water DIC  $\Delta^{14}\text{C}$  concentrations. For reference the atmospheric  $\text{CO}_2$   $\Delta^{14}\text{C}$  curve is shown. As example, potential calendar years of synthesis from matching  $\Delta^{14}\text{C}$  concentrations are given for station P167.

were synthesized after AD1950. Accordingly, pigment ages of bomb- $^{14}\text{C}$  containing pigments can only be estimated by comparison with the surface water  $\text{DIC}^{14}\text{C}$  record from AD1950 until the sampling year AD2008. Since measured bomb surface water  $\text{DIC}^{14}\text{C}$  values are only available for AD1988 (Jones and Gagnon, 1994), we use modelled bomb curve data (Figure 4.4, Table 4.3 in the Appendix) adapted to match measured pre-bomb, bomb, and post-bomb data (Jones and Gagnon, 1994; Ostlund and Dryssen, 1986, this study; Siani et al., 2000). Estimated average calendar years of pigment synthesis range from AD1956 to AD1969 (Table 4.1) because post-bomb surface DIC  $^{14}\text{C}$  concentrations have not equilibrated to values  $<30\text{\textperthousand}$  (Figure 4.4, Table 4.3 in the Appendix) until AD2008. Only for pyropheophytin *a* at station P128 (AD1963 or AD2009), and pyropheophytin *a* (AD1969 or 1981) and cyclopheophorbide *a* enol at station P167 (AD1964 or AD2002) two possible average synthesis years can be derived from comparison with the DIC  $^{14}\text{C}$  record. However, in all cases the earlier possible date is regarded more likely because of its similarity for estimated years of pigment synthesis at the other stations (AD1956 to AD1964) and, in the case of cyclopheophorbide *a* enol, with the date estimated for a second aliquot (AD1962) analysed separately. The modelled surface DIC  $^{14}\text{C}$  concentrations do not reach values high enough to correspond to that of the most  $^{14}\text{C}$ -enriched pigment, chlorophyll *a* at station P169 ( $181.12 \pm 17.1\text{\textperthousand}$ ). This might be caused by either uncertainties of the model related to the scarcity of input

data, since the chlorophyll *a*  $\Delta^{14}\text{C}$  value is in the range previously reported for northern hemisphere oceanic surface water DIC (e.g., Druffel, 1987), or contribution of terrestrial chlorophyll *a* such as from a leaf fragment, reflecting atmospheric bomb- $^{14}\text{C}$  concentrations. Overall, also bomb- $^{14}\text{C}$  containing pigments are older than expected. Considering that our estimate of blank carbon introduced during HPLC processing is associated with an uncertain error and that we cannot accurately determine the blank introduction during wet chemical sample preparation, the reported blank-corrected  $\Delta^{14}\text{C}$  concentrations may be slightly erroneous. An additional contribution of roughly 1-11  $\mu\text{g C}$  with radiocarbon-dead composition for most samples with sizes of approximately 30  $\mu\text{g}$  to 230  $\mu\text{g C}$  would change the  $^{14}\text{C}$  concentrations to values between 100 and 110‰. Such values equal surface water DIC  $^{14}\text{C}$  concentration integrated from AD1970 to AD1990. This is the time period of highest surface DI $^{14}\text{C}$  concentrations, which is coincident with an up to tenfold increase of the phytoplankton photosynthetic activity on the NW Black Sea shelf caused by anthropogenic eutrophication (Aubrey et al., 1996; Oguz, 2005, and references therein). Besides higher biomass quantity, pigment preservation should have been enhanced through reduced light penetration in the uppermost water column (Aubrey et al., 1996; Oguz, 2005), which likely limits photo-oxidation of pigments. Moreover, the eutrophication-triggered recurrent hypoxia of the shallow shelf bottom waters (Aubrey et al., 1996) should have further enhanced pigment preservation by decreasing both oxidation and especially grazing. Therefore, the preservation efficiency should have been considerably enhanced during this time period and through bioturbation (except P167) pigments synthesized during the eutrophication phase would become admixed with more recent pigments, which would explain why more recent pigment  $^{14}\text{C}$  concentrations are obscured.

If the decomposition of chlorophyll *a* to its successor pigments in the sediment occurred on timescales of several years to decades, the  $^{14}\text{C}$  concentrations of the latter within the same sedimentary layer as the precursor should decrease with increasing degradative loss of functional groups, i.e. a decrease in radiocarbon concentrations would be expected from chlorophyll *a* to pheophytin *a* and further to pyropheophytin *a* due to increasing time needed for the decompositional process. An evaluation of the timescales of pre- and post-depositional degradation processes is only possible for station P167, the only core location where bioturbation can be excluded to cause pigment age differences. Likewise, no age artefact from low sediment accumulation is expected since the sedimentation rate at this station is  $\sim 0.9 \text{ mm/yr}$  years (extrapolated from Gulin et al., 2002). Except for pyropheophytin *a* all pigment  $^{14}\text{C}$  concentrations agree within  $2\sigma$ -analytical uncertainty, thus, their decompositional conversion occurs within a few years. Although the  $^{14}\text{C}$  concentrations of pyropheophytin *a* are significantly different from the  $^{14}\text{C}$  concentrations of the other pigments at station P167, the calendar age difference is also only a few years ([Table 4.1](#)) caused by the steep gradient of bomb- $^{14}\text{C}$  incorporation

into surface DIC during the 1960s. However, other than expected pyropheophytin *a* is younger than chlorophyll *a* and pheophytin *a*. This pattern is also evident at stations P128, P177, and P120. These younger ages are coupled with a nitrogen isotopic depletion of pyropheophytin *a* compared to chlorophyll *a* and pheophytin *a* at the respective stations, which might be caused by seasonal nutrient variations. Since the spring bloom is associated with a pyropheophytin *a* mass flux maximum and the autumn bloom is coupled to a pheophytin *a* flux maximum (King, 1995), the  $^{14}\text{C}$  concentration differences between pyropheophytin *a* and the other pigments might also be driven by seasonality at the more offshore locations (P120 and P167). A difference in the average dwelling depths of diatoms (spring bloom) and coccolithophorides (autumn bloom) or seasonally varying DI $^{14}\text{C}$  concentrations (Broecker and Peng, 1980) could explain the pigment  $\Delta^{14}\text{C}$  differences. For the Black Sea seasonal variations in subsurface chlorophyll *a* depths have been reported (Chu et al., 2005) but seasonally integrated DI $^{14}\text{C}$  are not available.

The stable carbon and nitrogen isotopic composition of the individual pigments reflects the conditions at the time of synthesis. At station P128 the oldest pigment (pheophytin *a*) is approximately 700 years older than the youngest pigment (pyropheophytin *a*). Our data suggest that during that time period the nitrogen isotopic composition and, thus, the nutrient utilization pathway and source nitrate isotopic composition has not changed substantially if pigments are derived from phytoplankton. Likewise, no major changes of the nutrient source and utilization pathway are obvious at station P177 where the oldest (chlorophyll *a*) and the youngest (pheophytin *a*) measured pigments are even  $\sim$ 1200 years apart. If chlorophyll *a* and pheophytin *a* at these two river mouth stations is derived from terrestrial plants, such temporal assessment is invalid. All pigments clearly derive from phytoplankton at stations P120 and P169 where chlorophyll *a*  $\delta^{15}\text{N}$  values differ considerably from the  $\delta^{15}\text{N}$  values of the other pigments while their  $^{14}\text{C}$  concentration differences are insignificant. Apparently, for the NW Black Sea shelf spatial differences of the nutrient utilization pathway and seasonal variations of the isotopic composition of a nutrient source seem to have a stronger imprint on the stable isotopic composition than potential temporal changes during the last millennium.

Overall, combined  $\delta^{13}\text{C}$  and  $\delta^{15}\text{N}$  isotope analysis of pigments from NW Black Sea surface sediments identified their origin from a mainly nitrate utilizing phytoplanktonic community with additional contribution from diazotrophs towards the central ocean basin. Their  $^{14}\text{C}$  concentrations are much lower than expected as a result of protection against molecular degradation by processes such as association with minerals or eutrophication-induced hypoxia and light limitation. The isotopic heterogeneity due to seasonally varying isotopic compositions of the nutrient source, habitat, and the growth period appear at least as strong as long-term trends.

**Acknowledgements**

We thank Laurence Mee for providing N and P data. Birgit Meyer-Schack and Monika Segl are thanked for bulk  $\delta^{13}\text{C}$  and  $\delta^{15}\text{N}$  analysis and for assistance with vacuum line procedures.

This study was funded by the Helmholtz Young Investigator Group „Applications of molecular  $^{14}\text{C}$  analysis for the study of sedimentation processes and carbon cycling in marine sediments“ and a JSPS fellowship grant PE08543 to Stephanie Kusch. Additional funding was provided by GLOMAR (Bremen Graduate School for Global Change in the Marine Realm).

**4.5 SUPPLEMENTARY DATA****4.5.1 Stable nitrogen isotopic data**

sample	water depth [m]	$\delta^{15}\text{N}$ [%oo]
P128	0	8.21±0.2
	0	7.24±0.2
	15	4.93±0.2
P177	6	8.07±0.2
	12	7.99±0.2
	22	8.39±0.2
	22	6.95±0.2
P169	75	4.94±0.2
	92	4.96±0.2
P167	25	7.22±0.2
	70	7.68±0.2

Table 4.2 Seawater nitrate nitrogen isotopic composition.

#### 4.5.1 Bomb surface water DIC model results

calendar year	$\Delta^{14}\text{C} [\text{\textperthousand}] \text{ max}$	$\Delta^{14}\text{C} [\text{\textperthousand}] \text{ average}$	$\Delta^{14}\text{C} [\text{\textperthousand}] \text{ min}$
1940	-50.61	-54.11	-57.69
1941	-50.82	-54.26	-57.8
1942	-51.02	-54.42	-57.91
1943	-51.24	-54.58	-58.02
1944	-51.45	-54.75	-58.14
1945	-51.67	-54.92	-58.26
1946	-51.89	-55.09	-58.39
1947	-52.12	-55.26	-58.51
1948	-52.34	-55.43	-58.64
1949	-52.56	-55.61	-58.77
1950	-52.79	-55.78	-58.9
1951	-53.02	-55.96	-59.03
1952	-53.25	-56.14	-59.16
1953	-53.48	-56.32	-59.3
1954	-53.71	-56.51	-59.44
1955	-52.77	-55.66	-58.68
1956	-49.49	-52.77	-56.16
1957	-44.54	-48.41	-52.36
1958	-37.77	-42.43	-47.15
1959	-28.7	-34.42	-40.16
1960	-19.54	-26.31	-33.06
1961	-11.73	-19.36	-26.93
1962	-0.17	-9.1	-17.93
1963	26.75	14.61	2.72
1964	62.86	46.44	30.46
1965	90.13	70.65	51.72
1966	107.09	85.91	65.29
1967	117.92	95.82	74.28
1968	124.4	101.93	79.98
1969	129.04	106.41	84.25
1970	133.42	110.64	88.29
1971	136.95	114.11	91.66
1972	138.95	116.23	93.84
1973	139.07	116.67	94.57
1974	137.78	115.86	94.18
1975	136.29	114.85	93.6
1976	134.85	113.86	93.02
1977	133.34	112.78	92.34
1978	131.91	111.75	91.69
1979	130.31	110.56	90.89
1980	128.21	108.92	89.68
1981	125.7	106.9	88.12
1982	122.63	104.37	86.12
1983	118.65	101.03	83.39
1984	114.33	97.37	80.37
1985	110.56	94.17	77.74
1986	107.35	91.45	75.5
1987	104.17	88.75	73.27
1988	100.63	85.72	70.75
1989	97.03	82.63	68.15
1990	93.57	79.64	65.64
1991	90.08	76.62	63.09
1992	86.63	73.61	60.55
1993	83.2	70.63	58.01
1994	79.82	67.67	55.49
1995	76.58	64.83	53.06
1996	73.6	62.22	50.82
1997	70.97	59.9	48.84
1998	68.51	57.73	46.97
1999	66.08	55.59	45.13
2000	63.62	53.4	43.24
2001	61.11	51.19	41.33
2002	58.55	48.91	39.36
2003	55.93	46.59	37.34
2004	53.28	44.22	35.29
2005	50.63	41.86	33.23
2006	48.02	39.53	31.19
2007	45.45	37.23	29.18
2008	42.91	34.96	27.19

Table 4.3 Modelled surface water  $\Delta^{14}\text{C}$  results from 20 m water depth for the time interval AD1940 to AD2008 (sampling year).



## 5. SUMMARY AND PERSPECTIVES

The studies comprising this thesis traced various pre- and post-depositional processes affecting terrestrial and marine organic matter until final burial in marine sediments and successfully determined the respective timescales of those mechanisms:

Lateral sediment transport of organic matter within the southern and central Panama Basin during the late glacial and Holocene was identified as occurring within less than a few decades after particle formation as indicated by the radiocarbon ages of alkenones, foraminifera, and total organic carbon. Such timescales argue against both long-distance lateral transport and deposition of pre-aged allochthonous material from marine or terrestrial sources. The allochthonous material in the southern Panama Basin rather results from local particle winnowing within the east-west trending troughs, which are characteristic for the abyssal hill topography surrounding the core locations. Recently sedimented organic matter is returned into bottom waters from the kilometer-scale topographic highs by internal tides or bottom currents and becomes locally transported and redistributed within bottom nepheloid layers. As a result of such rapid and local transport the potential for temporal decoupling of proxies residing in different grain size fractions is minimized. Thus, comparison of various proxies for paleoceanographic reconstructions appears robust in the study area. Nevertheless, fast bottom currents, which episodically spill across the Carnegie Ridge from the Peru Basin transport coarser-grained particles downslope to the Southern Panama Basin. This process might bias paleoceanographic reconstructions based on foraminiferal tests for core Y69-71P.

**PERSPECTIVES** The identification of downslope transport of foraminifera down the Carnegie Ridge and its effect on foraminiferal  $^{14}\text{C}$  ages results in the need for a revised age model for core Y69-71P if it is to be used in studies of past climate change. A first correction of  $U_{37}^K$  based sea surface temperatures made here attenuates the previously observed temperature offsets of cores ME0005-24JC and Y69-71P. This offset is a paradox, since both cores should have virtually identical sea surface temperature records based on their proximity. However, even after age model correction the temperature offset remains for the late Holocene. The cause of this temperature offset, which might either be of environmental or analytical nature, needs to be identified by systematic re-assessment of core-top  $U_{37}^K$  or  $\text{TEX}_{86}$  analysis in comparison with in situ sea surface temperatures. Furthermore,  $^{230}\text{Th}$  dynamics need to be clarified, i.e., the affinity of  $^{230}\text{Th}$  to particle size and particle composition has to be accounted for in order to report reliable quantitative estimates of focusing in the Eastern Equatorial Pacific.

Average terrestrial residence times of long chain *n*-alkanes and *n*-fatty acids in different river catchments of the Black Sea were estimated to range from  $900\pm70$  to  $4400\pm170$  years. Evaluation of the controlling factors, which determine continental carbon turnover revealed drainage area size is the main control in climatically similar catchments. Larger areas are characterized by higher mean terrestrial residence time. In morphologically similar drainage areas average terrestrial residence time appears to be controlled by the climatic regime. Mediterranean climate type drainage areas seem to favor prolonged terrestrial residence compared to drainage areas under continental climate. In addition to river mouth stations, where riverine organic matter can be traced, along-transect data were used to assess potential additional sources contributing long chain plant waxes to the Black Sea. This approach enabled the identification of petrogenic *n*-alkanes, and aeolian *n*-alkanes and *n*-fatty acids contributing to the sedimentary biomarker pool. Such petrogenic contribution of *n*-alkanes implies average terrestrial residence times are more reliably represented by *n*-fatty acids. Terrigenous biomarkers are delivered to the offshore waters through aeolian transport. This fraction does not only consist of lipids immediately abraded from leaves but also receives a contribution from degraded agricultural soils of the northern Black Sea catchment as implied by the respective ages of *n*-alkanes and *n*-fatty acids at the offshore core locations.

**PERSPECTIVES** The reported terrestrial residence times are estimated using long chain *n*-alkanes and *n*-fatty acids. However, *n*-alkanes and *n*-fatty acids represent only a part of the lipid fraction and an even smaller fraction of all the terrestrial components biosynthesized on the continents. Thus, their radiocarbon ages do not characterize the ages of other terrigenous compounds, such as amino acids, carbohydrates, lignin, and other biopolymers. Since lipids have been shown to be older than corresponding amino acid or carbohydrate fractions in detrital aggregates, sediment floc, and sediments, more labile components should exhibit shorter whereas more refractory components should exhibit longer residence times. Accordingly, further assessment of terrestrial residence times using a comprehensive range of terrigenous biomarkers would be desirable. Moreover, to study the controls of terrestrial turnover recorded in marine sediments basins which receive input from rivers draining morphologically or climatically different catchments, such as the Caspian Sea (Volga, Terek, and Kura Rivers) or the Strait of Georgia (Columbia and Fraser Rivers), need to be investigated. In order to determine climate related changes of terrestrial residence within a catchment, down-core analyses are needed in study areas, such as anoxic basins with laminated sediments, where significant changes in the sedimentology can be excluded.

The radiocarbon concentrations of mainly phytoplanktonic chlorophyll *a*, pheophytin *a*, pyropheophytin *a*, and cyclopheophorbide *a* enol from Black Sea core top sediments translate into ages from 40 up to 1200 years. These unexpectedly high ages must result from efficient preservation mechanisms, such as association with minerals or water column hypoxia and light limitation induced by eutrophication. Simultaneous compound-specific stable carbon and nitrogen analysis revealed the environmental conditions during the time of pigment synthesis. The stable carbon isotopic composition is in agreement with marine photoautotrophic origin. The stable nitrogen isotopic composition indicates nitrate utilization as the major nitrogenous nutrient uptake pathway most evident at near-coast stations. Further offshore a contribution of pigments from diazotrophs is implied by depletion of the stable nitrogen isotopes. This spatial pattern in the composition of the phytoplanktonic community appears to have been rather constant over longer timescales. Differences of the stable carbon and nitrogen isotopic composition between old and young pigments seems to be as strong as the seasonal isotopic variations between pigments of virtually the same age caused by the isotopic variability of the nutrient source, growth period, and habitat.

**PERSPECTIVES** The findings of old chloro- and pheopigment radiocarbon ages strongly demonstrate that the degradation dynamics of pigments under natural conditions have yet not been fully understood. Fundamental research is necessary to gain more information about the controlling parameters of pigment preservation. Compound-specific radiocarbon analysis of pigments from different environmental settings is required to evaluate the preserved radiocarbon age structures. Additionally, compound-specific radiocarbon analysis of laboratory-cultured pigments will provide insights to the age relationships of precursor and successor pigments, which have been found to be partly inconsistent in this study.

The studies performed in this thesis have highlighted the great potential of compound-specific radiocarbon analysis to illuminate temporal scales of carbon cycle dynamics. For a broader implementation of this straight-forward method and future applications of compound-specific radiocarbon analysis some instrumental challenges need to be overcome.

**INSTRUMENTAL PERSPECTIVES** Compound-specific radiocarbon analysis is currently restricted to the sensitivity of the AMS systems. Improvements of these highly sophisticated systems have recently been achieved, but are not routinely employed. Routine operation of continuous-flow gas ion sources and the development of on-line combustion applications to AMS systems (e.g., GC/AMS or HPLC/AMS) will reduce background contamination associated with graphitization and allow the reduction of sample size requirements towards more

reliable ultra-microscale analysis. With advances in sample size requirements, investigations of potential procedural blanks associated with sample purification and processing are crucial. The development and routine use of small accelerators (currently  $^{14}\text{C}$  analysis is feasible at terminal voltages of 500kV, but reduction down to only 200kV has been achieved) will significantly reduce the investment and operating costs, decrease the space requirements, and increase sample throughput. This will make AMS systems more broadly available meeting the increasing demand and make compound-specific radiocarbon analysis amenable to wider applications in different disciplines.

**FUTURE APPLICATIONS** Compound-specific radiocarbon analysis has already and will further improve considerably our understanding of marine and terrestrial biogeochemistry. Future applications will include more profound investigations of process-specific compounds, for example, radiocarbon analysis of intact polar lipids will yield insights into the metabolism of deep biosphere archaea. Radiocarbon analysis of bacterial hopanoids, which hold the potential to be environmental, ecological, and phylogenetic biomarkers, will allow a better understanding about their biosynthesis and functioning, and provide insights to a vast array of biogeochemical cycles and their temporal scales. The most straightforward progress in compound-specific radiocarbon analysis will be its broad application to nucleic acids, the most specific biomarkers for any given organism. Overall, other prospective applications of compound-specific radiocarbon analysis to carbon cycle dynamics and their temporal scales will arise with analytical and technical progress in conjunction with further advancement and findings from studies linking microbiology and organic geochemistry.





## 6. REFERENCES

- Aller, R.C., Hall, P.O.J., Rude, P.D., Aller, J.Y. (1998) Biogeochemical heterogeneity and suboxic diagenesis in hemipelagic sediments of the Panama Basin. Deep Sea Research Part I: Oceanographic Research Papers. 45, 133-165.
- Altabet, M.A., Francois, R. (1994) Sedimentary Nitrogen Isotopic Ratio as a Recorder for Surface Ocean Nitrate Utilization. Global Biogeochem. Cycles. 8, doi: 10.1029/93GB03396.
- Arnold, J.R., Libby, W.F. (1949) Age Determinations by Radiocarbon Content: Checks with Samples of Known Age. Science. 110, 678-680.
- Arthur, M.A., Dean, W.E. (1998) Organic-Matter Production and Preservation and Evolution of Anoxia in the Holocene Black Sea. Paleoceanography. 13, 395-411.
- Asper, V.L., Honjo, S., Orsi, T.H. (1992) Distribution and transport of marine snow aggregates in the Panama Basin. Deep Sea Research Part A. Oceanographic Research Papers. 39, 939-952.
- Aubrey, D., Moncheva, S., Demirov, E., Diaconu, V., Dimitrov, A. (1996) Environmental changes in the western Black Sea related to anthropogenic and natural conditions. Journal of Marine Systems. 7, 411-425.
- Ayçik, G.A., Çetaku, D., Erten, H.N., Salihoglu, I. (2004) Dating of Black Sea sediments from Romanian coast using natural  $^{210}\text{Pb}$  and fallout  $^{137}\text{Cs}$ . Journal of Radioanalytical and Nuclear Chemistry. 259, 177-180.
- Bakan, G., Büyükgüngör, H. (2000) The Black Sea. Marine Pollution Bulletin. 41, 24-43.
- Banaru, D., Harmelin-Vivien, M., Gomoiu, M.-T., Onciu, T.-M. (2007) Influence of the Danube River inputs on C and N stable isotope ratios of the Romanian coastal waters and sediment (Black Sea). Marine Pollution Bulletin. 54, 1385-1394.
- Bard, E. (1988) Correction of Accelerator Mass Spectrometry  $^{14}\text{C}$  Ages Measured in Planktonic Foraminifera: Paleoceanographic Implications. Paleoceanography. 3, 635-645.
- Bard, E. (1998) Geochemical and geophysical implications of the radiocarbon calibration. Geochimica et Cosmochimica Acta. 62, 2025-2038.
- Bard, E. (2001) Paleoceanographic implications of the difference in deep-sea sediment mixing between large and fine particles. Paleoceanography. 16, 235-239.
- Bard, E., Hamelin, B., Fairbanks, R.G., Zindler, A. (1990) Calibration of the  $^{14}\text{C}$  timescale over the past 30,000 years using mass spectrometric U-Th ages from Barbados corals. Nature. 345, 405-410.
- Bard, E., Arnold, M., Fairbanks, R.G., Hamelin, B. (1993)  $^{230}\text{Th}$ - $^{234}\text{U}$  and  $^{14}\text{C}$  ages obtained by mass spectrometry on corals. Radiocarbon. 35, 191-199.
- Barker, S., Broecker, W.S., Clark, E., Hajdas, I. (2007) Radiocarbon age offsets of foraminifera resulting from differential dissolution and fragmentation within the sedimentary bioturbated zone. Paleoceanography. 22, PA2205, doi:10.1029/2006PA001354.
- Barnes, C.E., Cochran, J.K. (1991) Geochemistry of uranium in Black Sea sediments. Deep Sea Research. 38, S1237-S1254.
- Bauer, J.E., Williams, P.M., Druffel, E.R.M. (1992)  $^{14}\text{C}$  activity of dissolved organic carbon fractions in the north-central Pacific and Sargasso Sea. Nature. 357, 667-670.
- Beaulieu, S.E. (2002) Accumulation and fate of phytodetritus on the sea floor. Oceanography and Marine Biology: an annual review. 40, 171-232.
- Beck, J.W., Richards, D.A., Edwards, R.L., Silverman, B.W., Smart, P.L., Donahue, D.J., Herrera-Osterheld, S., Burr, G.S., Calsoyas, L., Jull, A.J.T., Biddulph, D. (2001)

- Extremely Large Variations of Atmospheric  $^{14}\text{C}$  Concentration During the Last Glacial Period. *Science*. 292, 2453-2458.
- Becker-Heidmann, P., Scharpenseel, H.-W., Wiechmann, H. (1996) Hamburg radiocarbon thin layer soils database. *Radiocarbon*. 38, 295-345.
- Beer, J., Siegenthaler, U., Bonani, G., Finkel, R.C., Oeschger, H., Suter, M., Wolfli, W. (1988) Information on past solar activity and geomagnetism from  $^{10}\text{Be}$  in the Camp Century ice core. *Nature*. 331, 675-679.
- Behrenfeld, M.J., Bale, A.J., Kolber, Z.S., Aiken, J., Falkowski, P.G. (1996) Confirmation of iron limitation of phytoplankton photosynthesis in the equatorial Pacific Ocean. *Nature*. 383, 508-511.
- Behrenfeld, M.J., Falkowski, P.G. (1997) Photosynthetic rates derived from satellite-based chlorophyll concentration. *Limnology and Oceanography*. 42, 1-20.
- Benthien, A., Müller, P.J. (2000) Anomalously low alkenone temperatures caused by lateral particle and sediment transport in the Malvinas Current region, western Argentine Basin. *Deep Sea Research Part I: Oceanographic Research Papers*. 47, 2369-2393.
- Benway, H.M., Haley, B.A., P., K.G., Mix, A.C. (2003) Adaptation of a Flow-Through Leaching Procedure for Mg/Ca Paleothermometry. *Geochem. Geophys. Geosyst.* 4, 1-15.
- Benway, H.M., Mix, A.C., Haley, B.A., Klinkhammer, G.P. (2006) Eastern Pacific Warm Pool paleosalinity and climate variability: 0–30 ky. *Paleoceanography*. 21, doi: 10.1029/2005PA001208.
- Berger, W.H. (1970) Planktonic Foraminifera: Selective solution and the lysocline. *Marine Geology*. 8, 111-138.
- Berger, W.H., Piper, D.J.W. (1972) Planktonic foraminifera: differential settling, dissolution, and redeposition. *Limnology and Oceanography*. 17, 275-287.
- Bianchi, T.S., Findlay, S. (1991) Decomposition of Hudson Estuary Macrophytes: Photosynthetic Pigment Transformations and Decay Constants. *Estuaries*. 14, 65-73.
- Bianchi, T.S., Dibb, J.E., Findlay, S. (1993) Early Diagenesis of Plant Pigments in Hudson River Sediments. *Estuarine, Coastal and Shelf Science*. 36, 517-527.
- Bienfang, P.K. (1980) Phytoplankton sinking rates in oligotrophic waters off Hawaii, USA. *Marine Biology*. 61, 69-77.
- Bienfang, P.K. (1981) Sinking rates of heterogeneous, temperate phytoplankton populations. *J. Plankton Res.* 3, 235-253.
- Bindoff, N.L., Willebrand, J., Artale, V., Cazenave, A., Gregory, J., Gulev, S., Hanawa, K., Le Quéré, C., Levitus, S., Nojiri, Y., Shum, C.K., Talley, L.D., Unnikrishnan, A. (2007) Observations: Oceanic Climate Change and Sea Level, in: Solomon, S., Qin, D., Manning, M., Chen, Z., Marquis, M., Averyt, K.B., Tignor, M., Miller, H.L., (Eds), *Climate Change 2007: The Physical Science Basis. Contribution of Working Group I to the Fourth Assessment Report of the Intergovernmental Panel on Climate Change*, Cambridge University Press, Cambridge.
- Birmili, W., Schepanski, K., Ansmann, A., Spindler, G., Tegen, I., Wehner, B., Nowak, A., Reimer, E., Mattis, I., Müller, K., Brüggemann, E., Gnauk, T., Herrmann, H., Wiedensohler, A., Althausen, D., Schladitz, A., Tuch, T., Löschau, G. (2008) A case of extreme particulate matter concentrations over Central Europe caused by dust emitted over the southern Ukraine. *Atmospheric Chemistry and Physics*. 8, 997-1016.

- Blair, N.E., Leithold, E.L., Ford, S.T., Peeler, K.A., Holmes, J.C., Perkey, D.W. (2003) The persistence of memory: the fate of ancient sedimentary organic carbon in a modern sedimentary system. *Geochimica et Cosmochimica Acta*. 67, 63-73.
- Blair, N.E., Leithold, E.L., Aller, R.C. (2004) From bedrock to burial: the evolution of particulate organic carbon across coupled watershed-continental margin systems. *Marine Chemistry*. 92, 141-156.
- Bohn, U., Neuhäusl, R., Gollub, G., Hettwer, C., Neuhäuslová, Z., Raus, T., Schlüter, H., Weber, H. (2003) Map of the Natural Vegetation of Europe. Scale 1:2 500 000., in: Federal Agency for Nature Conservation, B., Germany, (Ed), Landwirtschaftsverlag, Münster.
- Brandes, J.A., Devol, A.H., Yoshinari, T., Jayakumar, D.A., Naqvi, S.W.A. (1998) Isotopic composition of nitrate in the central Arabian Sea and eastern tropical North Pacific: A tracer for mixing and nitrogen cycles. *Limnology and Oceanography*. 43, 1680-1689.
- Brassell, S.C., Eglinton, G., Marlowe, I.T., Pflaumann, U., Sarnthein, M. (1986) Molecular stratigraphy: a new tool for climatic assessment. *Nature*. 320, 129-133.
- Breckle, S.-W., Agachanjanz, O., Rahmann, M. (1994) Spezielle Ökologie der Gemäßigten und Arktischen Zonen Euro-Nordasiens. *Zonobiom VI-IX*, Gustav Fischer Verlag, Stuttgart.
- Broecker, W.S. (2008) Excess sediment  $^{230}\text{Th}$ : Transport along the sea floor or enhanced water column scavenging? *Global Biogeochemical Cycles*. 22, GB1006, doi: 10.1029/2007GB003057.
- Broecker, W.S., Peng, T.H. (1980) Seasonal variability in the  $^{14}\text{C}/^{12}\text{C}$  ratio for surface ocean water *Geophys. Res. Lett.* 7, 1020-1022.
- Broecker, W.S., Mix, A.C., Andree, M., Oeschger, H. (1984) Radiocarbon measurements on co-existing benthic and planktonic foraminiferal shells: Potential for reconstructing ocean ventilation times over the past 20,000 years. *Nuclear Instruments and methods in Physics Research*. B5, 335-339.
- Broecker, W.S., Peng, T.-H., Ostlund, G., Stuiver, M. (1985) The Distribution of Bomb Radiocarbon in the Ocean. *J. Geophys. Res.* 90, 6953-6970.
- Broecker, W.S., Blanton, S., Smethie, W.M., Jr., Ostlund, G. (1991) Radiocarbon Decay and Oxygen Utilization in The Deep Atlantic Ocean. *Global Biogeochem. Cycles*. 5, 79-89.
- Burdige, D.J. (2005) Burial of terrestrial organic matter in marine sediments: A re-assessment. *Global Biogeochem. Cycles*. 19, doi: 10.1029/2004GB002368.
- Butzin, M., Roether, W. (2004) Tritium budget of the South Atlantic. *J. Geophys. Res.* 109, C03036, doi: 10.1029/2002JC001561.
- Calvert, S.E., Vogel, J.S., Southon, J.R. (1987) Carbon accumulation rates and the origin of the Holocene sapropel in the Black Sea. *Geology*. 15, 918-921.
- Calvert, S.E., Karlin, R.E., Toolin, L.J., Donahue, D.J., Southon, J.R., Vogel, J.S. (1991) Low organic carbon accumulation rates in Black Sea sediments. *Nature*. 350, 692-695.
- Camacho-Ibar, V.F., Aveytua-Alcázar, L., Carriquiry, J.D. (2003) Fatty acid reactivities in sediment cores from the northern Gulf of California. *Organic Geochemistry*. 34, 425-439.
- Canuel, E.A., Martens, C.S. (1996) Reactivity of recently deposited organic matter: Degradation of lipid compounds near the sediment-water interface. *Geochimica et Cosmochimica Acta*. 60, 1793-1806.

---

REFERENCES

- Carpenter, S.R., Elser, M.M., Elser, J.J. (1986) Chlorophyll production, degradation and sedimentation: implications for paleolimnology. *Limnology and Oceanography*. 31, 112-124.
- Cauwet, G., Déliat, G., Krastev, A., Shtereva, G., Becquevort, S., Lancelot, C., Momzikoff, A., Saliot, A., Cociasu, A., Popa, L. (2002) Seasonal DOC accumulation in the Black Sea: a regional explanation for a general mechanism. *Marine Chemistry*. 79, 193-205.
- Chamberlain, P.M., McNamara, N.P., Chaplow, J., Stott, A.W., Black, H.I.J. (2006) Translocation of surface litter carbon into soil by Collembola. *Soil Biology and Biochemistry*. 38, 2655-2664.
- Chavez, F.P., Barber, R.T. (1987) An estimate of new production in the equatorial Pacific. *Deep Sea Research Part A. Oceanographic Research Papers*. 34, 1229-1243.
- Chen, N., Bianchi, T.S., Bland, J.M. (2003) Implications for the role of pre- versus post-depositional transformation of chlorophyll-a in the Lower Mississippi River and Louisiana shelf. *Marine Chemistry*. 81, 37-55.
- Chicarelli, M.I., Hayes, J.M., Popp, B.N., Eckardt, C.B., Maxwell, J.R. (1993) Carbon and nitrogen isotopic compositions of alkyl porphyrins from the Triassic Serpiano oil shale. *Geochimica et Cosmochimica Acta*. 57, 1307-1311.
- Chikaraishi, Y., Naraoka, H., Poulsen, S.R. (2004) Hydrogen and carbon isotopic fractionations of lipid biosynthesis among terrestrial (C<sub>3</sub>, C<sub>4</sub> and CAM) and aquatic plants. *Phytochemistry*. 65, 1369-1381.
- Chikaraishi, Y., Matsumoto, K., Kitazato, H., Ohkouchi, N. (2007) Sources and transformation processes of pheopigments: Stable carbon and hydrogen isotopic evidence from Lake Haruna, Japan. *Organic Geochemistry*. 38, 985-1001.
- Chikaraishi, Y., Kashiyama, Y., Ogawa, N.O., Kitazato, H., Satoh, M., Nomoto, S., Ohkouchi, N. (2008) A compound-specific isotope method for measuring the stable nitrogen isotopic composition of tetrapyrroles. *Organic Geochemistry*. 39, 510-520.
- Chu, P.C., Ivanov, L.M., Margolina, T.M. (2005) Seasonal variability of the Black Sea chlorophyll-a concentration. *Journal of Marine Systems*. 56, 243-261.
- Clark, P.U., McCabe, A.M., Mix, A.C., Weaver, A.J. (2004) Rapid Rise of Sea Level 19,000 Years Ago and Its Global Implications. *Science*. 304, 1141-1144.
- Cline, J.D., Kaplan, I.R. (1975) Isotopic fractionation of dissolved nitrate during denitrification in the eastern tropical north pacific ocean. *Marine Chemistry*. 3, 271-299.
- Cociasu, A., Dorogan, L., Humborg, C., Popa, L. (1996) Long-term ecological changes in Romanian coastal Waters of the Black Sea. *Marine Pollution Bulletin*. 32, 32-38.
- Cole, J.J., Prairie, Y.T., Caraco, N.F., McDowell, W.H., Tranvik, L.J., Striegl, R.G., Duarte, C.M., Kortelainen, P., Downing, J.A., Middelburg, J.J., Melack, J. (2007) Plumbing the Global Carbon Cycle: Integrating Inland Waters into the Terrestrial Carbon Budget Ecosystems. 10, 172-185.
- Collister, J.W., Rieley, G., Stern, B., Eglinton, G., Fry, B. (1994) Compound-specific  $\delta^{13}\text{C}$  analyses of leaf lipids from plants with differing carbon dioxide metabolisms. *Organic Geochemistry*. 21, 619-627.
- Conte, M.H., Weber, J.C., Carlson, P.J., Flanagan, L.B. (2003) Molecular and carbon isotopic composition of leaf wax in vegetation and aerosols in a northern prairie ecosystem. *Oecologia*. 135, 67-77.

- Damon, P.E., Lerman, J.C., Long, A. (1978) Temporal Fluctuations of Atmospheric  $^{14}\text{C}$ : Causal Factors and Implications. *Annual Review of Earth and Planetary Sciences*. 6, 457-494.
- De La Rocha, C.L., Passow, U. (2007) Factors influencing the sinking of POC and the efficiency of the biological carbon pump. *Deep Sea Research Part II: Topical Studies in Oceanography*. 54, 639-658.
- Denman, K.L., Brasseur, G., Chidthaisong, A., Ciais, P., Cox, P.M., Dickinson, R.E., Hauglustaine, D., Heinze, C., Holland, E., Jacob, D., Lohmann, U., Ramachandran, S., da Silva Dias, P.L., Wofsy, S.C., Zhang, X. (2007) The Physical Science Basis. Contribution of Working Group I to the Fourth Assessment Report of the Intergovernmental Panel on Climate Change, in: Solomon, S., Qin, D., Manning, M., Chen, Z., Marquis, M., Averyt, K.B., Tignor, M., Miller, H.L., (Eds), *Climate Change 2007*, Cambridge university Press, Cambridge.
- Dickens, A.F., Gelinas, Y., Masiello, C.A., Wakeham, S., Hedges, J.I. (2004) Reburial of fossil organic carbon in marine sediments. *Nature*. 427, 336-339.
- Dolgilevich, M.J. (1997) Extent and Severity of Wind Erosion in the Ukraine International Symposium on Wind Erosion, Kansas State University, Manhattan, KA, USA. <http://www.weru.ksu.edu/symposium/proceed.htm>.
- Drenzek, N.J. (2007) The Temporal Dynamics of Terrestrial Organic Matter Transfer to the Oceans: Initial Assessment and Application, Ph.D. thesis, MIT/WHOI Joint Program in Oceanography/ Applied Ocean Science and Engineering.
- Drenzek, N.J., Montlucon, D.B., Yunker, M.B., Macdonald, R.W., Eglinton, T.I. (2007) Constraints on the origin of sedimentary organic carbon in the Beaufort Sea from coupled molecular  $^{13}\text{C}$  and  $^{14}\text{C}$  measurements. *Marine Chemistry*. 103, 146-162.
- Drenzek, N.J., Hughen, K.A., Montluçon, D.B., Southon, J.R., dos Santos, G.M., Druffel, E.R.M., Giosan, L., Eglinton, T.I. (2009) A new look at old carbon in active margin sediments. *Geology*. 37, 239-242.
- Driessen, P., Deckers, J., Spaargaren, O., Nachtergaele, F. (2001) Lecture Notes on the Major Soils of the World, World Soil Resources Reports 94, Food and Agriculture Organization of the United Nations, Rome.
- Druffel, E.R., Honjo, S., Griffin, S., Wong, C.S. (1986) Radiocarbon in particulate matter from the Eastern Sub-Arctic Pacific Ocean: evidence of a source of terrestrial carbon to the deep sea. *Radiocarbon*. 28, 397-407.
- Druffel, E.R.M. (1987) Bomb radiocarbon in the Pacific: Annual and seasonal timescale variations. *Journal of Marine Research*. 45, 667-698.
- Druffel, E.R.M., Williams, P.M., Bauer, J.E., Ertel, J.R. (1992) Cycling of Dissolved and Particulate Organic Matter in the Open Ocean. *J. Geophys. Res.* 97, 15639-15659.
- Druffel, E.R.M., Griffin, S., Honjo, S., Manganini, S.J. (1998) Evidence of Old Carbon in the Deep Water Column of the Panama Basin from Natural Radiocarbon Measurements. *Geophysical Research Letters*. 25, 1733-1736.
- Druffel, E.R.M., Bauer, J.E., Griffin, S., Beaupré, S.R., Hwang, J. (2008) Dissolved inorganic radiocarbon in the North Pacific Ocean and Sargasso Sea. *Deep Sea Research Part I: Oceanographic Research Papers*. 55, 451-459.
- Eckert, S., Schnetger, B., Brumsack, H.-J. (2009) Trace metal patterns in Black Sea sapropels as a chemostratigraphic tool, EGU General Assembly 2009, *Geophysical Research Abstracts Vol. 11*, Vienna, Austria, pp. EGU2009-9371.
- Edwards, R.L., Beck, J.W., Burr, G.S., Donahue, D.J., Chappell, J.M.A., Bloom, A.L., Druffel, E.R.M., Taylor, F.W. (1993) A Large Drop in Atmospheric  $^{14}\text{C}/^{12}\text{C}$  and

- Reduced Melting in the Younger Dryas, Documented with  $^{230}\text{Th}$  Ages of Corals. *Science*. 260, 962-968.
- Egbert, G.D., Ray, R.D., Bills, B.G. (2004) Numerical modeling of the global semidiurnal tide in the present day and in the last glacial maximum. *J. Geophys. Res.* 109, C03003, doi:10.1029/2003JC001973.
- Eglinton, G., Hamilton, R.J. (1967) Leaf Epicuticular Waxes. *Science*. 156, 1322-1335.
- Eglinton, T.I., Aluwihare, L.I., Bauer, J.E., Druffel, E.R.M., McNichol, A.P. (1996) Gas Chromatographic Isolation of Individual Compounds from Complex Matrices for Radiocarbon Dating. *Anal. Chem.* 68, 904-912.
- Eglinton, T.I., Benitez-Nelson, B.C., Pearson, A., McNichol, A.P., Baer, J.E., Druffel, E.R.M. (1997) Variability in Radiocarbon Ages of Individual Organic Compounds from Marine Sediments. *Science*. 277, 796-799.
- Eglinton, T.I., Eglinton, G., Dupont, L., Sholkovitz, E.R., Montluçon, D. (2002) Composition, age, and provenance of organic matter in NW African dust over the Atlantic Ocean. *Geochemistry Geophysics Geosystems*. 3, 1050, doi: 10.1029/2001GC000269.
- Eglinton, T.I., Repeta, D.J. (2003) Organic Matter in the Contemporary Ocean, in: Holland, H. D., Turekian, K. K. (Eds), *Treatise on Geochemistry*, Pergamon, Oxford, pp. 145-180.
- Eglinton, T.I., Eglinton, G. (2008) Molecular proxies for paleoclimatology. *Earth and Planetary Science Letters*. 275, 1-16.
- Enting, I.G., Wigley, T.M.L., Heimann, M. (1994) Future Emissions and Concentrations of Carbon Dioxide: Key Ocean/Atmosphere/Land Analyses, Technical Paper No 31, CSIRO Division of Atmospheric Research, Melbourne, Australia.
- Fairbanks, R.G., Sverdlove, M., Free, R., Wiebe, P.H., Be, A.W.H. (1982) Vertical distribution and isotopic fractionation of living planktonic foraminifera from the Panama Basin. *Nature*. 298, 841-844.
- Fairbanks, R.G., Mortlock, R.A., Chiu, T.-C., Cao, L., Kaplan, A., Guilderson, T.P., Fairbanks, T.W., Bloom, A.L., Grootes, P.M., Nadeau, M.-J. (2005) Radiocarbon calibration curve spanning 0 to 50,000 years BP based on paired  $^{230}\text{Th}/^{234}\text{U}/^{238}\text{U}$  and  $^{14}\text{C}$  dates on pristine corals. *Quaternary Science Reviews*. 24, 1781-1796.
- Falkowski, P.G. (2003) Biogeochemistry of Primary Production in the Sea, in: Holland, H. D., Turekian, K. K. (Eds), *Treatise on Geochemistry*, Pergamon, Oxford, pp. 185-213.
- Feldberg, M.J., Mix, A.C. (2003) Planktonic foraminifera, sea-surface temperatures, and mechanisms of oceanic change in the Peru and south equatorial currents, 0–150 ka BP. *Paleoceanography*. 18, PA1016. doi:10.1029/2001PA000740.
- Field, C.B., Behrenfeld, M.J., Randerson, J.T., Falkowski, P. (1998) Primary Production of the Biosphere: Integrating Terrestrial and Oceanic Components. *Science*. 281, 237-240.
- Fok-Pun, L., Komar, P.D. (1983) Settling velocities of planktonic foraminifera: density variations and shape effects. *Journal of Foraminiferal Research*. 13, 60-68.
- Forster, P., Ramaswamy, V., Artaxo, P., Berntsen, T., Betts, R., Fahey, D.W., Haywood, J., Lean, J., Lowe, D.C., Myhre, G., Nganga, J., Prinn, R., Raga, G., Schulz, M., Van Dorland, R. (2007) Changes in Atmospheric Constituents and in Radiative Forcing, in: Solomon, S., Qin, D., Manning, M., Chen, Z., Marquis, M., Averyt, K.B., Tignor, M., Miller, H.L., (Eds), *Climate Change 2007: The Physical Science Basis. Contribution of Working Group I to the Fourth Assessment Report of the*

- Intergovernmental Panel on Climate Change, Cambridge University Press, Cambridge.
- Francois, R., Frank, M., Rutgers van der Loeff, M., Bacon, M., P. (2004)  $^{230}\text{Th}$  normalization: An essential tool for interpreting sedimentary fluxes during the late Quaternary. *Paleoceanography*. 19, PA1018, doi:10.1029/2003PA000939.
- Francois, R., Frank, M., Rutgers van der Loeff, M., Bacon, M.P., Geibert, W., Kienast, S., Anderson, R.F., Bradtmiller, L., Chase, Z., Henderson, G., Marcantonio, F., Allen, S.E. (2007) Comment on "Do geochemical estimates of sediment focusing pass the sediment test in the equatorial Pacific?" by M. Lyle et al. *Paleoceanography*. 22, PA1216, doi:10.1029/2005PA001235.
- Freeman, K.H., Hayes, J.M. (1992) Fractionation of Carbon Isotopes by Phytoplankton and Estimates of Ancient CO<sub>2</sub> Levels. *Global Biogeochem. Cycles*. 6, doi: 10.1029/92GB00190.
- Friedrich, M., Remmeli, S., Kromer, B., Hofmann, J., Spurk, M., Felix Kaiser, K., Orcel, C., Küppers, M. (2004) The 12,460-Year Hohenheim Oak and Pine Tree-Ring Chronology from Central Europe—a Unique Annual Record for Radiocarbon Calibration and Paleoenvironment Reconstructions. *Radiocarbon*. 46, 1111-1122.
- Fuchsman, C.A., Murray, J.W., Konovalov, S.K. (2008) Concentration and natural stable isotope profiles of nitrogen species in the Black Sea. *Marine Chemistry*. 111, 90-105.
- Furlong, E.T., Carpenter, R. (1988) Pigment preservation and remineralization in oxic coastal marine sediments. *Geochimica et Cosmochimica Acta*. 52, 87-99.
- Gagosian, R.B., Peltzer, E.T., Zafiriou, O.C. (1981) Atmospheric transport of continentally derived lipids to the tropical North Pacific. *Nature*. 291, 312-314.
- Gagosian, R.B., Peltzer, E.T. (1986) The importance of atmospheric input of terrestrial organic material to deep sea sediments. *Organic Geochemistry*. 10, 661-669.
- Gislefoss, J.S., Nydal, R., Slagstad, D., Sonninen, E., Holmén, K. (1998) Carbon time series in the Norwegian sea. *Deep Sea Research Part I: Oceanographic Research Papers*. 45, 433-460.
- Giunta, S., Morigi, C., Negri, A., Guichard, F., Lericolais, G. (2007) Holocene biostratigraphy and paleoenvironmental changes in the Black Sea based on calcareous nannoplankton. *Marine Micropaleontology*. 63, 91-110.
- Godwin, H. (1962) Half-life of Radiocarbon. *Nature*. 195, 984-984.
- Goericke, R., Strom, S.L., Bell, M.A. (2000) Distribution and sources of cyclic pheophorbides in the marine environment. *Limnology and Oceanography*. 45, 200-211.
- Gong, C., Hollander, D.J. (1999) Evidence for differential degradation of alkenones under contrasting bottom water oxygen conditions: implication for paleotemperature reconstruction. *Geochimica et Cosmochimica Acta*. 63, 405-411.
- Goni, M.A., Ruttenberg, K.C., Eglinton, T.I. (1997) Sources and contribution of terrigenous organic carbon to surface sediments in the Gulf of Mexico. *Nature*. 389, 275-278.
- Goslar, T., Arnold, M., Bard, E., Kuc, T., Pazdur, M.F., Ralska-Jasiewiczowa, M., Rozanski, K., Tisnerat, N., Walanus, A., Wicik, B., Wieqkowski, K. (1995) High concentration of atmospheric  $^{14}\text{C}$  during the Younger Dryas cold episode. *Nature*. 377, 414-417.
- Goslar, T., Hercman, H., Pazdur, A. (2000) Comparison of U-series and radiocarbon dates of speleothems. *Radiocarbon*. 42, 403-414.
- Gossauer, A., Engel, N. (1996) Chlorophyll catabolism - structures, mechanisms, conversions. *Journal of Photochemistry and Photobiology B: Biology*. 32, 141-151.

- Griffith, D.R., Barnes, R.T., Raymond, P.A. (2009) Inputs of Fossil Carbon from Wastewater Treatment Plants to U.S. Rivers and Oceans. *Environmental Science & Technology.* 43, 5647-5651.
- Gruber, N., Keeling, C.D., Bates, N.R. (2002) Interannual Variability in the North Atlantic Ocean Carbon Sink. *Science.* 298, 2374-2378.
- Gulin, S.B. (2000) Recent changes of biogenic carbonate deposition in anoxic sediments of the Black Sea: sedimentary record and climatic implication. *Marine Environmental Research.* 49, 319-328.
- Gulin, S.B., Polikarpov, G.G., Egorov, V.N., Martin, J.M., Korotkov, A.A., Stokozov, N.A. (2002) Radioactive Contamination of the North-western Black Sea Sediments. *Estuarine, Coastal and Shelf Science.* 54, 541-549.
- Gulin, S.B., Polikarpov, G.G., Martin, J.M. (2003) Geochronological reconstruction of <sup>137</sup>Cs transport from the Coruh river to the SE Black Sea: comparative assessment of radionuclide retention in the mountainous catchment area. *Continental Shelf Research.* 23, 1811-1819.
- Haddad, R.I., Martens, C.S., Farrington, J.W. (1991) Quantifying early diagenesis of fatty acids in a rapidly accumulating coastal marine sediment. *Organic Geochemistry.* 19, 205-216.
- Hansman, R.L., Griffin, S., Watson, J.T., Druffel, E.R.M., Ingalls, A.E., Pearson, A., Aluwihare, L.I. (2009) The radiocarbon signature of microorganisms in the mesopelagic ocean. *Proceedings of the National Academy of Sciences.* 106, 6513-6518.
- Hayes, J.M., Takigiku, R., Ocampo, R., Callot, H.J., Albrecht, P. (1987) Isotopic compositions and probable origins of organic molecules in the Eocene Messel shale. *Nature.* 329, 48-51.
- Hedges, J.I. (1992) Global biogeochemical cycles: progress and problems. *Marine Chemistry.* 39, 67-93.
- Hedges, J.I., Ertel, J.R., Quay, P.D., Grootes, P.M., Richey, J.E., Devol, A.H., Farwell, G.W., Schmidt, F.W., Salati, E. (1986) Organic Carbon-14 in the Amazon River System. *Science.* 231, 1129-1131.
- Hedges, J.I., Keil, R.G. (1995) Sedimentary organic matter preservation: an assessment and speculative synthesis. *Marine Chemistry.* 49, 81-115.
- Hedges, J.I., Keil, R.G., Benner, R. (1997) What happens to terrestrial organic matter in the ocean? *Organic Geochemistry.* 27, 195-212.
- Hedges, J.I., Oades, J.M. (1997) Comparative organic geochemistries of soils and marine sediments. *Organic Geochemistry.* 27, 319-361.
- Hélie, J.-F., Hillaire-Marcel, C., Rondeau, B. (2002) Seasonal changes in the sources and fluxes of dissolved inorganic carbon through the St. Lawrence River-isotopic and chemical constraint. *Chemical Geology.* 186, 117-138.
- Hinrichs, K.-U., Hayes, J.M., Sylva, S.P., Brewer, P.G., DeLong, E.F. (1999) Methane-consuming archaeabacteria in marine sediments. *Nature.* 398, 802-805.
- Hinrichs, K.-U., Summons, R.E., Orphan, V., Sylva, S.P., Hayes, J.M. (2000) Molecular and isotopic analysis of anaerobic methane-oxidizing communities in marine sediments. *Organic Geochemistry.* 31, 1685-1701.
- Honjo, S. (1982) Seasonality and Interaction of Biogenic and Lithogenic Particulate Flux at the Panama Basin. *Science.* 218, 883-884.
- Honjo, S., Spencer, D.W., Gardner, W.D. (1992) A sediment trap intercomparison experiment in the Panama Basin, 1979. *Deep Sea Research Part A. Oceanographic Research Papers.* 39, 333-358.

- Hopmans, E.C., Weijers, J.W.H., Schefuß, E., Herfort, L., Sinninghe Damste, J.S., Schouten, S. (2004) A novel proxy for terrestrial organic matter in sediments based on branched and isoprenoid tetraether lipids. *Earth and Planetary Science Letters.* 224, 107-116.
- Houghton, R.A. (2003a) The Contemporary Carbon Cycle, in: Holland, H. D., Turekian, K. K. (Eds), *Treatise on Geochemistry*, Pergamon, Oxford, pp. 473-513.
- Houghton, R.A. (2003b) Why are estimates of the terrestrial carbon balance so different? *Global Change Biology.* 9, 500-509.
- Hoyt, P.B. (1966) Chlorophyll-type compounds in soil. II. their decomposition. *Plant and Soil.* 25, 313-328.
- Hughen, K.A., Overpeck, J.T., Lehman, S.J., Kashgarian, M., Southon, J., Peterson, L.C., Alley, R., Sigman, D.M. (1998) Deglacial changes in ocean circulation from an extended radiocarbon calibration. *Nature.* 391, 65-68.
- Hughen, K., Lehman, S., Southon, J., Overpeck, J., Marchal, O., Herring, C., Turnbull, J. (2004a)  $^{14}\text{C}$  Activity and Global Carbon Cycle Changes over the Past 50,000 Years. *Science.* 303, 202-207.
- Hughen, K.A., Baillie, M.G.L., Bard, E., Beck, J.W., Bertrand, C.J.H., Blackwell, P.G., Buck, C.E., Burr, G.S., Cutler, K.B., Damon, P.E., Edwards, R.L., Fairbanks, R.G., Friedrich, M., Guilderson, T.P., Kromer, B., McCormac, G., Manning, S., Ramsey, C.B., Reimer, P.J., Reimer, R.W., Remmeli, S., Southon, J.R., Stuiver, M., Talamo, S., Taylor, F.W., van der Plicht, J., Weyhenmeyer, C.E. (2004b) Marine04 Marine Radiocarbon Age Calibration, 0–26 Cal Kyr BP. *Radiocarbon.* 46, 1059-1086.
- Ingalls, A.E., Anderson, R.F., Pearson, A. (2004) Radiocarbon dating of diatom-bound organic compounds. *Marine Chemistry.* 92, 91-105.
- Ingalls, A.E., Shah, S.R., Hansman, R.L., Aluwihare, L.I., Santos, G.M., Druffel, E.R.M., Pearson, A. (2006) Quantifying archaeal community autotrophy in the mesopelagic ocean using natural radiocarbon. *Proceedings of the National Academy of Sciences.* 103, 6442-6447.
- Ivanova, E.V., Murdmaa, I.O., Chepalyga, A.L., Cronin, T.M., Pasechnik, I.V., Levchenko, O.V., Howe, S.S., Manushkina, A.V., Platonova, E.A. (2007) Holocene sea-level oscillations and environmental changes on the Eastern Black Sea shelf. *Palaeogeography, Palaeoclimatology, Palaeoecology.* 246, 228-259.
- Jaoshvili, S. (2002) The rivers of Black Sea, in: Khomerki, I., Gigineishvili, G., Kordzadze, A., (Eds), Technical Report, vol. 71, European Environment Agency, Copenhagen, Denmark.
- Jobbágy, E.G., Jackson, R.B. (2000) The vertical distribution of soil organic carbon and its relation to climate and vegetation. *Ecological Applications.* 10, 423-436.
- Jones, G.A., Gagnon, A.R. (1994) Radiocarbon chronology of Black Sea sediments. *Deep Sea Research Part I: Oceanographic Research Papers.* 41, 531-557.
- Kanduč, T., Szramek, K., Ogrinc, N., Walter, L.M. (2007) Origin and cycling of riverine inorganic carbon in the Sava River watershed (Slovenia) inferred from major solutes and stable carbon isotopes *Biogeochemistry.* 86, 137-154.
- Kao, S.-J., Liu, K.-K. (1996) Particulate organic carbon export from a subtropical mountainous river (Lanyang Hsi) in Taiwan. *Limnology and Oceanography.* 41, 1749-1757.
- Karlén, I., Olsson, I.U., Källburg, P., Kilici, S. (1968) Absolute determination of the activity of two  $^{14}\text{C}$  dating standards. *Arkiv Geofysik.* 4, 465-471.
- Kashiyama, Y., Ogawa, N.O., Kuroda, J., Shiro, M., Nomoto, S., Tada, R., Kitazato, H., Ohkouchi, N. (2008a) Diazotrophic cyanobacteria as the major photoautotrophs

- during mid-Cretaceous oceanic anoxic events: Nitrogen and carbon isotopic evidence from sedimentary porphyrin. *Organic Geochemistry*. 39, 532-549.
- Kashiyama, Y., Ogawa, N.O., Shiro, M., Tada, R., Kitazato, H., Ohkouchi, N. (2008b) Reconstruction of the biogeochemistry and ecology of photoautotrophs based on the nitrogen and carbon isotopic compositions of vanadyl porphyrins from Miocene siliceous sediments. *Biogeosciences*. 5, 797-816.
- Keil, R.G., Mayer, L.M., Quay, P.D., Richey, J.E., Hedges, J.I. (1997) Loss of organic matter from riverine particles in deltas. *Geochimica et Cosmochimica Acta*. 61, 1507-1511.
- Kessler, J.D., Reeburgh, W.S., Sounthor, J., Varela, R. (2005) Fossil methane source dominates Cariaco Basin water column methane geochemistry. *Geophys. Res. Lett.* 32, L12609, doi:10.1029/2005GL022984.
- Kessler, W.S. (2006) The circulation of the eastern tropical Pacific: A review. *Progress In Oceanography*. 69, 181-217.
- Key, R.M., Kozyr, A., Sabine, C.L., Lee, K., Wanninkhof, R., Bullister, J.L., Feely, R.A., Millero, F.J., Mordy, C., Peng, T.H. (2004) A global ocean carbon climatology: Results from Global Data Analysis Project (GLODAP). *Global Biogeochem. Cycles*. 18, GB4031, doi:10.1029/2004GB002247.
- Kienast, M., Kienast, S.S., Calvert, S.E., Eglinton, T.I., Mollenhauer, G., Francois, R., Mix, A.C. (2006) Eastern Pacific cooling and Atlantic overturning circulation during the last deglaciation. *Nature*. 443, 846-849.
- Kienast, S.S., Kienast, M., Mix, A.C., Calvert, S.E., Francois, R. (2007) Thorium-230 normalized particle flux and sediment focusing in the Panama Basin region during the last 30,000 years. *Paleoceanography*. 22, doi:10.1029/2006PA001357.
- Killops, S.D., Killops, V.J. (2004) An Introduction to Organic Geochemistry, Wiley-Blackwell, Malden.
- King, L.L. (1993) Chlorophyll Diagenesis in the Water Column and Sediments of the Black Sea, Ph.D. thesis, MIT/WHOI Joint Program in Oceanography/ Applied Ocean Science and Engineering.
- King, L.L. (1995) A mass balance of chlorophyll degradation product accumulation in Black Sea sediments. *Deep Sea Research Part I: Oceanographic Research Papers*. 42, 919-942.
- Kish, S. (2003) Changing Export Production in the Eastern Equatorial Pacific, 160 ka to Present. Unpublished MS Thesis, Oregon State University.
- Koch, P.L., Zachos, J.C., Gingerich, P.D. (1992) Correlation between isotope records in marine and continental carbon reservoirs near the Palaeocene/Eocene boundary. *Nature*. 358, 319-322.
- Kolber, Z.S., Barber, R.T., Coale, K.H., Fitzwateri, S.E., Greene, R.M., Johnson, K.S., Lindley, S., Falkowski, P.G. (1994) Iron limitation of phytoplankton photosynthesis in the equatorial Pacific Ocean. *Nature*. 371,
- Krupatkina, D.K., Finenko, Z.Z., Shalapyonok, A.A. (1991) Primary production and size-fractionated structure of the Black Sea phytoplankton in the winter-spring period. *Marine Ecology Progress Series*. 73, 25-31.
- Laird, N.P. (1971) Panama Basin Deep Water - Properties and Circulation. *Journal of Marine Research*. 29, 226-234.
- Larionov, G.A., Skidmore, E.L., Kiryukhina, Z.P. (1997) Wind Erosion in Russia: Spreading and Quantitative Assessment, International Symposium on Wind Erosion, Kansas State University, Manhattan, KA, USA. <http://www.weru.ksu.edu/symposium/proceed.htm>.

- Lehmann, M.M., Bernasconi, S.M., McKenzie, J.A., Barbieri, A., Simona, M., Veronesi, M. (2004) Seasonal variation of the  $\delta^{13}\text{C}$  and  $\delta^{15}\text{N}$  of particulate and dissolved carbon and nitrogen in Lake Lugano: Constraints on biogeochemical cycling in a eutrophic lake. *Limnology and Oceanography*. 49, 415-429.
- Levin, I., Kromer, B., Schoch-Fischer, H., Bruns, M., Munnich, M., Berdau, D., Vogel, J.C., Munnich, K.O. (1985) 25 Years of tropospheric  $^{14}\text{C}$  observations. *Radiocarbon*. 27, 1-19.
- Levin, I., Kromer, B. (1997) Twenty Years of Atmospheric  $^{14}\text{CO}_2$  Observations at Schauinsland Station, Germany. *Radiocarbon*. 39, 205-218.
- Levin, I., Hesshaimer, V. (2000) Radiocarbon - a unique tracer of global carbon cycle dynamics. *Radiocarbon*. 42, 69-80.
- Levin, I., Hammer, S., Kromer, B., Meinhardt, F. (2008) Radiocarbon observations in atmospheric CO<sub>2</sub>: Determining fossil fuel CO<sub>2</sub> over Europe using Jungfraujoch observations as background. *Science of The Total Environment*. 391, 211-216.
- Liu, K.-K., Kaplan, I.R. (1989) The eastern tropical Pacific as a source of  $^{15}\text{N}$ -enriched nitrate in seawater off southern California. *Limnology and Oceanography*. 34, 820-830.
- Locarnini, R.A., Mishonov, A.V., Antonov, J.J., Boyer, T.P., Garcia, H.E. (2006) World Ocean Atlas 2005, Volume 1: Temperature, in: Levitus, S., (Ed), NOAA Atlas NESDIS 61, U.S. Government Printing Office, Washington, D.C., p. 182.
- Lockheart, M.J., Van Bergen, P.F., Evershed, R.P. (1997) Variations in the stable carbon isotope compositions of individual lipids from the leaves of modern angiosperms: implications for the study of higher land plant-derived sedimentary organic matter. *Organic Geochemistry*. 26, 137-153.
- Longworth, B.E., Petsch, S.T., Raymond, P.A., Bauer, J.E. (2007) Linking lithology and land use to sources of dissolved and particulate organic matter in headwaters of a temperate, passive-margin river system. *Geochimica et Cosmochimica Acta*. 71, 4233-4250.
- Lonsdale, P. (1977) Inflow of bottom water to the Panama Basin. *Deep Sea Research*. 24, 1065-1094.
- Lonsdale, P., Malfait, B. (1974) Abyssal Dunes of Foraminiferal Sand on the Carnegie Ridge. *Bulletin of the Geological Society of America*. 85, 1697-1712.
- Loubere, P. (1999) A multiproxy reconstruction of biological productivity and oceanography in the eastern equatorial Pacific for the past 30,000 years. *Marine Micropaleontology*. 37, 173-198.
- Loubere, P. (2000) Marine control of biological production in the eastern equatorial Pacific Ocean. *Nature*. 406, 497-500.
- Loubere, P., Fariduddin, M., Murray, R.W. (2003) Patterns of export production in the eastern equatorial Pacific over the past 130,000 years. *Paleoceanography*. 18, doi:10.1029/2001PA000658.
- Loubere, P., Mekik, F., Francois, R., Pichat, S. (2004) Export fluxes of calcite in the eastern equatorial Pacific from the Last Glacial Maximum to present. *Paleoceanography*. 19, PA2018, doi:10.1029/2003PA000986.
- Loubere, P., Richaud, M. (2007) Some reconciliation of glacial-interglacial calcite flux reconstructions for the eastern equatorial Pacific. *Geochemistry Geophysics Geosystems*. 8, Q03008, doi:10.1029/2006GC001367.
- Louda, J.W., Li, J., Liu, L., Winfree, M.N., Baker, E.W. (1998) Chlorophyll-a degradation during cellular senescence and death. *Organic Geochemistry*. 29, 1233-1251.

- Lyle, M., Mix, A., Pisias, N. (2002) Patterns of CaCO<sub>3</sub> deposition in the eastern tropical Pacific Ocean for the last 150 kyr: Evidence for a southeast Pacific depositional spike during marine isotope stage (MIS) 2. *Paleoceanography*. 17, 1013, doi:10.1029/2000PA000538.
- Lyle, M., M., Pisias, N., Mix, A., Martinez, J.I., Paytan, A. (2005) Do geochemical estimates of sediment focusing pass the sediment test in the equatorial Pacific? *Paleoceanography*. 20, PA1005, doi:10.1029/2004PA001019.
- Lyle, M., Pisias, N., Paytan, A., Martinez, J.I., Mix, A. (2007) Reply to comment by R. Francois et al. on "Do geochemical estimates of sediment focusing pass the sediment test in the equatorial Pacific?": Further explorations of <sup>230</sup>Th normalization. *Paleoceanography*. 22, PA1217, doi:10.1029/2006PA001373.
- Ma, L., Dolphin, D. (1996) Stereoselective Synthesis of New Chlorophyll a Related Antioxidants Isolated from Marine Organisms. *The Journal of Organic Chemistry*. 61, 2501-2510.
- Malfait, B.T., Van Andel, T.H. (1980) A modern oceanic hardground on the Carnegie Ridge in the eastern Equatorial Pacific. *Sedimentology*. 27, 467-496. 1365-3091.
- Marcantonio, F., Anderson, R.F., Higgins, S., Stute, M., Schlosser, P., Kubik, P. (2001) Sediment focusing in the central equatorial Pacific Ocean. *Paleoceanography*. 16, 260-267.
- Marlowe, I.T., Brassell, S.C., Eglinton, G., Green, J.C. (1984) Long chain unsaturated ketones and esters in living algae and marine sediments. *Organic Geochemistry*. 6, 135-141.
- Martinez, I., Rincon, D., Yokoyama, Y., Barrows, T. (2006) Foraminifera and coccolithophorid assemblage changes in the Panama Basin during the last deglaciation: Response to sea-surface productivity induced by a transient climate change. *Palaeogeography, Palaeoclimatology, Palaeoecology*. 234, 114-126.
- Masiello, C.A., Druffel, E.R.M. (1998) Black Carbon in Deep-Sea Sediments. *Science*. 280, 1911-1913.
- Matile, P., Hörtensteiner, S., Thomas, H., Kräutler, B. (1996) Chlorophyll Breakdown in Senescent Leaves. *Plant Physiol.* 112, 1402-1409.
- Matsumoto, K., Kawamura, K., Uchida, M., Shibata, Y., Yoneda, M. (2001) Compound Specific Radiocarbon and  $\delta^{13}\text{C}$  Measurements of Fatty Acids in a Continental Aerosol Sample. *Geophys. Res. Lett.* 28, doi: 2001GL013599.
- Mayer, L.M. (1994a) Relationships between mineral surfaces and organic carbon concentrations in soils and sediments. *Chemical Geology*. 114, 347-363.
- Mayer, L.M. (1994b) Surface area control of organic carbon accumulation in continental shelf sediments. *Geochimica et Cosmochimica Acta*. 58, 1271-1284.
- Mazaud, A., Laj, C., Bard, E., Arnold, M., Tric, E. (1991) Geomagnetic field control of <sup>14</sup>C production over the last 80 ky: implications for the radiocarbon time-scale. *Geophysical Research Letters*. 18, 1885-1888.
- McCarthy, J.J., Yilmaz, A., Coban-Yildiz, Y., Nevins, J.L. (2007) Nitrogen cycling in the offshore waters of the Black Sea. *Estuarine, Coastal and Shelf Science*. 74, 493-514.
- McCormac, F.G., Hogg, A.G., Blackwell, P.G., Buck, C.E., Higham, T.F.G., Reimer, P.J. (2004) SHcal04 Southern Hemisphere calibration, 0-11.0 cal kyr BP. *Radiocarbon*. 46, 1087-1092.
- McIlvin, M.R., Altabet, M.A. (2005) Chemical Conversion of Nitrate and Nitrite to Nitrous Oxide for Nitrogen and Oxygen Isotopic Analysis in Freshwater and Seawater. *Analytical Chemistry*. 77, 5589-5595.

- McNichol, A.P., Osborne, E.A., Gagnon, A.R., Fry, B., Jones, G.A. (1994) TIC, TOC, DIC, DOC, PIC, POC - unique aspects in the preparation of oceanographic samples for  $^{14}\text{C}$ -AMS. Nuclear Instruments and Methods in Physics Research Section B: Beam Interactions with Materials and Atoms. 92, 162-165.
- Meyers, P.A. (1994) Preservation of elemental and isotopic source identification of sedimentary organic matter. Chemical Geology. 114, 289-302.
- Minagawa, M., Wada, E. (1986) Nitrogen isotope ratios of red tide organisms in the East China Sea: A characterization of biological nitrogen fixation. Marine Chemistry. 19, 245-259.
- Mix, A.C. (2006) Running hot and cold in the eastern equatorial Pacific. Quaternary Science Reviews. 25, 1147-1149.
- Mollenhauer, G., Eglington, T.I., Ohkouchi, N., Schneider, R.R., Muller, P.J., Grootes, P.M., Rullkötter, J. (2003) Asynchronous alkenone and foraminifera records from the Benguela Upwelling System. *Geochimica et Cosmochimica Acta*. 67, 2157-2171.
- Mollenhauer, G., Kienast, M., Lamy, F., Meggers, H., Schneider, R.R., Hayes, J.M., Eglington, T.I. (2005a) An evaluation of  $^{14}\text{C}$  age relationships between co-occurring foraminifera, alkenones, and total organic carbon in continental margin sediments. *Paleoceanography*. 20, PA1016, doi:10.1029/2004PA001103.
- Mollenhauer, G., Montlucon, D., Eglington, T.I. (2005b) Radiocarbon Dating of Alkenones from Marine Sediments: II. Assessment of Carbon Process Blanks. *Radiocarbon*. 47, 413-424.
- Mollenhauer, G., McManus, J.F., Benthien, A., Muller, P.J., Eglington, T.I. (2006) Rapid lateral particle transport in the Argentine Basin: Molecular  $^{14}\text{C}$  and  $^{230}\text{Th}_{\text{xs}}$  evidence. *Deep Sea Research Part I: Oceanographic Research Papers*. 53, 1224-1243.
- Mollenhauer, G., Eglington, T.I. (2007) Diagenetic and sedimentological controls on the composition of organic matter preserved in California Borderland Basin sediments. *Limnology and Oceanography*. 52, 558-576.
- Mollenhauer, G., Rethemeyer, J. (2009) Compound-specific radiocarbon analysis – analytical challenges and applications. *IOP Conf. Series: Earth and Environmental Science*. 5, doi:10.1088/1755-1307/5/1/012006.
- Montoya, J.P., Carpenter, E.J., Capone, D.G. (2002) Nitrogen fixation and nitrogen isotope abundances in zooplankton of the oligotrophic North Atlantic. *Limnology and Oceanography*. 47, 1617-1628.
- Moore, T.C., Jr., Heath, G.R., Kowsmann, R.O. (1973) Biogenic sediments of the Panama Basin. *Journal of Geology*. 81, 458-472.
- Moreth, C.M., Yentsch, C.S. (1970) The role of chlorophyllase and light in the decomposition of chlorophyll from marine phytoplankton. *Journal of Experimental Marine Biology and Ecology*. 4, 238-249.
- Müller, P.J., Kirst, G., Ruhland, G., von Storch, I., Rosell-Melé, A. (1998) Calibration of the alkenone paleotemperature index U37K' based on core-tops from the eastern South Atlantic and the global ocean (60°N-60°S). *Geochimica et Cosmochimica Acta*. 62, 1757-1772.
- Murray, J.W., Fuchsman, C., Kirkpatrick, J., Paul, B., Konovalov, S.K. (2005) Species and  $\delta^{15}\text{N}$  signatures of nitrogen transformations in the suboxic zone of the Black Sea. *Oceanography*. 18, 36-47.
- NOSAMS (2008) General Statement of  $^{14}\text{C}$  Procedures at the National Ocean Sciences AMS Facility. <http://www.nosams.whoi.edu/images/amsgenst.pdf>
- NOSAMS (2009a) Laboratory Capabilities. <http://www.nosams.whoi.edu/about/index.html>.

- NOSAMS (2009b) Sample Types and Processes. <http://www.nosams.whoi.edu/clients/processes.html>.
- Nydal, R., Lövseth, K. (1983) Tracing Bomb  $^{14}\text{C}$  in the Atmosphere 1962-1980. *J. Geophys. Res.* 88, 3621-3642.
- Oades, J.M. (1988) The retention of organic matter in soils Biogeochemistry. 5, 35-70.
- Oberhuber, M., Berghold, J., Breuker, K., Hörtensteiner, S., Kräutler, B. (2003) Breakdown of chlorophyll: A nonenzymatic reaction accounts for the formation of the colorless "nonfluorescent" chlorophyll catabolites. *Proceedings of the National Academy of Sciences of the United States of America.* 100, 6910-6915.
- Ocampo, R., Sachs, J.P., Repeta, D.J. (1999) Isolation and structure determination of the unstable  $13^2$ ,  $17^3$ -Cyclopheophorbide *a* enol from recent sediments. *Geochimica et Cosmochimica Acta.* 63, 3743-3749.
- Oguz, T. (2005) Long-Term Impacts of Anthropogenic Forcing on the Black Sea Ecosystem. *Oceanography.* 18, 112-121.
- Oguz, T., Malanotte-Rizzoli, P., Aubrey, D. (1995) Wind and thermohaline circulation of the Black Sea driven by yearly mean climatological forcing. *Journal of Geophysical Research.* 100, 6845-6863.
- Ohkouchi, N., Kawamura, K., Kawahata, H., Taira, A. (1997) Latitudinal distributions of terrestrial biomarkers in the sediments from the Central Pacific. *Geochimica et Cosmochimica Acta.* 61, 1911-1918.
- Ohkouchi, N., Eglinton, T.I., Keigwin, L.D., Hayes, J.M. (2002) Spatial and Temporal Offsets Between Proxy Records in a Sediment Drift. *Science.* 298, 124-1227.
- Ohkouchi, N., Eglinton, T.I., Hayes, J.M. (2003) Radiocarbon dating of individual fatty acids as a tool for refining Antarctic margin sediment chronologies. *Radiocarbon.* 45, 17-24.
- Ohkouchi, N., Eglinton, T.I., Hughen, K.A., Roosen, E., Keigwin, L.D. (2005a) Radiocarbon Dating of Alkenones from Marine Sediments: III. Influence of Solvent Extraction Procedures on  $^{14}\text{C}$  Measurements of Foraminifera. *Radiocarbon.* 47, 425-432.
- Ohkouchi, N., Nakajima, Y., Okada, H., Ogawa, N.O., Suga, H., Oguri, K., Kitazato, H. (2005b) Biogeochemical processes in the saline meromictic Lake Kaiike, Japan: implications from molecular isotopic evidences of photosynthetic pigments. *Environmental microbiology.* 7, 1009-1016.
- Ohkouchi, N., Xu, L., Reddy, C.M., Montlucon, D., Eglinton, T.I. (2005c) Radiocarbon Dating of Alkenones from Marine Sediments: I. Isolation Protocol. *Radiocarbon.* 47, 401-412.
- Ohkouchi, N., Kashiyama, Y., Kuroda, J., Ogawa, N.O., Kitazato, H. (2006) The importance of diazotrophic cyanobacteria as primary producers during Cretaceous Oceanic Anoxic Event 2. *Biogeosciences.* 3, 467-478.
- Ohkouchi, N., Nakajima, Y., Ogawa, N.O., Chikaraishi, Y., Suga, H., Sakai, S., Kitazato, H. (2008) Carbon isotopic composition of the tetrapyrrole nucleus in chloropigments from a saline meromictic lake: A mechanistic view for interpreting the isotopic signature of alkyl porphyrins in geological samples. *Organic Geochemistry.* 39, 521-531.
- Ostlund, H.G., Dryssen, D. (1986) Renewal rates of Black Sea deep water, Proceedings of the chemical and physical oceanography of the Black Sea, International meeting, University of Göteborg, Göteborg, Sweden.
- Owens, T.G., Falkowski, P.G. (1982) Enzymatic degradation of chlorophyll *a* by marine phytoplankton in vitro. *Phytochemistry.* 21, 979-984.

- Panin, N., Jipa, D. (2002) Danube River Sediment Input and its Interaction with the North-western Black Sea. *Estuarine, Coastal and Shelf Science.* 54, 551-562.
- Paytan, A., Kastner, M., Chavez, F.P. (1996) Glacial to Interglacial Fluctuations in Productivity in the Equatorial Pacific as Indicated by Marine Barite. *Science.* 274, 1355-1357.
- Pearson, A., McNichol, A.P., Schneider, R.J., Reden, K.F.v., Zheng, Y. (1998) Microscale AMS  $^{14}\text{C}$  measurement at NOSAMS. *Radiocarbon.* 40, 61-75.
- Pearson, A., Eglinton, T.I. (2000) The origin of *n*-alkanes in Santa Monica Basin surface sediment: a model based on compound-specific  $\Delta^{14}\text{C}$  and  $\delta^{13}\text{C}$  data. *Organic Geochemistry.* 31, 1103-1116.
- Pearson, A., McNichol, A.P., Benitez-Nelson, B.C., Hayes, J.M., Eglinton, T.I. (2001) Origins of lipid biomarkers in Santa Monica Basin surface sediment: a case study using compound-specific  $\Delta^{14}\text{C}$  analysis. *Geochimica et Cosmochimica Acta.* 65, 3123-3137.
- Pearson, A., Seewald, J.S., Eglinton, T.I. (2005) Bacterial incorporation of relict carbon in the hydrothermal environment of Guaymas Basin. *Geochimica et Cosmochimica Acta.* 69, 5477-5486.
- Pearson, P.N., Palmer, M.R. (2000) Atmospheric carbon dioxide concentrations over the past 60 million years. *Nature.* 406, 695-699.
- Pedersen, T.F. (1983) Increased productivity in the eastern equatorial Pacific during the last glacial maximum (19,000 to 14,000 yr B.P.). *Geology.* 11, 16-19.
- Pena, L.D., Cacho, I., Ferretti, P., Hall, M.A. (2008) El Nino Southern Oscillation like variability during glacial terminations and interlatitudinal teleconnections. *Paleoceanography.* 23, PA3101, doi:10.1029/2008PA001620.
- Pennington, J.T., Mahoney, K.L., Kuwahara, V.S., Kolber, D.D., Calienes, R., Chavez, F.P. (2006) Primary production in the eastern tropical Pacific: A review. *Progress In Oceanography.* 69, 285-317.
- Peters, K.E., Walters, C.C., Moldowan, J.M. (2005) *The Biomarker Guide*, Cambridge University Press, Cambridge.
- Petit, J.R., Jouzel, J., Raynaud, D., Barkov, N.I., Barnola, J.M., Basile, I., Bender, M., Chappellaz, J., Davis, M., Delaygue, G., Delmotte, M., Kotlyakov, V.M., Legrand, M., Lipenkov, V.Y., Lorius, C., Pepin, L., Ritz, C., Saltzman, E., Stievenard, M. (1999) Climate and atmospheric history of the past 420,000 years from the Vostok ice core, Antarctica. *Nature.* 399, 429-436.
- Petsch, S.T., Eglinton, T.I., Edwards, K.J. (2001)  $^{14}\text{C}$ -Dead Living Biomass: Evidence for Microbial Assimilation of Ancient Organic Carbon During Shale Weathering. *Science.* 292, 1127-1131.
- Pisias, N.G., Mix, A.C. (1997) Spatial and Temporal Oceanographic Variability of the Eastern Equatorial Pacific During the Late Pleistocene: Evidence from Radiolaria Microfossils *Paleoceanography.* 12, 381-393.
- Popa, A. (1997) Environment changes in the Danube Delta caused by the hydrotechnical works on the Sf. Gheorghe branch. *Geo-Eco-Marina.* 2, 135-147.
- Post, W.M., Pastor, J., Zinke, P.J., Stangenberger, A.G. (1985) Global patterns of soil nitrogen storage. *Nature.* 317, 613-616.
- Prahl, F.G., Wakeham, S.G. (1987) Calibration of unsaturation patterns in long-chain ketone compositions for palaeotemperature assessment. *Nature.* 330, 367-369.
- Prahl, F.G., Mix, A.C., Sparrow, M.A. (2006) Alkenone paleothermometry: Biological lessons from marine sediment records off western South America. *Geochimica et Cosmochimica Acta.* 70, 101-117.

- Preoteasa, L., Roberts, H.M., Duller, G.A.T., Vespremeanu-Stroe, A. (2009) Late-Holocene coastal dune system evolution in the Danube Delta, NW Black Sea Basin Journal of Coastal Research. S56, 347-351.
- Raymond, P.A., Bauer, J.E. (2001a) Riverine export of aged terrestrial organic matter to the North Atlantic Ocean. *Nature*. 409, 497-500.
- Raymond, P.A., Bauer, J.E. (2001b) Use of  $^{14}\text{C}$  and  $^{13}\text{C}$  natural abundances for evaluating riverine, estuarine, and coastal DOC and POC sources and cycling: a review and synthesis. *Organic Geochemistry*. 32, 469-485.
- Reddy, C.M., Xu, L., Quinn, J.G., Hartmann, P.C. (2002) Investigating the radiocarbon content of the unresolved complex mixture. *Abstr. Am. Chem. Soc. Div. Environ. Chem.* 224, 32.
- Reimer, P.J., Baillie, M.G.L., Bard, E., Bayliss, A., Beck, J.W., Bertrand, C.J.H., Blackwell, P.G., Buck, C.E., Burr, G.S., Cutler, K.B., Damon, P.E., Edwards, R.L., Fairbanks, R.G., Friedrich, M., Guilderson, T.P., Hogg, A.G., Hughen, K.A., Kromer, B., McCormac, G., Manning, S., Ramsey, C.B., Reimer, R.W., Remmele, S., Southon, J.R., Stuiver, M., Talamo, S., Taylor, F.W., van der Plicht, J., Weyhenmeyer, C.E. (2004a) IntCal04 Terrestrial Radiocarbon Age Calibration, 0–26 Cal Kyr BP. *Radiocarbon*. 46, 1029-1058.
- Reimer, P.J., Brown, T.A., Reimer, R.W. (2004b) CALIBomb - bomb radiocarbon calibration (<http://intcal.qub.ac.uk/CALIBomb/frameset.html>).
- Reimer, P.J., Brown, T.A., Reimer, R.W. (2004c). Discussion: Reporting and calibration of post-bomb  $^{14}\text{C}$  data. *Radiocarbon*. 46, 1299-1304.
- Reimer, P.J., Baillie, M.G.L., Bard, E., Bayliss, A., Beck, J.W., Blackwell, P.G., Bronk Ramsey, C., Buck, C.E., Burr, G.S., Edwards, R.L., Friedrich, M., Grootes, P.M., Guilderson, T.P., Hajdas, I., Heaton, T.J., Hogg, A.G., Hughen, K.A., Kaiser, K.F., Kromer, B., McCormac, F.G., Manning, S.W., Reimer, R.W., Richards, D.A., Southon, J.R., Talamo, S., Turney, C.S.M., van der Plicht, J., Weyhenmeyer, C.E. (2009) IntCal09 and Marine09 Radiocarbon Age Calibration Curves, 0–50,000 Years cal BP. *Radiocarbon*. 51, 1111-1150.
- Repeta, D.J., Simpson, D.J. (1991) The distribution and recycling of chlorophyll, bacteriochlorophyll and carotenoids in the Black Sea. *Deep Sea Research*. 38, S969-S984.
- Reschke, S., Ittekkot, V., Panin, N. (2002) The Nature of Organic Matter in the Danube River Particles and North-western Black Sea Sediments. *Estuarine, Coastal and Shelf Science*. 54, 563-574.
- Rethemeyer, J., Kramer, C., Gleixner, G., Wiesenberg, G.L.B., Schwark, L., Andersen, N., Nadeau, M.-J., Grootes, P.M. (2004) Complexity of soil organic matter: AMS  $^{14}\text{C}$  analysis of soil lipid fractions and individual compounds. *Radiocarbon*. 46, 465-473.
- Rho, J., Bauman, A., Boettger, H., Yen, T. (1973) A search for porphyrin biomarkers in nonesuch shale and extraterrestrial samples. *Origins of Life and Evolution of Biospheres*. 4, 69-77.
- Riley, G., Collier, R.J., Jones, D.M., Eglinton, G., Eakin, P.A., Fallick, A.E. (1991) Sources of sedimentary lipids deduced from stable carbon-isotope analyses of individual compounds. *Nature*. 352, 425-427.
- Riley, G., Collister, J.W., Stern, B., Eglinton, G. (1993) Gas chromatography/isotope ratio mass spectrometry of leaf wax n-alkanes from plants of differing carbon dioxide metabolisms. *Rapid Communications in Mass Spectrometry*. 7, 488-491.

- Rontani, J.-F., Harji, R., Guasco, S., Prahl, F.G., Volkman, J.K., Bhosle, N.B., Bonin, P. (2008) Degradation of alkenones by aerobic heterotrophic bacteria: Selective or not. *Organic Geochemistry*. 39, 34-51.
- Ruff, M., Wacker, L., Gäggeler, H.W., Suter, M., Synal, H.-A., Szidat, S. (2007) A Gas Ion Source for Radiocarbon Measurements at 200 kV. *Radiocarbon*. 49, 307-314
- Rühlemann, C., Butzin, M. (2006) Alkenone temperature anomalies in the Brazil-Malvinas Confluence area caused by lateral advection of suspended particulate material. *Geochem. Geophys. Geosyst.* 7, Q10015, doi:10.1029/2006GC001251.
- Sachs, J.P., Repeta, D.J., Goericke, R. (1999) Nitrogen and carbon isotopic ratios of chlorophyll from marine phytoplankton. *Geochimica et Cosmochimica Acta*. 63, 1431-1441.
- Sackett, W.M., Poag, C.W., Eadie, B.J. (1974) Kerogen Recycling in the Ross Sea, Antarctica. *Science*. 185, 1045-1047.
- Saliot, A., Derieux, S., Sadouni, N., Bouloubassi, I., Filliaux, J., Dagaut, J., Momzikoff, A., Gondry, G., Guillou, C., Breas, O., Cauwet, G., Deliat, G. (2002) Winter and Spring Characterization of Particulate and Dissolved Organic Matter in the Danube-Black Sea Mixing Zone. *Estuarine, Coastal and Shelf Science*. 54, 355-367.
- Sanger, J.E. (1988) Fossil pigments in paleoecology and paleolimnology. *Palaeogeography, Palaeoclimatology, Palaeoecology*. 62, 343-359.
- Santos, G.M., Southon, J.R., Griffin, S., Beaupre, S.R., Druffel, E.R.M. (2007) Ultra small-mass AMS  $^{14}\text{C}$  sample preparation and analyses at KCCAMS/UCI Facility. *Nuclear Instruments and Methods in Physics Research Section B: Beam Interactions with Materials and Atoms*. 259, 293-302.
- Sarnthein, M., Winn, K., Duplessy, J.C., Fontugne, M.R. (1988) Global Variations of Surface Ocean Productivity in Low and Mid Latitudes: Influence on CO<sub>2</sub> Reservoirs of the Deep Ocean and Atmosphere During the Last 21,000 Years. *Paleoceanography*. 3, 361-399.
- Schlünz, B., Schneider, R.R. (2000) Transport of terrestrial organic carbon to the oceans by rivers: re-estimating flux- and burial rates *International Journal of Earth Sciences*. 88, 599-606.
- Schouten, S., Klein Breteler, W.C.M., Blokker, P., Schogt, N., Rijpstra, W.I.C., Grice, K., Baas, M., Sinninghe Damsté, J.S. (1998) Biosynthetic effects on the stable carbon isotopic compositions of algal lipids: implications for deciphering the carbon isotopic biomarker record. *Geochimica et Cosmochimica Acta*. 62, 1397-1406.
- Schouten, S., Hopmans, E.C., Schefu, E., Sinninghe Damste, J.S. (2002) Distributional variations in marine crenarchaeotal membrane lipids: a new tool for reconstructing ancient sea water temperatures? *Earth and Planetary Science Letters*. 204, 265-274.
- Schramm, A., Stein, M., Goldstein, S.L. (2000) Calibration of the  $^{14}\text{C}$  time scale to >40 ka by  $^{234}\text{U}$ - $^{230}\text{Th}$  dating of Lake Lisan sediments (last glacial Dead Sea). *Earth and Planetary Science Letters*. 175, 27-40.
- Schrum, C., Staneva, J., Stanev, E., Özsoy, E. (2001) Air-sea exchange in the Black Sea estimated from atmospheric analysis for the period 1979-1993. *Journal of Marine Systems*. 31, 3-19.
- Shah, S.R., Pearson, A. (2007) Ultra-Microscale (5-25 µg C) Analysis of Individual Lipids by  $^{14}\text{C}$  AMS: Assessment and Correction for Sample Processing Blanks. *Radiocarbon*. 49, 69-82.

- Siani, G., Paterne, M., Arnold, M., Bard, E., Mativier, B., Tisnerat, N., Bassinot, F. (2000) Radiocarbon Reservoir Ages In The Mediterranean Sea And Black Sea. *Radiocarbon*. 42, 271-280.
- Siddall, M., Anderson, R.F., Winckler, G., Henderson, G.M., Bradtmiller, L.I., McGee, D., Franzese, A., Stocker, T.F., Müller, S.A. (2008) Modeling the particle flux effect on distribution of  $^{230}\text{Th}$  in the equatorial Pacific. *Paleoceanography*. 23, PA2208, doi:10.1029/2007PA001556.
- Sigman, D.M., Altabet, M.A., McCorkle, D.C., Francois, R., Fischer, G. (2000) The  $\delta^{15}\text{N}$  of nitrate in the Southern Ocean: Nitrogen cycling and circulation in the ocean interior. *J. Geophys. Res.* 105, 19599-19614.
- Sigman, D.M., Granger, J., DiFiore, P.J., Lehmann, M.M., Ho, R., Cane, G., van Geen, A. (2005) Coupled nitrogen and oxygen isotope measurements of nitrate along the eastern North Pacific margin. *Global Biogeochem. Cycles*. 19, doi:10.1029/2005GB002458.
- Simoneit, B.R.T. (1977a) The Black Sea, a sink for terrigenous lipids. *Deep Sea Research*. 24, 813-830.
- Simoneit, B.R.T. (1977b) Organic matter in eolian dusts over the Atlantic Ocean. *Marine Chemistry*. 5, 443-464.
- Smith, C.R., Pope, R.H., DeMaster, D.J., Magaard, L. (1993) Age-dependent mixing of deep-sea sediments. *Geochimica et Cosmochimica Acta*. 57, 1473-1488.
- Smittenberg, R.H., Eglinton, T.I., Schouten, S., Damste, J.S.S. (2006) Ongoing Buildup of Refractory Organic Carbon in Boreal Soils During the Holocene. *Science*. 314, 1283-1286.
- SooHoo, J.B., Kiefer, D.A. (1982a) Vertical distribution of phaeopigments-I. A simple grazing and photooxidative scheme for small particles. *Deep Sea Research Part A. Oceanographic Research Papers*. 29, 1539-1551.
- SooHoo, J.B., Kiefer, D.A. (1982b) Vertical distribution of phaeopigments-II. Rates of production and kinetics of photooxidation. *Deep Sea Research Part A. Oceanographic Research Papers*. 29, 1553-1563.
- Sorokin, Y.I. (1983) The Black Sea, in: Ketchum, B.H., (Ed), *Ecosystems of the World - Estuaries and Enclosed Seas*, Elsevier Scientific Publishing Company, Amsterdam, pp. 253-292.
- Southon, J.R., Nelson, D.E., Vogel, J.S. (1990) A Record of Past Ocean-Atmosphere Radiocarbon Differences from the Northeast Pacific. *Paleoceanography*. 5, 197-206.
- Spooner, N., Getliff, J.M., Teece, M.A., Parkes, R.J., Leftley, J.W., Harris, P.G., Maxwell, J.R. (1995) Formation of mesopyrophyaeophorbide a during anaerobic bacterial degradation of the marine prymnesiophyte *Emiliania huxleyi*. *Organic Geochemistry*. 22, 225-229.
- Strous, M., Jetten, M.S.M. (2004) Anaerobic oxidation of methane and ammonium. *Annual Review of Microbiology*. 58, 99-117.
- Stuiver, M., Polach, H.A. (1977) Reporting of  $^{14}\text{C}$  Data. *Radiocarbon*. 19, 355-363.
- Stuiver, M., Quay, P.D. (1980) Changes in Atmospheric Carbon-14 Attributed to a Variable Sun. *Science*. 207, 11-19.
- Stuiver, M., Quay, P.D., Ostlund, H.G. (1983) Abyssal Water Carbon-14 Distribution and the Age of the World Oceans. *Science*. 219, 849-851.
- Stuiver, M., Braziunas, T.F., Becker, B., Kromer, B. (1991) Climatic, solar, oceanic, and geomagnetic influences on late-glacial and holocene atmospheric  $^{14}\text{C}/^{12}\text{C}$  change. *Quaternary Research*. 35, 1-24.

- Stuiver, M., Becker, B. (1993) High-precision decadal calibration of the radiocarbon time scale, AD 1950-6000 BC. *Radiocarbon*. 35, 35-65.
- Stuiver, M., Braziunas, T., F. (1993) Modeling atmospheric  $^{14}\text{C}$  influences and  $^{14}\text{C}$  ages of marine samples to 10,000BC. *Radiocarbon*. 35, 137-189.
- Stuiver, M., Reimer, P.J., Reimer, R. (2010) CALIB - radiocarbon calibration, version 6.0 (<http://intcal.qub.ac.uk/calib/>).
- Suess, H.E. (1955) Radiocarbon Concentration in Modern Wood. *Science*. 122, 415-417.
- Suess, H.E. (1986) Secular variations of cosmogenic  $^{14}\text{C}$  on Earth; their discovery and interpretation. *Radiocarbon*. 28, 259-265.
- Sun, M.-Y., Lee, C., Aller, R.C. (1993a) Laboratory studies of oxic and anoxic degradation of chlorophyll-a in Long Island Sound sediments. *Geochimica et Cosmochimica Acta*. 57, 147-157.
- Sun, M., Lee, C., Aller, R.C. (1993b) Anoxic and oxic degradation of  $^{14}\text{C}$ -labeled chloropigments and a  $^{14}\text{C}$ -labeled diatom in Long Island Sound sediments. *Limnology and Oceanography*. 38, 1438-1451.
- Sun, M.-Y., Wakeham, S.G. (1994) Molecular evidence for degradation and preservation of organic matter in the anoxic Black Sea Basin. *Geochimica et Cosmochimica Acta*. 58, 3395-3406.
- Sun, M.-Y., Zou, L., Dai, J., Ding, H., Culp, R.A., Scranton, M.I. (2004) Molecular carbon isotopic fractionation of algal lipids during decomposition in natural oxic and anoxic seawaters. *Organic Geochemistry*. 35, 895-908.
- Sundquist, E.T., Visser, K. (2003) The Geologic History of the Carbon Cycle, in: Holland, H. D., Turekian, K. K. (Eds), *Treatise on Geochemistry*, Pergamon, Oxford, pp. 425-472.
- Taguchi, S., Laws, E.A., Bidigare, R.R. (1993) Temporal variability in chlorophyll a and phaeopigment concentrations during incubations in the absence of grazers. *Marine Ecology Progress Series*. 101, 45-53.
- Takahashi, K., Be, A.W.H. (1984) Planktonic foraminifera: factors controlling sinking speeds. *Deep Sea Research Part A. Oceanographic Research Papers*. 31, 1477-1500.
- Tavernier, E., Dudal, R., Osmond, D., Moormann, F. (1963) Soil map of Europe. Scale 1:2 500 000, in: Food and Agriculture Organization of the United Nations, (Ed).
- Teodoru, C.R., Friedl, G., Friedrich, J., Roehl, U., Sturm, M., Wehrli, B. (2007) Spatial distribution and recent changes in carbon, nitrogen and phosphorus accumulation in sediments of the Black Sea. *Marine Chemistry*. 105, 52-69.
- Thomsen, L., Gust, G. (2000) Sediment erosion thresholds and characteristics of resuspended aggregates on the western European continental margin. *Deep Sea Research Part I: Oceanographic Research Papers*. 47, 1881-1897.
- Thomson, J., Cook, G.T., Anderson, R., MacKenzie, A.B., Harkness, D.D., McCave, I.N. (1995) Radiocarbon age offsets in different-sized carbonate components of deep-sea sediments. *Radiocarbon*. 37, 91-101.
- Thunell, R.C., Keir, R.S., Honjo, S. (1981) Calcite Dissolution: An in situ Study in the Panama Basin. *Science*. 212, 659-661.
- Tissot, B.P., Welte, D.H. (1978) Petroleum Formation and Occurrence. A New Approach to Oil and Gas Exploration, Springer, Berlin.
- Toggweiler, J., Dixon, K., Bryan, K. (1989) Simulations of Radiocarbon in a Coarse-Resolution World Ocean Model 1. Steady State Prebomb Distributions. *J. Geophys. Res.* 94, 8217-8242.

- Tolmazin, D. (1985) Changing Coastal oceanography of the Black Sea. I: Northwestern Shelf. *Progress In Oceanography*. 15, 217-276.
- Treibs, A. (1936) Chlorophyll- und Häminderivate in organischen Mineralstoffen. *Angewandte Chemie*. 49, 682-686.
- Trumbore, S.E. (1993) Comparison of Carbon Dynamics in Tropical and Temperate Soils Using Radiocarbon Measurements. *Global Biogeochem. Cycles*. 7, 275-290.
- Trumbore, S.E. (1997) Potential responses of soil organic carbon to global environmental change. *Proceedings of the National Academy of Sciences of the United States of America*. 94, 8284-8291.
- Trumbore, S. (2009) Radiocarbon and Soil Carbon Dynamics. *Annual Review of Earth and Planetary Sciences*. 37, 47-66.
- Trumbore, S.E., Chadwick, O.A., Amundson, R. (1996) Rapid Exchange Between Soil Carbon and Atmospheric Carbon Dioxide Driven by Temperature Change. *Science*. 272, 393-396.
- Turnewitsch, R., Reyss, J.-L., Nylander, J., Waniek, J.J., Lampitt, R.S. (2008) Internal tides and sediment dynamics in the deep sea--Evidence from radioactive  $^{234}\text{Th}/^{238}\text{U}$  disequilibria. *Deep Sea Research Part I: Oceanographic Research Papers*. 55, 1727-1747.
- Uchida, M., Shibata, Y., Kawamura, K., Kumamoto, Y., Yoneda, M., Ohkushi, K.i., Harada, N., Hirota, M., Mukai, H., Tanaka, A., Kusakabe, M., Morita, M. (2001) Compound-specific radiocarbon ages of fatty acids in marine sediments from the western North Pacific. *Radiocarbon*. 43, 949-956.
- Uchida, M., Shibata, Y., Ohkushi, K.i., Yoneda, M., Kawamura, K., Morita, M. (2005) Age discrepancy between molecular biomarkers and calcareous foraminifera isolated from the same horizons of Northwest Pacific sediments. *Chemical Geology*. 218, 73-89.
- Valentine, D.L. (2002) Biogeochemistry and microbial ecology of methane oxidation in anoxic environments: a review. *Antonie van Leeuwenhoek*. 81, 271-282.
- Van Andel, T.H. (1973) Texture and dispersal of sediments in the Panama Basin. *Journal of Geology*. 81, 434-457.
- Van Andel, T.H., Ross Heath, G., Malfait, B.T., Heinrichs, D.F., Ewing, J.I. (1971) Tectonics of the Panama Basin, Eastern Equatorial Pacific. *Geological Society of America Bulletin*. 82, 1489-1508.
- Velinsky, D.J., Fogel, M.L., Todd, J.F., Tebo, B.M. (1991) Isotopic fractionation of dissolved ammonium at the oxygen-hydrogen sulfide interface in anoxic waters. *Geophys. Res. Lett.* 18, 10.1029/91GL00344.
- Völker, A.H.L., Grootes, P.M., Nadeau, M.-J., Sarnthein, M. (2000) Radiocarbon levels in the Iceland Sea from 25-53kyr and their link to the earth's magnetic field intensity. *Radiocarbon*. 42, 437-452.
- Volkman, J.K., Eglington, G., Corner, E.D.S., Forsberg, T.E.V. (1980a) Long-chain alkenes and alkenones in the marine coccolithophorid *Emiliania huxleyi*. *Phytochemistry*. 19, 2619-2622.
- Volkman, J.K., Johns, R.B., Gillan, F.T., Perry, G.J., Bavor Jr, H.J. (1980b) Microbial lipids of an intertidal sediment-I. Fatty acids and hydrocarbons. *Geochimica et Cosmochimica Acta*. 44, 1133-1143.
- Voss, M., Dippner, J.W., Montoya, J.P. (2001) Nitrogen isotope patterns in the oxygen-deficient waters of the Eastern Tropical North Pacific Ocean. *Deep Sea Research Part I: Oceanographic Research Papers*. 48, 1905-1921.

- Wakeham, S.G. (1996) Aliphatic and polycyclic aromatic hydrocarbons in Black Sea sediments. *Marine Chemistry.* 53, 187-205.
- Wakeham, S.G. (2006) Radiocarbon Compositions of Biomarkers in Sediment Traps and Surface Sediments in the Ocean, 2006 Ocean Sciences Meeting. *Eos Trans. AGU,* 87 (36), Ocean Sci. Meet. Suppl., pp. OS16K-05.
- Wang, X.C., Druffel, E.R.M., Lee, C. (1996) Radiocarbon in organic compound classes in particulate organic matter and sediment in the deep northeast Pacific Ocean. *Geophysical Research Letters.* 23, 3583-3586.
- Wang, X.-C., Druffel, E.R.M., Griffin, S., Lee, C., Kashgarian, M. (1998) Radiocarbon studies of organic compound classes in plankton and sediment of the northeastern Pacific Ocean. *Geochimica et Cosmochimica Acta.* 62, 1365-1378.
- Watkins, J.M., Mix, A.C., Wilson, J. (1996) Living Planktic Foraminifera: Tracers of circulation and productivity in the central equatorial Pacific. *Deep Sea Research II.* 43, 1257-1282.
- Weijers, J.W.H., Schouten, S., van den Donker, J.C., Hopmans, E.C., Sinninghe Damsté, J.S. (2007) Environmental controls on bacterial tetraether membrane lipid distribution in soils. *Geochimica et Cosmochimica Acta.* 71, 703-713.
- Williams, P.M., Druffel, E.R.M. (1987) Radiocarbon in dissolved organic matter in the central North Pacific Ocean. *Nature.* 330, 246-248.
- Willkomm, H. (1976) Age Determination in Quaternary. *Radiocarbon Dating and Age Estimation with Other Methods of Nuclear Physics,* Verlag Karl Thiemic, München.
- Wyrtki, K. (1967) Circulation and Water Masses in the Eastern Equatorial Pacific Ocean. *International Journal of Oceanology and Limnology.* 1, 117-147.
- Ziervogel, K., Bohling, B. (2003) Sedimentological parameters and erosion behaviour of submarine coastal sediments in the south-western Baltic Sea *Geo-Marine Letters.* 23, 43-52.
- Zimmerman, A.R., Goyne, K.W., Chorover, J., Komarneni, S., Brantley, S.L. (2004) Mineral mesopore effects on nitrogenous organic matter adsorption. *Organic Geochemistry.* 35, 355-375.



## 7. ACKNOWLEDGEMENTS

This thesis “**TRACING TIME IN THE OCEAN: UNREVALING DEPOSITIONAL AND PRESERVATIONAL TIMESCALES USING COMPOUND-SPECIFIC RADIOCARBON ANALYSIS OF BIOMARKERS FROM MARINE SEDIMENTS**” was founded within the Helmholtz Young Investigators Group “Applications of molecular  $^{14}\text{C}$  analysis for the study of sedimentation processes and carbon cycling in marine sediments”. Additional funding was provided by the Japan Society for Promotion of Science (JSPS fellowship PE08543) and the Bremen Graduate School “Global Change in the Marine Realm” (GLOMAR).

I would like to especially thank **GESINE MOLLENHAUER** for giving me the opportunity to join her working group and entrusting me with this project in the fascinating and fiddly field of compound-specific radiocarbon analysis. I want to thank you for your supervision, for always having time and advice, and for your support upon my own ideas – you did a great job. Additionally, I would like to thank **KAI-UWE HINRICHES** for reviewing this thesis and joining my thesis committee. Moreover I thank **RALF TIEDEMANN** for participating in my thesis committee.

I enjoyed being a member of the Young Investigators Group with the other members **JANET RETHEMEYER**, **MARIA WINTERFELD**, **SVEN KRETSCHMER**, and **RALPH KREUTZ**. I would like to thank Janet for 3 marvellous years sharing an office. I will never forget the fun we had. Maria made survival of the last months much easier by her highly appreciated company and friendship. Ralph is acknowledged for the maintenance of all GCs, and the PCGC and HPLC systems – this made my compound-specific radiocarbon analyses possible.

I furthermore want to acknowledge our **MARINE GEOCHEMISTRY WORKING GROUP** at **AWI**. Special thanks to **JANA FRIEDRICH** for the chance to join her *RV Poseidon* cruise P363 (Black Sea), which allowed to get core-top sample material appropriate for compound-specific radiocarbon dating and, thus, set the basis for projects II and III.

I also want to express many thanks to **NAO OHKOUCHI**, **CHIRO KASHIYAMA**, **NANA OGAWA** and all members of the **BIOGEOCHEMISTRY WORKING GROUP** at **JAMSTEC** for giving me the opportunity to join their group and laboratory facilities for 3 months and who made it possible to successfully finish our project (III).

Furthermore, I am grateful to **BIRGIT MEYER-SCHACK**, **MONIKA SEGL** and **HELLA BUSCOFF** for their support and help with vacuum line sample preparation and C/N analysis.

Many thanks to **HENNING KUHNERT**, **THOMAS FELIS**, **ENNO SCHEFUB**, and **FLORIAN ROMMERSKIRCHEN** for any help they provided during the last years.

I am indebted to **ALEX NICHOLS** and **DAVE HESLOP** for proof-reading.

Finally I would like to thank **ALL FRIENDS** who made my time in Bremen fun.



## 8. APPENDIX

### A.1 LIST OF ABBREVIATIONS

$\text{Al}_2\text{O}_3$	aluminium oxide
AMS	Accelerator Mass Spectrometry
ASE	accelerated solvent extraction
BP	before present
C	carbon
$^{12}\text{C}$	carbon with atomic mass 12
$^{13}\text{C}$	carbon with atomic mass 13
$^{14}\text{C}$	carbon with atomic mass 14 (radiocarbon)
$\text{CaCO}_3$	carbonate
cal yrs BP	calibrated $^{14}\text{C}$ years before present
CAM	Crassulacean Acid Metabolism
$\text{CO}_2$	carbon dioxide
$\text{CuO}$	copper oxide
DAD	Diode Array Detector
EA	Elemental Analyser
FAME	fatty acid methyl ester
FID	Flame Ionisation Detector
GC	Gas Chromatography
GDGT	glycerol dialkyl glycerol tetraether
HCl	hydrogen chloride
HPLC	High Performance Liquid Chromatography
$\text{H}_3\text{PO}_4$	phosphoric acid
IRMS	Isotope Ratio Mass Spectrometry
mbsl	meters below sea level
meV	million electron Volts
MS	Mass Spectrometry
mV	million Volts
OC	organic carbon
OM	organic matter
PCGC	Preparative Column Gas Chromatography
PDB	PeeDee Belemnite
PFC	Preparative Fraction Collector
rpm	revolutions per minute
$\text{SiO}_2$	silicon dioxide (silica)
SOC	soil organic carbon
SST	sea surface temperature
TEP	transparent extrapolymeric particles
$^{230}\text{Th}$	Thorium with atomic mass 230
$^{230}\text{Th}_{\text{xs}}$	$^{230}\text{Th}_{\text{excess}}$
TLE	total lipid extract
TOC	total organic carbon
VPDB	Vienna PeeDee Belemnite

yrs BP	conventional $^{14}\text{C}$ years before present
$\%C_{\text{petro}}$	percent petrogenic carbon
$\%C_{\text{org}}$	percent organic carbon
$\%N_{\text{total}}$	percent total nitrogen

## A.1 LIST OF FIGURES

Figure 1.1 The global carbon cycle.....	1
Figure 1.2 Simplified illustration of the distribution of radiocarbon .....	3
Figure 1.3 Schematic diagram of the NOSAMS tandemron AMS system.....	5
Figure 1.4 Atmospheric $^{14}\text{CO}_2$ concentrations ( $\Delta^{14}\text{C}$ ) for the time period AD1795-2009... .	9
Figure 1.5 Clipping of the IntCal04 and Marine04 calibration curves showing the deviation between conventional $^{14}\text{C}$ age and calendar age as derived from dendrochronologically dated tree rings, foraminifera in varved sediments or $^{230}\text{Th}/^{234}\text{U}$ -dated corals.....	10
Figure 1.6 Simplified diagram of a Soxhlet apparatus.....	13
Figure 1.7 Schematic of a Gas Chromatograph and the chromatographic separation. ....	14
Figure 1.8 Diagram of the PCGC system used for biomarker purification in this thesis..	15
Figure 1.9 Diagram of an HPLC system as used in this thesis. .....	16
Figure 1.10 Diagram of the EA/IRMS system used in this thesis. .....	17
Figure 1.11 Example molecular structures of lipid and tetrapyrrole biomarkers discussed in this thesis. .....	18
Figure 2.1 Study area and core locations. ....	27
Figure 2.2 High resolution swath bathymetry image showing the abyssal hill topography around cores ME0005A-24JC and Y69-71P.....	28
Figure 2.3 Conventional radiocarbon ages of alkenones, foraminifera ( <i>N. dutertrei</i> ) and Total Organic Carbon (TOC) for core ME0005A-24JC. ....	31
Figure 2.4 Conventional radiocarbon ages of alkenones, foraminifera ( <i>N. dutertrei</i> and <i>G. sacculifer</i> ) and Total Organic Carbon (TOC) for core Y69-71P. ....	33
Figure 2.5 Conventional radiocarbon ages of alkenones, foraminifera ( <i>N. dutertrei</i> and <i>G. sacculifer</i> ) and Total Organic Carbon (TOC) for core MC16. ....	34
Figure 2.6 $U_{37}^K$ derived SSTs for core ME0005-24JC and Y69-71P.....	45
Figure 3.1 Study area with core locations. ....	52
Figure 3.2 A) BIT-Index; B) Concentrations of $C_{27+29+31+33}$ n-alkanes. ....	57
Figure 3.3 Radiocarbon data ( $\Delta^{14}\text{C}$ ) for core locations along river-mouth to deep-basin transects. ....	60
Figure 4.1 Study area showing core locations.....	79
Figure 4.2 Stable nitrogen and carbon isotopic composition ( $\delta^{13}\text{C}$ and $\delta^{15}\text{N}$ ) of purified chloro- and pheo-pigments. ....	85
Figure 4.3 Radiocarbon concentrations ( $\Delta^{14}\text{C}$ ) of purified chloro- and pheo-pigments. ...	86
Figure 4.4 Modelled Black Sea surface water DIC $\Delta^{14}\text{C}$ concentrations. ....	90



## A.1 LIST OF TABLES

<b>Table 1.1</b> Rounding off convention for conventional radiocarbon ages as reported by NOSAMS.....	9
<b>Table 2.1</b> Core locations .....	27
<b>Table 2.2</b> Radiocarbon data of foraminifera, TOC and alkenones of cores ME0005A-24JC, Y69-71P and MC16. ....	32
<b>Table 2.3</b> Receipt numbers from NOSAMS and Leibniz laboratory. ....	47
<b>Table 3.1</b> Drainage area characteristics of the investigated river transects.....	53
<b>Table 3.2</b> Core locations along river-mouth to deep-basin transects.....	54
<b>Table 3.3</b> Expected core top ages based on published sedimentation rates without and with the influence of bioturbation and Isoprenoid Tetraether Index at each station. ....	58
<b>Table 3.4</b> Radiocarbon and stable carbon isotopic data along river-mouth to deep-basin transects. ....	59
<b>Table 3.5</b> Average terrestrial residence times for the investigated river catchments deduced from the core locations closest to the river mouths. ....	65
<b>Table 3.6</b> Radiocarbon contents and conventional radiocarbon ages of n-C <sub>29+31</sub> alkanes corrected for petrogenic contribution.....	70
<b>Table 3.7</b> TOC radiocarbon and stable carbon isotopic data for stations without compound-specific radiocarbon data. ....	74
<b>Table 3.8</b> Geochemical proxy data along river-mouth to deep-basin transects. ....	75
<b>Table 4.1</b> Blank-corrected radiocarbon ( $\Delta^{14}\text{C}$ ) and stable isotopic composition ( $\delta^{13}\text{C}$ and $\delta^{15}\text{N}$ ) of purified chloro- and pheopigments, bivalve shells, total organic carbon (TOC), and bulk sediment. ....	84
<b>Table 4.2</b> Seawater nitrate nitrogen isotopic composition.....	94
<b>Table 4.3</b> Modelled surface water DI <sup>14</sup> C results from 20 m water depth for the time interval AD1940 to AD2008 (sampling year). ....	95





